이학박사 학위논문

Morphology and Thickness Control of 2D structures via Crystallization-Driven Self-Assembly of Block Copolymers Having Discrete Poly(lactic acid)s

단일 분자량을 갖는 락틱애씨드 블록공중합체의 결정화 자기조립을 통한 이차원 구조의 형태와 두께 조절 연구

2022년 8월

서울대학교 대학원

화학부 고분자화학전공

권용범

Morphology and Thickness ontrol of 2D structures via Crystallization-Driven Self-Assembly of Block Copolymers Having Discrete Poly(lactic acid)s

by

Yongbeom Kwon

Supervised by

Professor Kyoung Taek Kim

A Dissertation
Submitted to the Faculty of
Seoul National University (SNU)
in Partial Fulfillment of
the Requirements for the Degree of
Doctor of Philosophy

August 2022

Department of Chemistry
Graduate School
Seoul National University

Morphology and Thickness Control of 2D structures via Crystallization-Driven Self-Assembly of Block Copolymers Having Discrete Poly(lactic acid)s

지도교수 김 경 택

이 논문을 이학박사 학위논문으로 제출함

2022년 6월

서울대학교 대학원

화학부 고분자화학 전공

권 용 범

권용범의 이학박사 학위논문을 인준함

2022년 6월

위 원 장 이 연 (인)

부위원장 김 경 택 (인)

위 원 손 병 혁 (인)

위 원 최 태 림 (인)

위 원 곽 민 석 (인)

Abstract

Discrete polymers composed of an exact number of repeating units have attracted considerable interest as model systems to examine the behavior of polymers having chemical structures without statistical distribution. Self-assembly of discrete block copolymers has indicated that dispersity has a dramatic influence on the self-assembled structures. The use of discrete polymers for self-assembly provides a means to the control morphology and thickness of structures. It allows discrete polymers to be used as a potential candidate for the creation of advanced materials.

In chapter 2, we report the crystallization-driven self-assembly (CDSA) of block copolymers (BCPs) built with monodisperse poly(lactic acid) (MPLA) composed of enantiomeric repeating units joined in a defined sequence. The CDSA of the BCPs composed of crystallizable MPLA and solvent-soluble poly(ethylene glycol) (PEG) produced two-dimensional (2D) nanostructures. The morphology was transformed by a systematic change in the number and the sequence of enantiomeric repeating units comprising the MPLA block. This effect was more pronounced in the CDSA of a stereocomplex of a pair of BCPs having MPLA blocks configured in a complementary manner.

In chapter 3, the crystallites created by CDSA of stereoblock copolymers composed of MPLA and PEG were investigated to control the chain-folding. The CDSA of these BCPs, [DLA_n]-[LLA_n]-*b*-PEG, resulted in the formation of platelets having crystalline cores composed of the folded stereoblock PLAs via intramolecular stereocomplexation of [DLA_n] and [LLA_n] in solution. Precise control of the number and sequence of repeating units of stereoblock PLAs allowed us to control the thickness of the unilamellar crystallites, which were proportional to the number of lactic acid

units consisting of [DLA_n] and [LLA_n] domains.

In chapter 4, stereoblock copolymers having a mismatch in lactic acid units were synthesized by an iterative convergent method. The CDSA of mismatched stereoblock copolymers formed micro-sized structures. Extra DLAs in mismatched stereoblock copolymers contributed to the stacking of stereocomplex. The stacking driven by extra DLAs leads to the formation of micro-sized structures. Possible crystal models were suggested based on the assembled structures and XRD analysis.

Keywords: Discrete polymer, Iterative convergent synthesis, Crystallization-driven self-assembly, 2D structure, Stereoblock copolymer, Stereocomplex, Chain-folding, Micro-sized structure, Stereocomplex stacking.

Student Number: 2016-20333

Table of Contents

List of Figures

results from background scattering (Kapton tape).

Figure 1-7. (a) Schematic representation of the formation of diamond-shaped "patchy" platelet block co-micelles through seeded growth. TEM images of (b) diblock and (c) tetra-block platelet co-micelles. The samples for TEM were not stained. (d) AFM image and (e) height profile of diblock platelet co-micelle.

Figure 1-8. TEM images obtained from 1 g L^{-1} chloroform solutions of (a) $P1_{50}$-*b*-$P2_{22}$ after 1 h, and (b) after 1 d aging at 25 C, (c) $P1_{50}$-*b*-$P2_{33}$, (d) $P1_{50}$-*b*-$P2_{44}$, (e) $P1_{50}$-*b*-$P2_{55}$, and (f) $P1_{50}$-*b*-$P2_{66}$ without aging (scale bar for (b)–(f), 200 nm). Plots of the DP of P2 versus (g) average width (W_n) of the core of the 1D nanofibers compared to the theoretical length of the fully stretched P2 block, and (h) W_n after staining with RuO_4 vapour.

Figure 1-9. Morphological transition and the changes to the crystallinity on mixing of two homochiral cylinders 3 and 4. Conducted at 65 °C with the addition of fresh THF (final solvent composition THF/H_2O 20/80 v/v). (a) Cartoon illustration showing the morphological transition from homochiral cylinders 3 and 4 to stereocomplex spheres. Scale bar = 500 nm (b) FT-IR spectra of dried nanoparticles, which reveal the wavenumber of carbonyl group vibration of poly(lactide) shifted from 1,758 to 1,750 cm^{-1} over time. Scale bar = 500 nm. (c–g) TEM images, which illustrate the length of the cylindrical micelles decreased while the population of spherical micelles increased over time. Scale bars = 500 nm. (h) TEM expansion of 62 h time point. Scale bar = 100 nm. (i) WAXD diffractograms illustrating that the intensity of stereocomplex Bragg peak at a 2θ value of 12° increased gradually, whereas the intensity of homochiral Bragg peak at a 2θ value of

16.6 º decreased significantly over time. TEM samples were prepared by slow drying and negatively stained using PTA.

Figure 1-10. Assessment of micelle accumulation in MDA-MB-436 MCTSs using (a) confocal microscopy images taken at 50 μm depth from the spheroid surface. For MCTSs treated with spherical micelles and rod-like micelles with different lengths, (b) their total fluorescence intensities per unit area at cross-section were measured and compared. (c) Penetration of six different micelles in MCTS in periphery, intermediate and core regions at 50 μm depth. Data points represent mean ± standard deviation in each area, n = 3 MCTSs. Statistically significant differences between each region are denoted by (*), and in all cases $p < 0.05$.

Figure 1-11. (a) Schematic illustration of the preparation of low dispersity B−A−B segmented nanofibers with a central $PDHF_{14}$-*b*-PEG_{227} segment (A) and terminal $PDHF_8$-*b*-$P3EHT_{25}$-*b*-PEG_{113} segments (B). (b) TEM image of B−A−B segmented nanofibers (L_n = 739 nm, L_w/L_n = 1.02) in THF:MeOH (1:9, v/v) prepared from the epitaxial growth of $PDHF_8$-*b*-$P3EHT_{25}$-*b*-PEG_{113} unimers from $PDHF_{14}$-*b*-PEG_{227} seed micelles (L_n = 247 nm, L_w/L_n = 1.04). (c) LCSM image of B−A−B segmented nanofibers (L_n = 3473 nm, L_w/L_n = 1.03) in THF:MeOH (1:9, v/v) prepared from the epitaxial growth of $PDHF_8$-*b*-$P3EHT_{25}$-*b*-PEG_{113} unimers from $PDHF_{14}$-*b*-PEG_{227} seed micelles (L_n = 972 nm, L_w/L_n = 1.02). LCSM image was taken with both blue (PDHF) and red (P3EHT) channels. Scale bars: (b) 1 μm and (c) 10 μm.

Figure 2-1. Schematic representation of the formation of various nanostructures through crystallization-driven self-assembly. (a) CDSA of BCPs with a discrete number of repeating units and stereochemical

sequence of MPLA blocks and resulting 2D nanostructures. (b) CDSA of the SCs of a pair of BCPs having a mismatch in the size and stereochemical sequence of MPLA blocks and assembled structures.

Figure 2-2. (a) Gel-permeation chromatography (GPC) analysis of [LA_n] (b) Combined MALDI-TOF mass spectra of MPLA. (c) GPC analysis of [LA_n]-*b*-PEG. (d) Combined MALDI-TOF mass spectra of [LA_n]-*b*-PEG.

Figure 2-3. 2D nanostructures obtained from the CDSA of [DLA_{32n}]-*b*-PEG (n = 1, 2). (a,b) TEM images (c–f) AFM images, and height profiles of diamond- and truncated diamond crystallites. (a,c,e) [DLA_{32}]-*b*-PEG. (b,d,f) [DLA_{64}]-*b*-PEG. TEM samples were stained with a 1 wt% solution of phosphortungstic acid in water.

Figure 2-4. 2D crystallites with different shapes formed by the CDSA of diblock copolymers [DLA_{32}-*x*LA_8]-*b*-PEG (*x* = D, L, or D/L) or [DLA_{72}]-*b*-PEG. (a–d) TEM images, (e–h) AFM images, and (i–l) height profiles of leaf- and diamond-shaped crystallites. (a,e,i) [DLA_{40}]-*b*-PEG. (b,f,j) [DLA_{72}]-*b*-PEG. (c,g,k) [DLA_{32}-D/LLA_8]-*b*-PEG. (d,h,l) [DLA_{32}-LLA_8]-*b*-PEG. TEM samples were stained with a 1 wt% solution of phosphortungstic acid in water.

Figure 2-5. DSC results (second cooling scans, ramp rate = 10 ºC min^{-1}, T_c) of MPLA-*b*-PEG prepared by the CDSA of [DLA_{32}-*x*LA_8]-*b*-PEG (*x* = D, L, or D/L) or [DLA_{32}]-*b*-PEG.

Figure 2-6. Assembled structures with different shapes from mismatched SCs. (a–c) TEM images of incomplete SC. (a) Nanoparticles prepared by co-self-assembly of [DLA_{40}]-*b*-PEG/[LLA_{32}]-*b*-PEG (1:1 mol/mol, D/L = 1.250). (b) Vesicles formed by co-self-assembly of [DLA_{64}]-*b*-

PEG/[LLA_{32}]-*b*-PEG (1:1 mol/mol, D/L = 2.000). (c) Triangular 2D structures prepared by co-self-assembly of [DLA_{72}]-*b*-PEG/[LLA_{64}]-*b*-PEG (1:1 mol/mol, D/L = 1.125). (d,e) AFM image and height profile of vesicles formed by co-self-assembly of [DLA_{64}]-*b*-PEG/[LLA_{32}]-*b*-PEG (1:1 mol/mol, D/L = 2.000). (f,g) AFM image and height profile of triangular 2D structures by co-self-assembly of [DLA_{72}]-*b*-PEG/[LLA_{64}]-*b*-PEG (1:1 mol/mol, D/L = 1.125). TEM samples were stained with a 1 wt% solution of phosphortungstic acid in water.

Figure 2-7. 2D crystallites formed from SCs having stereochemical sequence. (a–d) TEM images, (e–h) AFM images, and height profiles of SC crystallites. (a,c,e,g) Triangular 2D structures by co-self-assembly of [DLA_{32}-D/LLA_8]-*b*-PEG/[LLA_{40}]-*b*-PEG (1:1 mol/mol).

Figure 2-8. (a) DSC (second heating scans, ramp rate = 10 °C min^{-1}, T_m) and (b) FT-IR results of the SCs prepared by the CDSA of [DLA_{32}-*x*LA_8]-*b*-PEG/[LLA_{40}]-*b*-PEG.

Figure 3-1. Schematic representation of the intermolecular and intramolecular stereocomplexation of [DLA_n]-[LLA_n]-*b*-PEG.

Figure 3-2. (a) Combined MALDI-TOF spectra of monodisperse PLA. (b) Combined MALDI-TOF spectra of [LLA_{16}]-*b*-PEG and [DLA_n]-[LLA_n]-*b*-PEG. (c) GPC analysis of [LLA_{16}]-*b*-PEG and [DLA_n]-[LLA_n]-*b*-PEG. (d) CD spectra of [DLA_{16}], [LLA_{16}], and [DLA_n]-[LLA_n]-*b*-PEG.

Figure 3-3. 2D nanostructures obtained from the CDSA of [DLA_{16}]-[LLA_{16}]-b-PEG (ethanol, 75°C, slow cooling, 16 h aging, dilution with water). (a, b) TEM images, (c–f) AFM images, and height profiles of ill-defined nanostructures. (a, c, e) 1 mg/mL, (b, d, f) 0.01 mg/mL. TEM

samples were stained using a 1 wt% solution of phosphotungstic acid in water.

Figure 3-4. Plot of the relative size of the nanostructures of [DLA_{16}]-[LLA_{16}]-*b*-PEG in solution (filled square: concentration 1 mg/mL in ethanol, filled circle: 0.01 mg/mL in ethanol, and open triangle: 1 mg/mL acetonitrile) versus time. The relative size was determined by DLS. The sameple solution was slowly cooled from 75 °C to room temperature during the measurement. The sizes after 12 h of aging: 390.5 nm (1 mg/mL in ethanol), 437.8 nm (0.01 mg/mL in ethanol), 183.7 nm (1 mg/mL in acetonitrile).

Figure 3-5. 2D nanostructures obtained from the CDSA of [DLA_{16}]-[LLA_{16}]-*b*-PEG (Acetonitrile, 75 °C, slow cooling, 16 h aging, dilution with water). (a–d) AFM images, and height profiles of defined nanostructures. (a, c) 1 mg/mL, (b, d) 2.5 mg/mL. (e) XRD patterns of the crystallite obtained from [LLA_{32}]-*b*-PEG and [DLA_{16}]-[LLA_{16}]-*b*-PEG in acetonitrile solution. (f) Differential scanning calorimetry (DSC) thermograms (second heating scans, ramp rate = 10 ºC min^{-1}, T_m) of the nanostructures prepared by the CDSA of [LLA_{32}]-*b*-PEG and [DLA_{16}]-[LLA_{16}]-*b*-PEG.

Figure 3-6. 2D nanostructures obtained from the CDSA of [DLA_{24}]-[LLA_{24}]-*b*-PEG (IPA/THF 9:1 or 3:1 vol %, 75°C, slow cooling, 24 h aging, dilution with water). (a–c) AFM images, (d–f) height profiles of nanostructures. (a, d) 1 mg/mL (IPA/THF 9:1 vol %), (b, e) 0.01 mg/mL (IPA/THF 9:1 vol %), (c, f) 1 mg/mL (IPA/THF 3:1 vol %).

Figure 3-7. (a) Synthesis of [DLA_{16}]-*rac*VLA^{NH2}-[LLA_{16}]-*b*-PEG. (b) Schematic representation of the intramolecular stereocomplexation and apex-labeling of [DLA_{16}]-*rac*VLA^{NH2}-[LLA_{16}]-*b*-PEG.

Figure 3-8. (a) MALDI-TOF spectra of [DLA_{16}]-*rac*VLA-allyl (blue) and [DLA_{16}]-*rac*VLA (black). (b) Combined MALDI-TOF spectra of [DLA_{16}]-[LLA_{16}]-*b*-PEG (black), [DLA_{16}]-*rac*VLA-[LLA_{16}]-*b*-PEG (red), and [DLA_{16}]-*rac*VLA^{NH2}-[LLA_{16}]-*b*-PEG (blue). Mass of VLA–H_2O: 98.10 Da, cysteamine: 77.15 Da.

Figure 3-9. 2D nanostructures obtained from the CDSA of (a–c) [DLA_{16}]-*rac*VLA^{NH2}-[LLA_{16}]-*b*-PEG and (d) [DLA_{16}]-*rac*VLA^{F}-[LLA_{16}]-*b*-PEG (1 mg/mL in ethanol, 75 °C, slow cooling, 16 h aging, dilution with water). (a) TEM image, (b,c) AFM images and height profiles, (d) CLSM image of the nanostructures.

Figure 4-1. (a) Combined MALDI-TOF spectra of [DLA_n]-[LLA_m]-*b*-PEG. (b) CD spectra of [D/LLA_{32}], and [DLA_{32}]-[LLA_{16}]-*b*-PEG.

Figure 4-2. Micro-sized triangular structures obtained from the CDSA of [DLA_{32}]-[LLA_{16}]-*b*-PEG (ethanol, 75 ºC, slow cooling, 12 h aging). (a) TEM image, (b) SEM image, (c,d) AFM image and height profile of micro-sized structure.

Figure 4-3. XRD patterns of the crystallite obtained from [DLA_{32}]-*b*-PEG and [DLA_{32}]-[LLA_{16}]-*b*-PEG in ethanol solution.

Figure 4-4. Micro-sized triangular structures obtained from the CDSA of [DLA_{24}]-[LLA_{16}]-*b*-PEG (ethanol, 75 ºC, slow cooling, 12 h aging). (a,b) TEM images of micro-sized structure.

Figure 4-5. (a) XRD pattern of the crystallite obtained from [DLA_{24}]-[LLA_{16}]-*b*-PEG in ethanol solution. (b) DSC thermograms of the self-

assembled structures prepared by the CDSA of [DLA_{40}]-*b*-PEG and [DLA_{24}]-[LLA_{16}]-*b*-PEG.

Figure 4-6. Schematic representation of the crystal models for [DLA_{32}]-[LLA_{16}]-*b*-PEG. Stacking of stereocomplex is induced by (a) homo crystallization or (b) stereocomplexation of extra DLA units.

List of Tables

List of Schemes

Chapter 1. Introduction

1.1 Discrete synthetic macromolecules

Controlled/living polymerization furnished controllability over the average molecular weight, dispersity, architecture of the formed polymers, which provides an opportunity in functional polymer design and materials.[1,2] However, the sequence and molecular weight distribution of macromolecules remained as challenges of polymer chemistry. Inspired by the functionality of biomacromolecules such as proteins or DNA, the synthesis of uniform macromolecules with unprecedented properties has attracted great interest. The synthesis of discrete polymers which were comprised of an exact number of monomers has depended on the iterative single monomer addition (Figure 1-1).[3,4] This strategy has the advantage to control the sequence and the polymer length absolutely. However, with the increase in the number of monomers or molecular weight, this strategy is inefficient because of the required number of reactions and purifications.

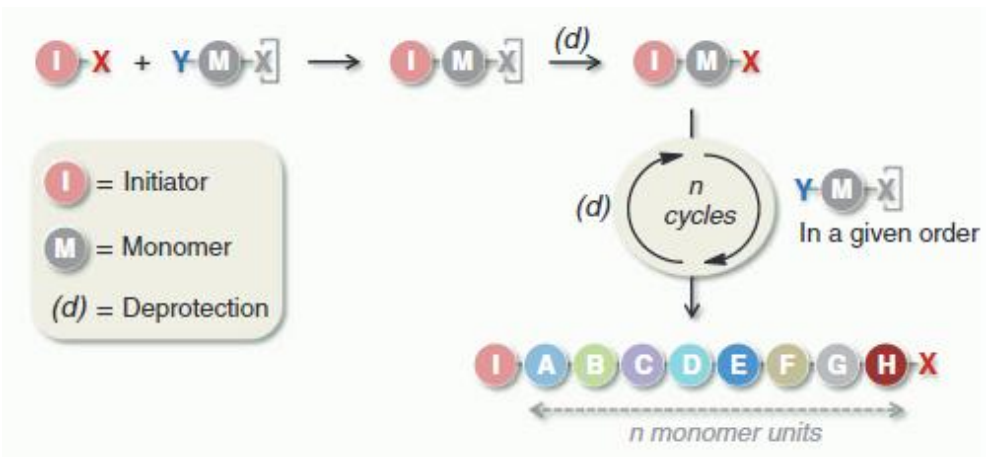

Figure 1-1. Schematic representation of iterative single monomer addition.[4]

Due to the limitation of iterative single monomer addition, new synthetic strategies for discrete polymers have been researched.[5] Recently, synthetic strategies have focussed on the simplified synthetic procedure. For example, the protecting group required for preventing polymerization is excluded by choosing orthogonal building blocks[6] and the unreacted monomers are removed simply using precipitation of positively charged macromolecules and extraction of liquid phase support.[7] The developments of these synthetic approaches including the iterative exponential growth (Figure 1-2) and the cross-convergent synthesis (Figure 1-3) have permitted the synthesis of high-molecular-weight discrete polymers with defined sequences.[8,9] These approaches resolved prerequisites regarding scalability and the chain length of the polymers, which led to the study of behavior and application of synthetic polymers with defined sequences.

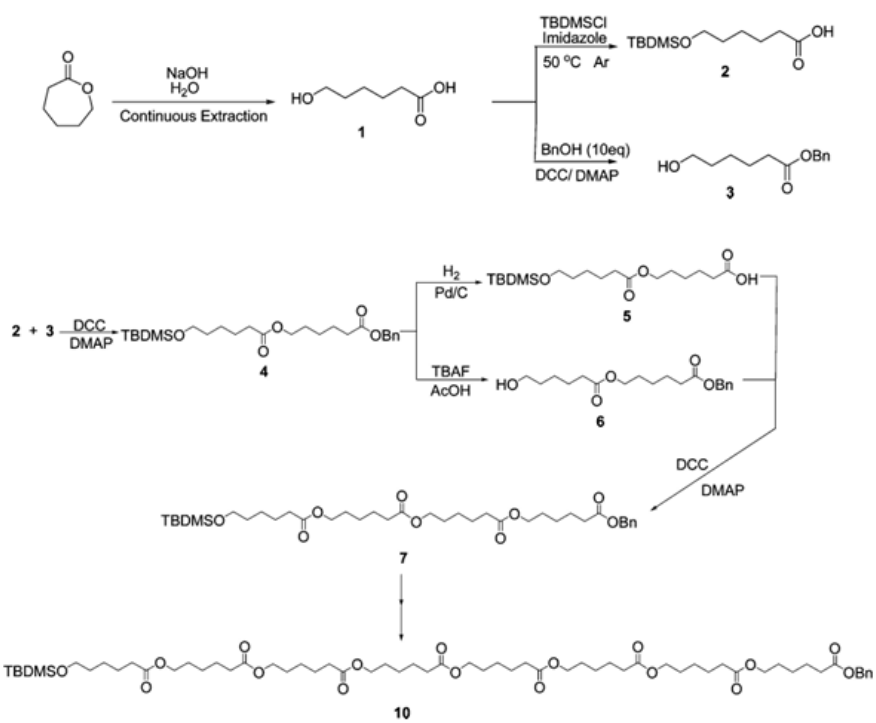

Figure 1-2. Schematic representation of the iterative exponential growth of molecularly defined caprolactone oligomers and polymers.[8]

Macromolecular data storage is one of the notable applications of sequence-defined polymers. The demand for storing data has increased geometrically, therefore a number of research about alternatives to current data storage methods are proceeding nowadays.[10,11] While DNA which is one of the options for data storage has some of the inherent drawbacks such as hydrolysis of phosphodiester bonds, expensive, and restricted number of building blocks, sequence-defined polymers are more suitable for alternation of encoding information in terms of price and various building blocks.[12–14] A number of different monomers can be incorporated into sequence-defined polymers by utilizing the diverse chemical reactions. This advantage enables sequence-defined polymers to encode data efficiently. Boukis and Meier established protocol for data storage based on Biginelli and Passerini reaction with the high structural variety of monomers (Figure 1-4).[15] This approach allowed them to achieve an information density of up to 24 bits per repeat unit.

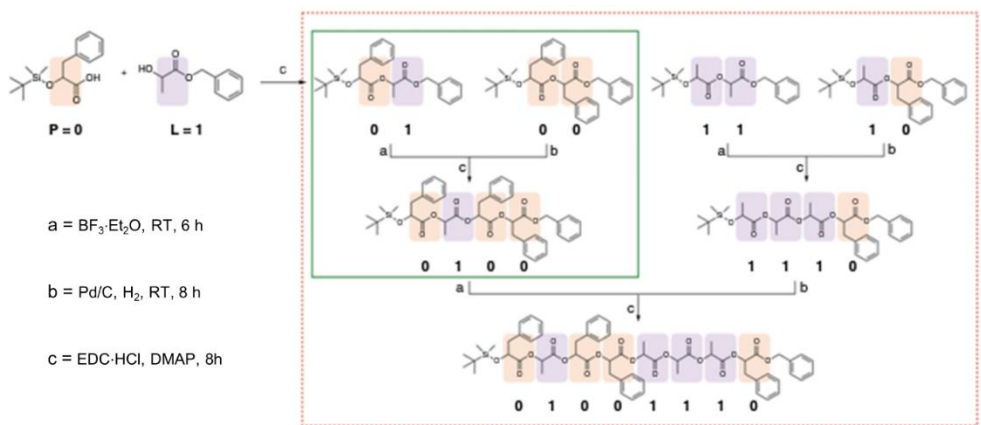

Figure 1-3. Schematic representation of the cross-convergent synthesis of poly(α-hydroxy acid). Four dyads of phenyllactic acid (P representing 0) and lactic acid (L representing 1) were used as the constituent units of poly(α-hydroxy acid).[9]

Kim et al. demonstrated an increase in capacity of data storage can also be accomplished via the synthesis of poly(α-hydroxy acid) (PAH) composed of a large discrete number of monomers in an absolutely defined aperiodic sequence (Figure 1-5).[9] The scalable synthesis of a binary encoded, high molecular weight PAH (up to 38 kDa) by using cross-convergent pathway, combined with preparative size exclusion chromatography as an purification method. Digital information can be stored in the aperiodic sequence of poly (phenyllactic-co-lactic acid), built via the direct translation of binary code to the chemical structure built with four dyads of monomers as constituent units. The encoded information can be decoded by a tandem mass technique utilizing MALDI-TOF MS/MS. This method allows synthesis of sequence-defined poly(α-hydroxy acid) in a minimal number of coupling steps and higher storage density (bit/Da).

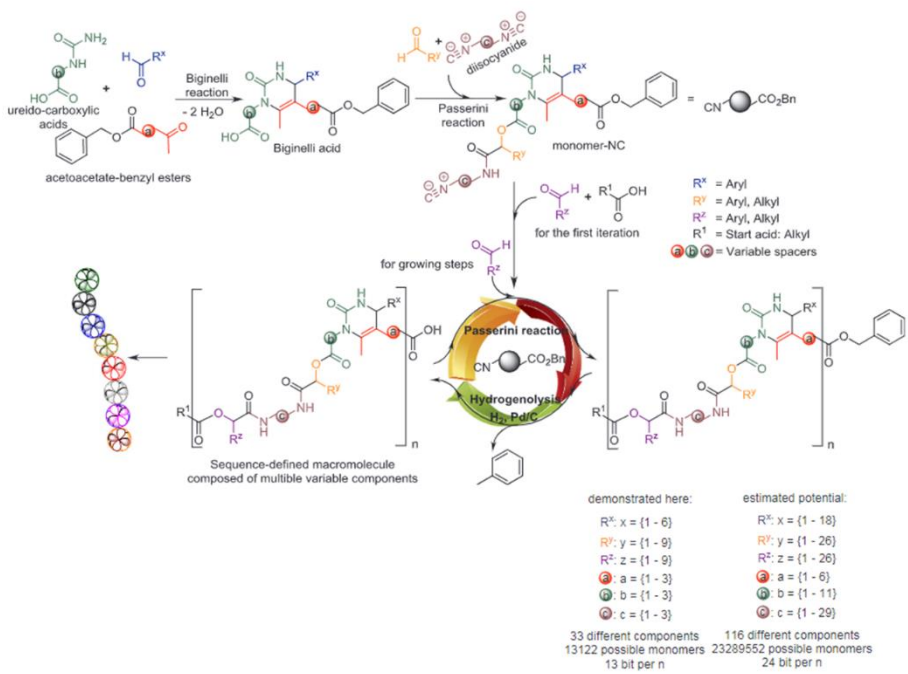

Figure 1-4. Schematic representation of the synthesis of sequence-defined macromolecules via the Biginelli and the Passerini multicomponent reactions. The variation of all components can potentially provide 24 bit per

repeating unit.[15]

The self-assembly of amphiphilic block copolymers is widely studied and has emerged as a versatile approach to form well-defined nanostructures.[16–19] This phenomenon is a result of the incompatibility between the hydrophilic and hydrophobic blocks, which separate to minimalize the interfacial energy. Controlling the molecular weights and molecular weight distributions of the constituting polymer blocks is significant for the regulation of the self-assembly behavior of block copolymers.[20–22] However, theoretical, and computational models often assume discrete block copolymers, instead of the disperse block copolymers which have the nature of the actual polymers used in experimental studies.[23,24] Therefore, these models do not reflect the actual behavior of block copolymers and do not consider variation that is derived from molecular weight distribution. Nevertheless, the continuous progress of the synthetic approach for sequence-defined polymers has nowadays enabled the scalable synthesis and study of discrete polymers.[25–28]

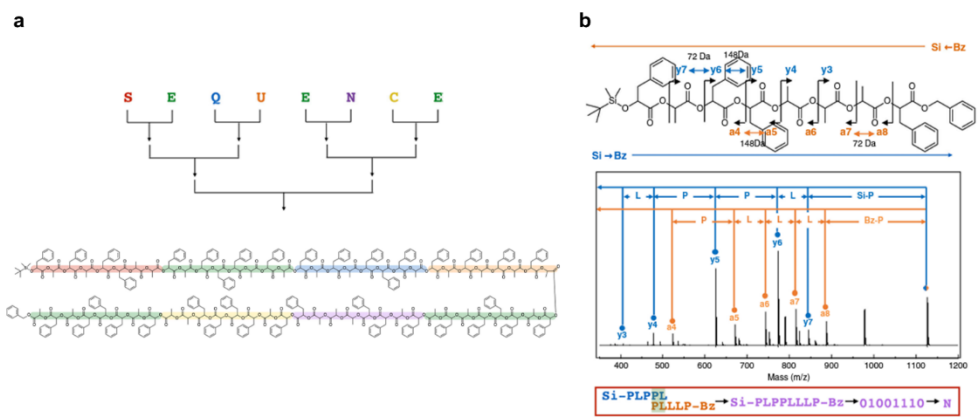

Figure 1-5. (a) PAH containing the 64-bit digital information encoding SEQUENCE. (b) MALDI-TOF MS/MS spectrum of a PAH, in which 8-bit information corresponding to the letter N was stored. Two series of

fragments (ai and yi fragments) could be read simultaneously in the spectrum. The PAH sequence was decoded by reading the spectrum in both directions relative to the molecular ion peak $[M+Na]^+$. The deciphered chemical sequence (Si-PLPPLLLP-Bz) was converted to digital code (01001110), which represented the letter N.[9]

Meijer et al. reported that the effect of dispersity on the self-assembly of dimethylsiloxane-lactic acid diblock copolymers and oligo(tetraethylene glycol)-poly(lactic acid)-oligo(tetraethylene glycol) ABA-type triblock copolymers.[29,30] Discrete oligodimethylsiloxane was synthesized by utilizing a new synthetic protocol, while the synthesis of discrete oligo(lactic acid) followed an established iterative synthesis. Ligation of these two blocks provided diblock co-oligomers with extremely low molar mass dispersities ($Đ \leq 1.00002$). Disperse diblock co-oligomers composed of dimethylsiloxane and lactic acid were previously examined, which showed a high incompatibility between the blocks. Compared with disperse diblock co-oligomers which did not indicate any clue for an ordered structure, extremely low disperse diblock co-oligomers exhibited sharp order–disorder transitions of phase-separated morphologies (Figure 1-6).[29] The importance of uniformity was demonstrated repeatedly when they investigated discrete ABA-type triblock copolymers. Isotactic L-lactic acid 16-mers were selected as the hydrophobic blocks and modified to couple with discrete oligo(tetraethylene glycol) at the both chain ends. Self-assembly of discrete ABA triblock copolymers showed uniform nanofibers and two-dimensional sheets, however such uniformity of assembled structures decreased when they used disperse oligomers for self-assembly.[30] Furthermore, sharp melt transitions and crystallization-driven gelation were found on discrete triblock copolymers.

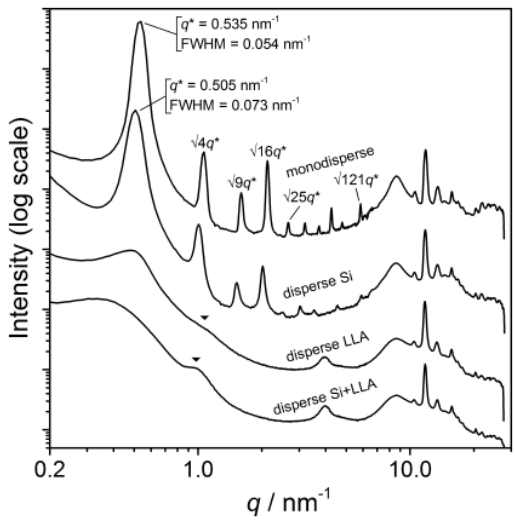

Figure 1-6. Room-temperature SAXS data for discrete and (partially) disperse oDMS-oLLA BCOs. The data are shifted vertically for clarity. Select higher order reflections are indicated as q/q* values or with black triangles. fwhm = full width at half-maximum. The broad peak at q = 4 nm^{-1} results from background scattering (Kapton tape).[29]

1.2 Crystallization-driven self-assmbly

The crystallization-driven self-assembly (CDSA) of block copolymers with a crystalline, core-forming block has aroused great attention due to the unique properties of two-dimensional (2D) planar structures that originate from very thin and flat morphology.[31–33] Uniform and stable 2D materials that have been widely used in organic electronics, membranes, and optical devices can be created by bottom-up assembly of block copolymers containing crystalline core-forming block.[34–36] Previosly, various crystalline blocks made of poly(ferrocenyl dimethylsilane),[37,38] enantiomeric poly(lactic acid),[39,40] poly(ε-caprolactone),[41] or poly(*p*-phenylenevinylene)[42] were used to prepare amphiphilic block copolymers that self-assemble into

2D polymeric nanosheets. These crystalline homopolymers were coupled with soluble corona blocks such as poly(ethylene glycol), poly(acrylic acid), or poly(2-vinylpyridine), which enhances the colloidal stability of the resulting 2D structures.

Manners et al. demonstrated that a wide range of polydisperse fiber-like micelles with crystalline core could be processed by seeded growth method.[37,38] Crystallizable seeds derived from the sonication of polydisperse micelles grow up by the addition of a solution of molecularly dissolved block copolymer with the crystalline core in a suitable organic solvent. This growth produces low dispersity fibers of a length controlled by the ratio of added block copolymer to seed. This method is termed "living" CDSA owing to the similarity between this process and living polymerizations. Futhermore, complex and hierarchical 2D nanoparticles could be formed via living CDSA using the sequential addition of different polymers (Figure 1-7).[43] Quasi-1D small seeds for complex and hierarchical assemblies were prepared by sonication of self-nucleated platelets. Then, the sequential addition of unimers and the polymer blend to the seeds produced diblock and tetra-block platelet co-micelles.

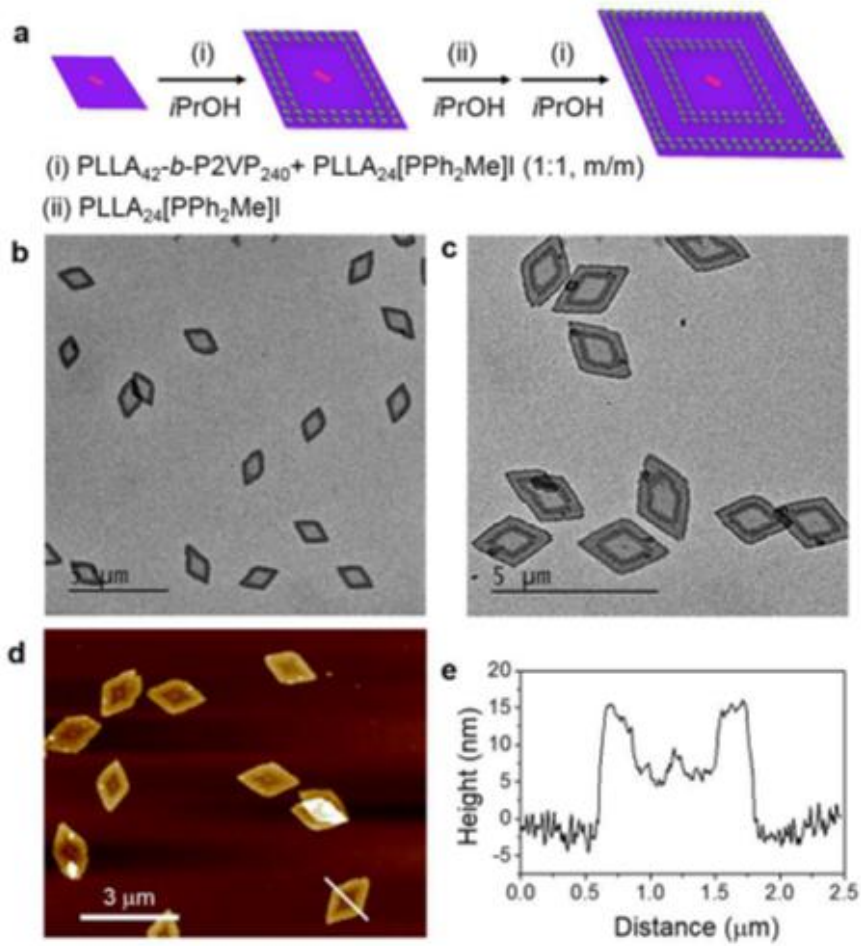

Figure 1-7. (a) Schematic representation of the formation of diamond-shaped "patchy" platelet block co-micelles through seeded growth. TEM images of (b) diblock and (c) tetra-block platelet co-micelles. The samples for TEM were not stained. (d) AFM image and (e) height profile of diblock platelet co-micelle.[43]

Choi et al. reported rapid formation and real-time observation of conjugated nanofibers by living CDSA.[44] Although the living CDSA has excellent controllability to morphology and uniformity, it generally takes several hours to days for well-defined nanostructures. To achieve the rapid

formation and real-time observation of nanostructures formed by living CDSA, they developed one-pot technique named Polymerization-Induced CDSA (PI-CDSA) and strategy termed *In situ* Nanoparticlization of Conjugated Polymers (INCP). They utilized seeded growth of fully conjugated block copolymers for spontaneous formation of nanostructures and retarded the fast aggregation by incorporating soluble dihexyl side chains. As a results, rapid formation of the long fibers with high rigidity and low width dispersities was observed using real-time monitoring (Figure 1-8).[44]

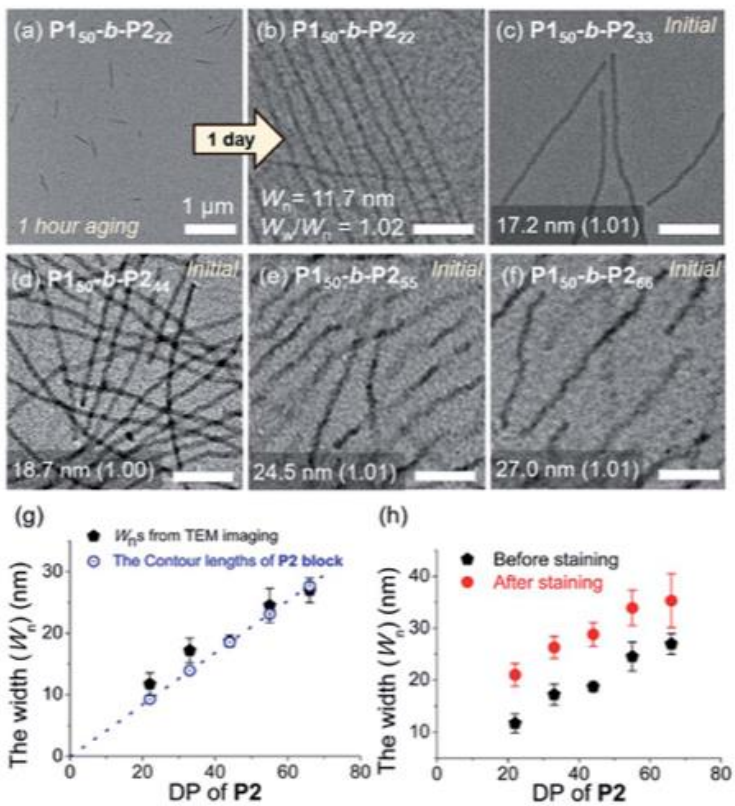

Figure 1-8. TEM images obtained from 1 g L^{-1} chloroform solutions of (a) P1$_{50}$-*b*-P2$_{22}$ after 1 h, and (b) after 1 d aging at 25 C, (c) P1$_{50}$-*b*-P2$_{33}$, (d) P1$_{50}$-*b*-P2$_{44}$, (e) P1$_{50}$-*b*-P2$_{55}$, and (f) P1$_{50}$-*b*-P2$_{66}$ without aging (scale bar for (b)–(f), 200 nm). Plots of the DP of P2 versus (g) average width (W_n) of the

core of the 1D nanofibers compared to the theoretical length of the fully stretched P2 block, and (h) W_n after staining with RuO_4 vapour.[44]

O'Reilly et al. used the stereocomplexation of isotactic poly(L-lactide) and poly(D-lactide) for the structural reorganization of nanoparticles.[45] Stereocomplexation is a general co-crystallization behavior between different polymers with complementary configurations.[46] Due to the unique structural characteristics of polymer stereocomplexes, stereocomplex crystallization endows the polymers with improved physical and mechanical properties. Co-crystallization of block copolymers consisting of complementary configurations led to morphological transitions induced by stereocomplexation (Figure 1-9).[45] Cylindrical micelles formed by self-assembly of each block copolymers were mixed and aged in CDSA condition. They observed a marked decrease in lengths of cylindrical micelles and increase in the number of spherical micelles, which demonstrated the ability to trigger the morphological transition through stereocomplexation.

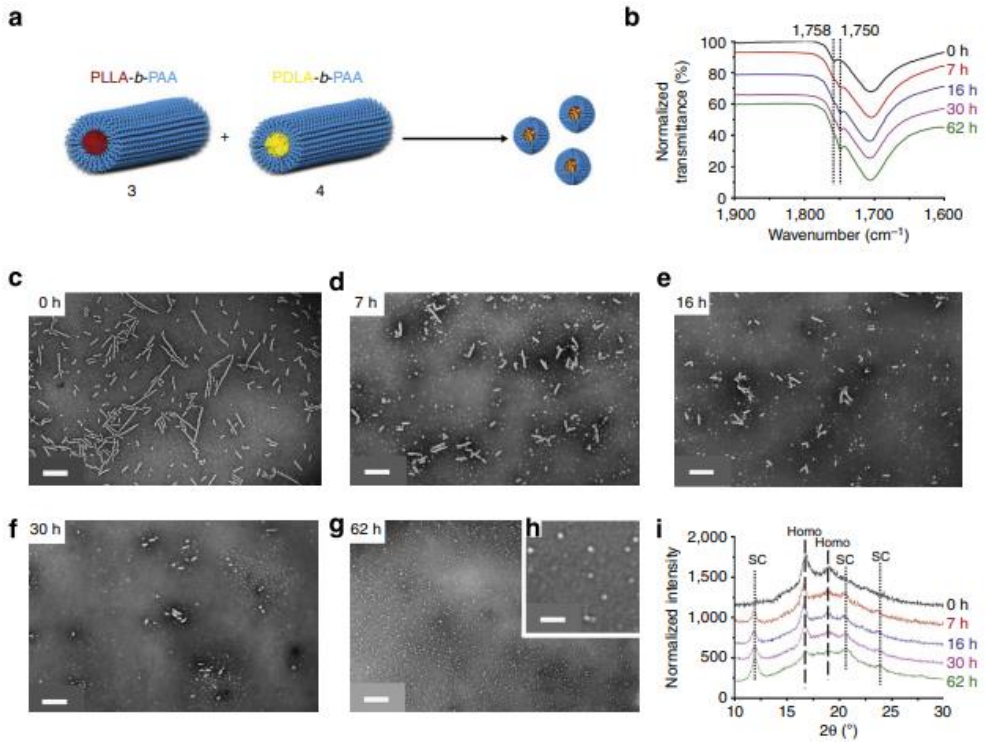

Figure 1-9. Morphological transition and the changes to the crystallinity on mixing of two homochiral cylinders 3 and 4. Conducted at 65 ºC with the addition of fresh THF (final solvent composition THF/H_2O 20/80 v/v). (a) Cartoon illustration showing the morphological transition from homochiral cylinders 3 and 4 to stereocomplex spheres. Scale bar = 500 nm (b) FT-IR spectra of dried nanoparticles, which reveal the wavenumber of carbonyl group vibration of poly(lactide) shifted from 1,758 to 1,750 cm^{-1} over time. Scale bar = 500 nm. (c–g) TEM images, which illustrate the length of the cylindrical micelles decreased while the population of spherical micelles increased over time. Scale bars = 500 nm. (h) TEM expansion of 62 h time point. Scale bar = 100 nm. (i) WAXD diffractograms illustrating that the intensity of stereocomplex Bragg peak at a 2θ value of 12º increased gradually, whereas the intensity of homochiral Bragg peak at a 2θ value of 16.6 º decreased significantly over time. TEM samples were prepared by

slow drying and negatively stained using PTA.[45]

1.3 Potential applications for crystallization-driven self-assembly

The living CDSA which provides ability to control the demensions and shape of nanostructures gives a potential advantage in biomedical applications.[47,48] Due to the different circulation times and uptake rates of polydisperse 1D fiber-like micelles, uniform nanostructures formed by living CDSA have emerged as promising candidates for nanomedicine.[49,50] Rigid rod-like micelles with uniform width and narrow length distribution prepared from living CDSA of a polyferrocenylsilane diblock copolymer showed that both shape and size were found to have a marked effect on cellular uptake and penetration into multicellular tumor spheroids formed by the same cell lines.[51] The highest cell-uptake and the deepest penetration into the tumor models were found in low dispersity fiber-like micelles with an elongated shape and short length.

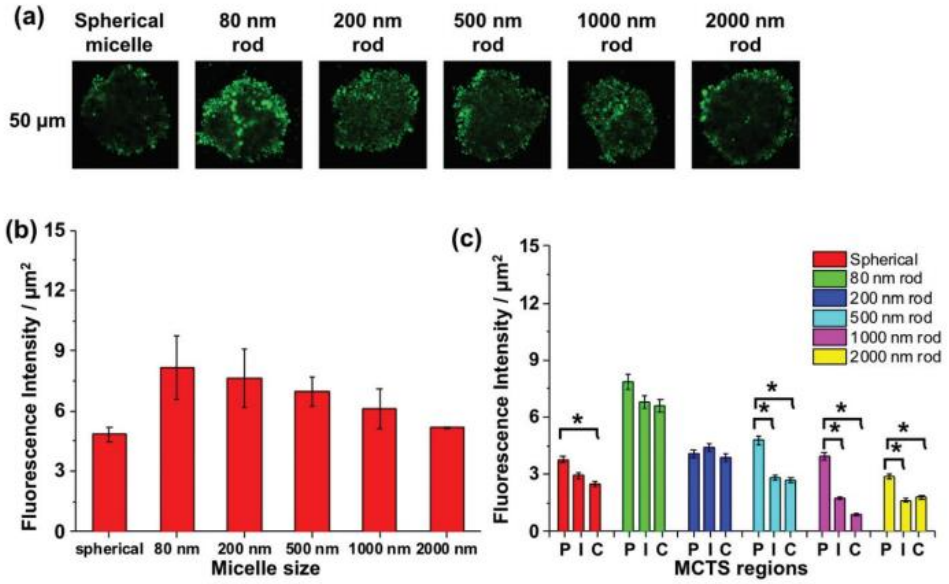

Figure 1-10. Assessment of micelle accumulation in MDA-MB-436 MCTSs using (a) confocal microscopy images taken at 50 µm depth from the spheroid surface. For MCTSs treated with spherical micelles and rod-like micelles with different lengths, (b) their total fluorescence intensities per unit area at cross-section were measured and compared. (c) Penetration of six different micelles in MCTS in periphery, intermediate and core regions at 50 µm depth. Data points represent mean ± standard deviation in each area, n = 3 MCTSs. Statistically significant differences between each region are denoted by (*), and in all cases $p < 0.05$.[51]

Conductive polymers have been widely used for photovoltaics, light-emitting devices, field-effect transistors and sensors.[52,53] The formation of uniform electroactive nanostructures with high colloidal stability, predetermined size, and spatially controlled functionality has been a major challenge.[54] The strong π–π interaction among conjugated polymers causes easy aggregation and disruption, which leads to uncontrolled self-assembly.

The living CDSA is a promising method to solve this problem. Segmented nanofibers with controlled dimensions were fabricated using the living CDSA of poly(3-(2'-ethylhexyl)thiophene) as energy-accepting outer core and poly(dihexylfluorene) as energy-donationg inner core.[55] It was demonstrated that Forster resonance energy transfer from the PDHF inner core to the lower energy P3EHT outer core was enhanced compared to the analogous coaxial structure in which the P3EHT block was solvated.

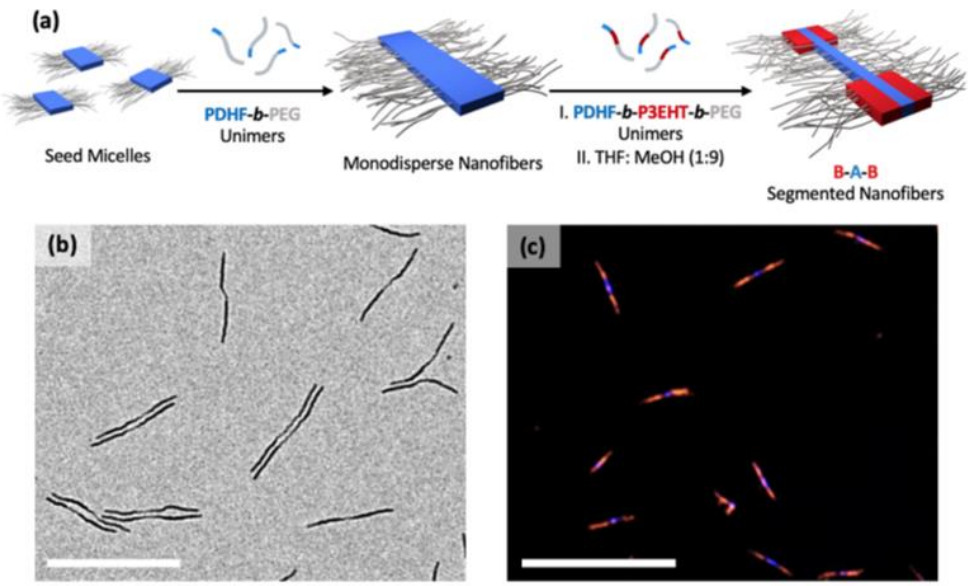

Figure 1-11. (a) Schematic illustration of the preparation of low dispersity B−A−B segmented nanofibers with a central $PDHF_{14}$-*b*-PEG_{227} segment (A) and terminal $PDHF_8$-*b*-$P3EHT_{25}$-*b*-PEG_{113} segments (B). (b) TEM image of B−A−B segmented nanofibers (L_n = 739 nm, L_w/L_n = 1.02) in THF:MeOH (1:9, v/v) prepared from the epitaxial growth of $PDHF_8$-*b*-$P3EHT_{25}$-*b*-PEG_{113} unimers from $PDHF_{14}$-*b*-PEG_{227} seed micelles (L_n = 247 nm, L_w/L_n = 1.04). (c) LCSM image of B−A−B segmented nanofibers (L_n = 3473 nm, L_w/L_n = 1.03) in THF:MeOH (1:9, v/v) prepared from the epitaxial growth of $PDHF_8$-*b*-$P3EHT_{25}$-*b*-PEG_{113} unimers from $PDHF_{14}$-*b*-PEG_{227} seed micelles (L_n = 972 nm, L_w/L_n = 1.02). LCSM image was taken with both

blue (PDHF) and red (P3EHT) channels. Scale bars: (b) 1 μm and (c) 10 μm.[55]

1.4 Summary of thesis

This dissertation reports the synthesis of discrete polymer and CDSA of crystalline block copolymers with a crystalline core-forming block. The existing limitation of the synthesis of discrete polymer was resolved through various synthetic strategies such as iterative exponential growth, cross-convergent method, and liquid phase support. These advances were applied to explore the unique properties of synthetic polymers with the absence of structural uncertainty. Living CDSA of various block copolymers having crystalline block have realized the formation of low-dimentional nanostructures with well-defined shape and size. This allowed for the potential use of uniform 2D nanostructures in the biomedical application and optoeletronics.

In Chapter 2, block copolymers composed of monodisperse poly(lactic acid)s (MPLA) with defined stereochemical sequences were synthesized using iterative convergent synthesis. The effect of a discrete number of units and stereochemical sequence on crystallites was investigated by CDSA of block copolymers with MPLA. This effect was more pronounced in the CDSA of a stereocomplex of a pair of BCPs with MPLA configured in a complementary manner. Unique nanostructures such as 2D triangles and vesicle-like structures were formed through incomplete stereocomplexation inducing regular nanostructures by attenuating crystallization kinetics.

In Chapter 3, a series of stereoblock copolymers were synthesized by

joining discrete oligo D- and L-lactic acid and poly(ethylene glycol) hydrophilic block. The thickness of 2D nanostructures could be controlled by the chain-folding of stereoblock copolymers via intramolecular stereocomplexation. To demonstrate the chain-folding of stereoblock copolymers, the insertion of a vinyl monomer in the middle of stereoblock was conducted. Apex labeling with fluorescein dye was proceeded by thiol-ene and isocyanate-amine reaction. Fluorescence on the surface of 2D nanostructures was confirmed through confocal microscopy.

In Chapter 4, stereoblock copolymers having a mismatch in lactic acid units were synthesized. This mismatch inducing incomplete stereocomplexation retarded crystallization of block copolymers, which lead to the formation of uniform triangular structures. Unlike previous strudies, micro-sized triangular structures were formed by intermolecular stereocomplexation. This is probably due to the stacking of stereocomplex. Extra D-lactic acids constituting mismatched streoblock copolymers contribute to stacking of streocomplex.

Excerpts from the following chapters have already been published:

Chapter 2: Kwon, Y.; Kim, K. T. Crystallization-Driven Self-Assembly of Block Copolymers Having Monodisperse Poly(lactic acid)s with Defined Stereochemical Sequences. *Macromolecules* **2021**, *54*, 10487–10498.

Chapter 3: Kwon, Y.; Ma, H.; Kim, K. T. Self-Assembly of Stereoblock Copolymers Driven by the Chain Folding of Discrete Poly(D-lactic acid-*b*-L-lactic acid) via Intramolecular Stereocomplexation. *Macromolecules* **2022**, *55,* 2768–2776.

1.5 References

1. Grubbs, R. B.; Grubbs, R. H. 50th Anniversary Perspective: Living Polymerization−Emphasizing the Molecule in Macromolecules. *Macromolecules* **2017**, *50*, 6979−6997.
2. Matyjaszewski, K.; Spanswick, J. Controlled/living radical polymerization. *Mater. Today* **2005,** *8*, 26−33.
3. Merrifield, R. B. Solid phase peptide synthesis. I. The synthesis of a tetrapeptide. *J. Am. Chem. Soc.* **1963,** *85,* 2149−2154.
4. Lutz, J.-F.; Ouchi, M.; Liu, D. R.; Sawamoto, M. Sequence-Controlled Polymers. *Science* **2013,** *341,* 1238149.
5. Aksakal, R.; Mertens, C.; Soete, M.; Badi, N.; Prez, F. D. Applications of Discrete Synthetic Macromolecules in Life and Materials Science: Recent and Future Trends. *Adv. Sci.* **2021,** *8,* 2004038.
6. Zhao, B.; Gao, Z.; Zheng, Y.; Gao, C. Scalable Synthesis of Positively Charged Sequence-Defined Functional Polymers. *J. Am. Chem. Soc.* **2019,** *141,* 4541−4546.
7. Dong, R.; Liu, R.; Gaffney, P. R. J.; Schaepertoens, M.; Marchetti, P.; Williams, C. M.; Chen, R.; Livingston, A. G. Sequence-defined multifunctional polyethers via liquid-phase synthesis with molecular sieving. *Nat. Chem.* **2019**, *11*, 136−145.
8. Takizawa, K.; Tang, C.; Hawker, C. J. Molecularly Defined Caprolactone Oligomers and Polymers: Synthesis and Characterization. *J. Am. Chem. Soc.* **2008,** *130,* 1718−1726.
9. Lee, J. M.; Koo, M. B.; Lee, S. W.; Lee, H.; Kwon, J.; Shim, Y. H.; Kim, S. Y.; Kim, K. T. High-Density Information Storage in an Absolutely Defined Aperiodic Sequence of Monodisperse Copolyester. *Nat. Commun.* **2020,** *11,* No. 56.

10. Zhirnov, V.; Zadegan, R. M.; Sandhu, G. S.; Church, G. M.; Hughes, W. L. Nucleic acid memory. *Nat. Mater.* **2016,** *15,* 366−370.
11. Rutten, M. G. T. A.; Vaandrager, F. W.; Elemans, J. A. A. W.; Nolte, R. J. M. Encoding information into polymers. *Nat. Rev. Chem.* **2018**, *2*, 365−381.
12. Erlich, Y.; Zielinski, D. DNA Fountain enables a robust and efficient storage architecture. *Science* **2017**, *355*, 950−954.
13. Azzarito, V.; Long, K.; Murphy, N. S.; Wilson, A. J. Inhibition of α-helix-mediated protein–protein interactions using designed molecules *Nat. Chem.* **2013**, *5*, 161−173.
14. Colquhoun, H.; Lutz, J.-F. Information-containing macromolecules. *Nat. Chem.* **2014,** *6,* 455−456.
15. Boukis, A. C.; Meier, M. A. R. Data storage in sequence-defined macromolecules via multicomponent reactions. *Eur. Polym. J.* **2018,** *104,* 32−38.
16. van Hest, J. C. M.; Delnoye, D. A. P.; Baars, M. H. P.; van Genderen, M. H. P. Meijer, E. W. Polystyrene-Dendrimer Amphiphilic Block Copolymers with a Generation-Dependent Aggregation. *Science* **1995**, *268*, 1592−1595.
17. Zhang, L.; Eisenberg, A. Multiple Morphologies of "Crew-Cut" Aggregates of Polystyrene-*b*-poly(acrylic acid) Block Copolymers. *Science* **1995,** *268*, 1728−1731.
18. Kim, K. T.; Meeuwissen, S. A.; Nolte, R. J. M.; van Hest, J. C. M. Smart nanocontainers and nanoreactors. *Nanoscale* **2010,** *2,* 844−858.
19. La, Y.; Park, C.; Shin, T. J.; Joo, S. H.; Kang, S.; Kim, K. T. Mesoporous monoliths of inverse bicontinuous cubic phases of block copolymer bilayers. *Nat. Chem.* **2014,** *6,* 534−541.
20. Terreau, O.; Luo, L.; Eisenberg, A. Effect of Poly(acrylic acid) Block Length Distribution on Polystyrene-b-Poly(acrylic acid) Aggregates in

Solution. 1. Vesicles. *Langmuir* **2003,** *19,* 5601–5607.

21. Doncom, K. E. B.; Blackman, L. D.; Wright, D. B.; Gibson, M. I.; O'Reilly, R. K. Dispersity effects in polymer self-assemblies: a matter of hierarchical control. *Chem. Soc. Rev.* **2017,** *46,* 4119–4134.
22. Ha, S.; La, Y.; Kim, K. T. Polymer Cubosomes: Infinite Cubic Mazes and Possibilities. *Acc. Chem. Res.* **2020,** *53,* 620–631.
23. Leibler, L. Theory of Microphase Separation in Block Copolymers. *Macromolecules* **1980,** *13,* 1602–1617.
24. Mai, Y.; Eisenberg, A. Self-assembly of block copolymers. *Chem. Soc. Rev.* **2012,** *41,* 5969–5985.
25. Hawker, C. J.; Malmström, E. E.; Frank, C. W.; Kampf, J. P. Exact Linear Analogs of Dendritic Polyether Macromolecules: Design, Synthesis, and Unique Properties. *J. Am. Chem. Soc.* **1997,** *119,* 9903–9904.
26. Takizawa, K.; Nulwala, H.; Hu, J.; Yoshinaga, K.; Hawker, C. J. Molecularly Defined (L)-Lactic Acid Oligomers and Polymers: Synthesis and Characterization. *J. Polym. Sci., Part A: Polym. Chem.* **2008,** *46,* 5977−5990.
27. French, A. C.; Thompson, A. L.; Davis, B. G. High-Purity Discrete PEG-Oligomer Crystals Allow Structural Insight. *Angew. Chem. Int. Ed.* **2009,** *48,* 1248–1252.
28. Koo, M. B.; Lee, S. W.; Lee, J. M.; Kim, K. T. Iterative Convergent Synthesis of Large Cyclic Polymers and Block Copolymers with Discrete Molecular Weights. *J. Am. Chem. Soc.* **2020,** *142,* 14028−14032.
29. Van Genabeek, B.; Lamers, B. A. G.; de Waal, B. F. M.; van Son, M. H. C.; Palmans, A. R. A.; Meijer, E. W. Amplifying (Im)perfection: The Impact of Crystallinity in Discrete and Disperse Block Co-oligomers. *J. Am. Chem. Soc.* **2017,** *139,* 14869–14872.

30. Das, A.; Petkau-Milroy, K.; Klerks, G.; B. van Genabeek, B.; Lafleur, R. P. M.; Palmans, A. R. A.; Meijer, E. W. Consequences of Dispersity on the Self-Assembly of ABA-Type Amphiphilic Block Co-Oligomers. *ACS Macro Lett.* **2018,** *7,* 546–550.
31. Zhang, X.; Xie, Y. Recent advances in free-standing two-dimensional crystals with atomic thickness: design, assembly and transfer strategies. *Chem. Soc. Rev.* **2013,** *42,* 8187–8199.
32. Boott, C. E.; Nazemi, A.; Manners, I. Synthetic covalent and non-covalent 2D materials. *Angew. Chem. Int. Ed.* **2015,** *54,* 13876–13894.
33. Zhuang, X.; Mai, Y.; Wu, D.; Zhang, F.; Feng, X. Two-dimensional soft nanomaterials: a fascinating world of materials. *Adv. Mater.* **2015,** *27,* 403–427.
34. Zeng, M.; Xiao, Y.; Liu, J.; Yang, K.; Fu, L. Exploring Two Dimensional Materials toward the Next-Generation Circuits: From Monomer Design to Assembly Control. *Chem. Rev.* **2018,** *118,* 6236−6296.
35. Zhuang, X.; Mai, Y.; Wu, D.; Zhang, F.; Feng, X. Two dimensional soft nanomaterials: a fascinating world of materials. *Adv. Mater.* **2015,** *27,* 403−427.
36. Wang, Z.; Jingjing, Q.; Wang, X.; Zhang, Z.; Chen, Y.; Huang, X.; Huang, W. Two-dimensional light-emitting materials: preparation, properties and applications. *Chem. Soc. Rev.* **2018,** *47,* 6128−6174.
37. Gilroy, J. B.; Gädt, T.; Whittell, G. R.; Chabanne, L.; Mitchels, J. M.; Richardson, R. M.; Winnik, M. A.; Manners, I. Monodisperse cylindrical micelles by crystallization-driven living self-assembly. *Nat. Chem.* **2010,** *2,* 566–570.
38. Hudson, Z. M.; Boott, C. E.; Robinson, M. E.; Rupar, P. A.; Winnik, M. A.; Manners, I. Tailored hierarchical micelle architectures using living

crystallization-driven self-assembly in two dimensions. *Nat. Chem.* **2014,** *6,* 893−898.

39. Kwon, Y.; Kim, K. T. Crystallization-Driven Self-Assembly of Block Copolymers Having Monodisperse Poly(lactic acid)s with Defined Stereochemical Sequences. *Macromolecules* **2021,** *54,* 10487−10498.
40. Kwon, Y.; Ma, H.; Kim, K. T. Self-Assembly of Stereoblock Copolymers Driven by the Chain Folding of Discrete Poly(D-lactic acid-*b*-L-lactic acid) via Intramolecular Stereocomplexation. *Macromolecules* **2022,** *55,* 2768−2776.
41. Ganda, S.; Dulle, M.; Drechsler, M.; Förster, B.; Förster, S.; Stenzel, M. H. Two-Dimensional Self-Assembled Structures of Highly Ordered Bioactive Crystalline-Based Block Copolymers. *Macromolecules* **2017,** *50,* 8544−8553.
42. Han, L.; Wang, M.; Jia, X.; Chen, W.; Qian, H.; He, F. Uniform two-dimensional square assemblies from conjugated block copolymers driven by π−π interactions with controllable sizes. *Nat. Commun.* **2018,** *9,* 865−877.
43. He, X.; He, Y.; Hsiao, M.-S.; Harniman, R. L.; Pearce, S.; Winnik, M. A.; Manners, I. Complex and Hierarchical 2D Assemblies via Crystallization-Driven Self-Assembly of Poly(L-lactide) Homopolymers with Charged Termini. *J. Am. Chem. Soc.* **2017,** *139,* 9221–9228.
44. Yang, S.; Choi, T.-L. Rapid formation and real-time observation of micron-sized conjugated nanofibers with tunable lengths and widths in 20 minutes by living crystallization-driven self-assembly. *Chem. Sci.* **2020,** *11,* 8416–8424.
45. Sun, L.; Pitto-Barry, A.; Kirby, N.; Schiller, T. L.; Sanchez, A. M.; Dyson, M. A.; Sloan, J.; Wilson, N. R.; O'Reilly, R. K.; Dove, A. P. Structural reorganization of cylindrical nanoparticles triggered by

polylactide stereocomplexation. *Nat. Commun.* **2014,** *5,* 5746.

46. Xie, Q.; Yu, C.; Pan, P. In *Crystallization in Multiphase Polymer Systems;* Thomas, S.; Arif P, M.; Gowd, E. B.; Kalarikkal, N.; Eds.; Elsevier: 2018; Chapter 17, pp 535−573.
47. Yu, W.; Liu, R.; Zhou, Y.; Gao, H. Size-Tunable Strategies for a Tumor Targeted Drug Delivery System. *ACS Cent. Sci.* **2020,** *6,* 100–116.
48. Jiang, W.; Kim, B. Y. S.; Rutka, J. T.; Chan, W. C. W. Nanoparticle-mediated cellular response is size-dependent. *Nat. Nanotechnol.* **2008,** *3,* 145–150.
49. Geng, Y.; Dalhaimer, P.; Cai, S.; Tsai, R.; Tewari, M.; Minko, T.; Discher, D. E. Shape effects of filaments versus spherical particles in flow and drug delivery. *Nat. Nanotechnol.* **2007,** *2,* 249–255.
50. Zhao, J.; Lu, H.; Xiao, P.; Stenzel, M. H. Cellular Uptake and Movement in 2D and 3D Multicellular Breast Cancer Models of Fructose-Based Cylindrical Micelles That Is Dependent on the Rod Length. *ACS Appl. Mater. Interfaces* **2016,** *8,* 16622–16630.
51. Yu, Q.; Roberts, M. G.; Houdaihed, L.; Liu, Y.; Ho, K.; Walker, G.; Allen, C.; Reilly, R. M.; Manners, I.; Winnik, M. A. Investigating the influence of block copolymer micelle length on cellular uptake and penetration in a multicellular tumor spheroid model. *Nanoscale* **2021,** *13,* 280–291.
52. Li, X.; Wang, X.; Zhang, L.; Lee, S.; Dai, H. Chemically Derived, Ultrasmooth Graphene Nanoribbon Semiconductors. *Science* **2008,** *319,* 1229–1232.
53. Grimsdale, A. C.; Chan, K. L.; Martin, R. E.; Jokisz, P. G.; Holmes, A. B. Synthesis of Light-Emitting Conjugated Polymers for Applications in Electroluminescent Devices. *Chem. Rev.* **2009,** *109,* 897–1091.
54. MacFarlane, L. R.; Shaikh, H.; Garcia-Hernandez, J. D.; Vespa, M.; Fukui, T.; Manners, I. Functional nanoparticles through π-conjugated

polymer self-assembly. *Nat. Rev. Mater.* **2020,** *6,* 7–26.

55. Shaikh, H.; Jin, X.-H.; Harniman, R. L.; Richardson, R. M.; Whittell, G. R.; Manners, I. Solid-State Donor−Acceptor Coaxial Heterojunction Nanowires via Living Crystallization-Driven Self-Assembly. *J. Am. Chem. Soc.* **2020,** *142,* 13469–13480.

Chapter 2. Crystallization-Driven Self-Assembly of Block Copolymers having Monodisperse Poly(lactic acid)s with Defined Stereochemical Sequences

2.1 Abstract

Monodisperse polymers composed of a discrete number of repeating units have attracted considerable interest as model systems to investigate the behavior of polymers having chemical structures without statistical distribution. Herein, we report the crystallization-driven self-assembly (CDSA) of block copolymers (BCPs) built with monodisperse poly(lactic acid) (MPLA) composed of enantiomeric repeating units connected in a defined sequence and poly(ethylene glycol) (PEG). The morphology of self-assembled nanostructures was transformed by a systematic change in the number and the sequence of enantiomeric lactic acid units of MPLA blocks. This effect was more pronounced in the CDSA of a stereocomplex (SC) of a pair of BCPs having MPLA blocks configured in a complementary manner. When the size of the MPLA blocks was mismatched, a pair of the consequent BCPs self-assembled into nanostructures from nanoparticles to two-dimensional (2D) triangles and vesicles. In addition, on mismatching the stereochemical sequences of MPLA blocks forming the SC, the nanostructures of a BCP pair exhibited a transition from ill-defined structures to 2D triangular structures. Our results suggest that the low-dimensional nanostructures created by the crystallization of MPLA-b-PEG could be manipulated by their precisely defined molecular weight and stereochemical sequences.

2.2 Introduction

The molecular weights, molecular weight distributions, and the sequences of monomers are key determinants of the properties of synthetic polymers and copolymers.[1–3] However, unlike biopolymers such as DNA and proteins, synthetic polymers exhibit statistical distribution in their molecular weights and often exhibit randomness in the sequence of monomers. Inspired by the biological functions arising from the well-defined chemical structures of biopolymers, the synthesis of polymers without molecular weight distribution and sequence uncertainty has been pursued extensively in polymer chemistry. The synthesis of monodisperse polymers has relied mostly on the sequential addition of individual monomers via solid-phase synthesis.[4–6] However, with the increase in molecular weight or number of repeating units, their synthesis becomes difficult, which limits the availability of monodisperse polymers and the study of their properties.[7–10] Recent developments of synthetic strategies including the iterative exponential growth and the cross-convergent synthesis have allowed the synthesis of high molecular-weight monodisperse polymers with defined sequences.[11–16] These advances have provided the opportunities to study the behavior of synthetic polymers with defined sequences and absence of structural uncertainty.[17–19] Furthermore, monodisperse and sequence-defined polymers offer the opportunity to explore unprecedented applications of the polymeric materials owing to the precisely defined chemical and physical properties dictated by their chemical structures.[20–22]

The self-assembly of amphiphilic block copolymers (BCPs) is a phenomenon in which controlling the molecular weights and molecular weight distributions of the constituting polymer blocks is significant for the regulation of the self-assembly behavior of BCPs.[23–26] For example, the

molecular weights of the polymer blocks and the molecular weight ratios of these blocks determine the size and morphology of the self-assembled BCP structures. It was demonstrated that the magnitude of molecular weight distribution of a BCP imposes an adverse effect on the formation of well-defined nanostructures via self-assembly.[27,28]

Particularly, the crystallization-driven self-assembly (CDSA) of BCPs having a core-forming crystalline block in solution is of great interest as the crystallization of core-forming polymers require a precise control of their stereochemical structures, molecular weights, and molecular weight distributions. Controlled polymerization methods such as living ring-opening polymerization (ROP) have been employed to synthesize BCPs with well-defined crystalline polymer blocks such as polyferrocenylsilane (PFS),[29–31] poly(lactic acid) (PLA),[32–40] and conjugated polymers.[41–43] Low dimensional nanostructures with well-defined size, shape, and functions have been realized by living CDSA of various BCPs.[44–46] However, the CDSA of BCPs built with monodisperse polymer blocks and the effects of the absence of molecular weight distribution (in the crystal-forming polymer block) on its self-assembly has only been recently investigated.[47,48] Significantly, the contribution of the stereochemical sequence of the core-forming polymer block to the shape of nanostructures formed by CDSA has not been investigated.

Here we report the synthesis of monodisperse poly(lactic acid) (MPLAs) consisting of a discrete number of enantiomeric monomers linked in a pre-defined sequence. An iterative convergent approach with orthogonally protected dimers of enantiopure L-lactic acid or D-lactic acid, as building blocks, was applied to synthesize MPLAs with configured molecular weight and stereochemical sequences composed of ~72 repeating units. The resulting MPLAs ($Đ$ = 1) were coupled to poly(ethylene glycol)

(PEG) (M_n = 2 kDa, $Đ$ = 1.04) to yield MPLA-*b*-PEG that could self-assemble in ethanol (EtOH) via the crystallization of core-forming MPLA blocks. The analysis of the height profiles of self-assembled structures using atomic force microscopy (AFM) suggested that enantiopure MPLAs fold at ~ 32 repeating units to form crystallites in the core of two-dimensional (2D) nanostructures created by CDSA of BCPs in EtOH (Figure 2-1a). The morphology of the 2D nanostructures of MPLA-*b*-PEG was transformed by changing the number of repeating units and the sequence of enantiomeric repeating units in the MPLA block (Figure 2-1a). The CDSA of a stereocomplex (SC) of a BCP pair composed of complementarily configured MPLA blocks, poly(D-lactic acid)-*b*-poly(ethylene glycol) ([DLA_n]-*b*-PEG) and poly(L-lactic acid)-*b*-PEG ([LLA_n]-*b*-PEG) produced 2D nanostructures. The effects of the number of enantiomeric repeating units and their sequences on the morphology of the self-assembled structures were more pronounced in CDSA of the SCs. Particularly, the morphology of the 2D nanostructures formed by CDSA of BCP pairs transformed from irregular structures to triangular platelets and vesicles when there was an increase in the size mismatch between enantiomeric MPLA blocks forming the SC (Figure 2-1b). This effect of the mismatch in the number of D- and L-lactic acid in the MPLA pair was also found when two MPLAs possessed the same number of repeating units but different stereochemical sequences (Figure 2-1b). The results suggested that the shape of low-dimensional nanostructures created by the crystallization of discrete polymers could be manipulated by their precisely defined stereochemical sequences.

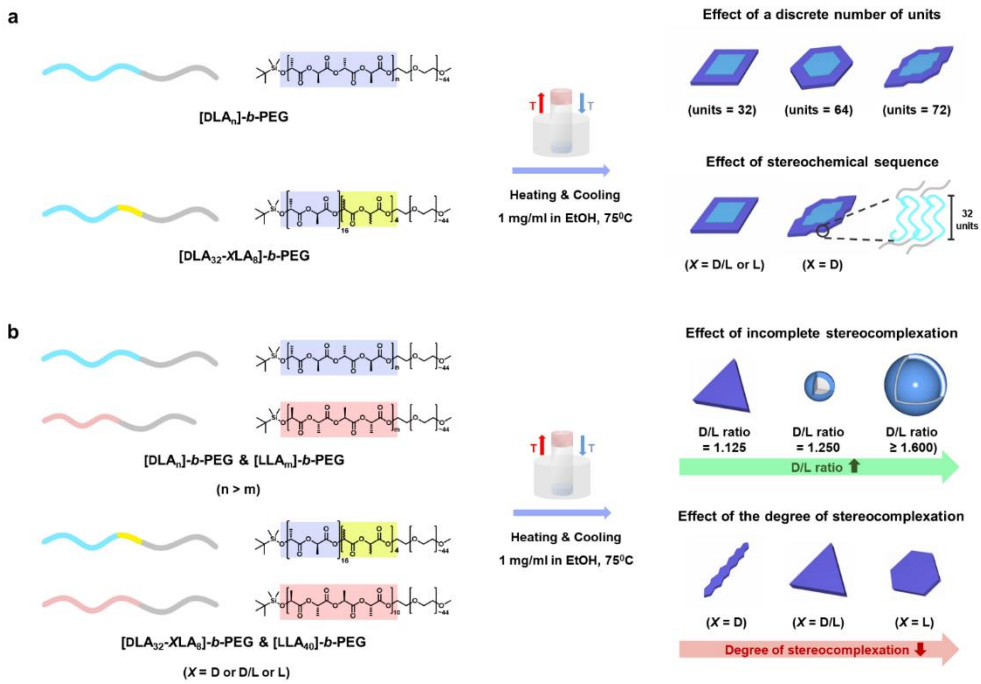

Figure 2-1. Schematic representation of the formation of various nanostructures through crystallization-driven self-assembly. (a) CDSA of BCPs with a discrete number of repeating units and stereochemical sequence of MPLA blocks and resulting 2D nanostructures. (b) CDSA of the SCs of a pair of BCPs having a mismatch in the size and stereochemical sequence of MPLA blocks and assembled structures.

2.3 Results and discussion

Synthesis of BCPs having MPLA with defined stereochemical sequences. Enantiopure MPLAs, poly(L-lactic acid) [LLA_n], and poly(D-lactic acid) [DLA_n] comprising 32 or 64 repeating units were synthesized by the iterative convergence of enantiomeric lactic acid dimers [LLA_2] or [DLA_2] having t-butyldimethylsilyl (TBDMS) and benzyl ester (Bn) protecting groups as building blocks.[13] The orthogonal deprotection of each

protecting group and the subsequent esterification of deprotected [LA_2]-OH and [LA_2]-COOH with 1-ethyl-3-(3- dimethylaminopropyl)carbodiimide (EDC) yielded a tetramer of lactic acid having the same protecting groups. The repetitions of these convergent steps produced MPLAs composed of the desired number of repeating units (Scheme 2-1).

Scheme 2-1. Iterative convergent syntheses of [DLA_{32}-*x*LA_8]-*b*-PEG and [DLA_{72}]-*b*-PEG.

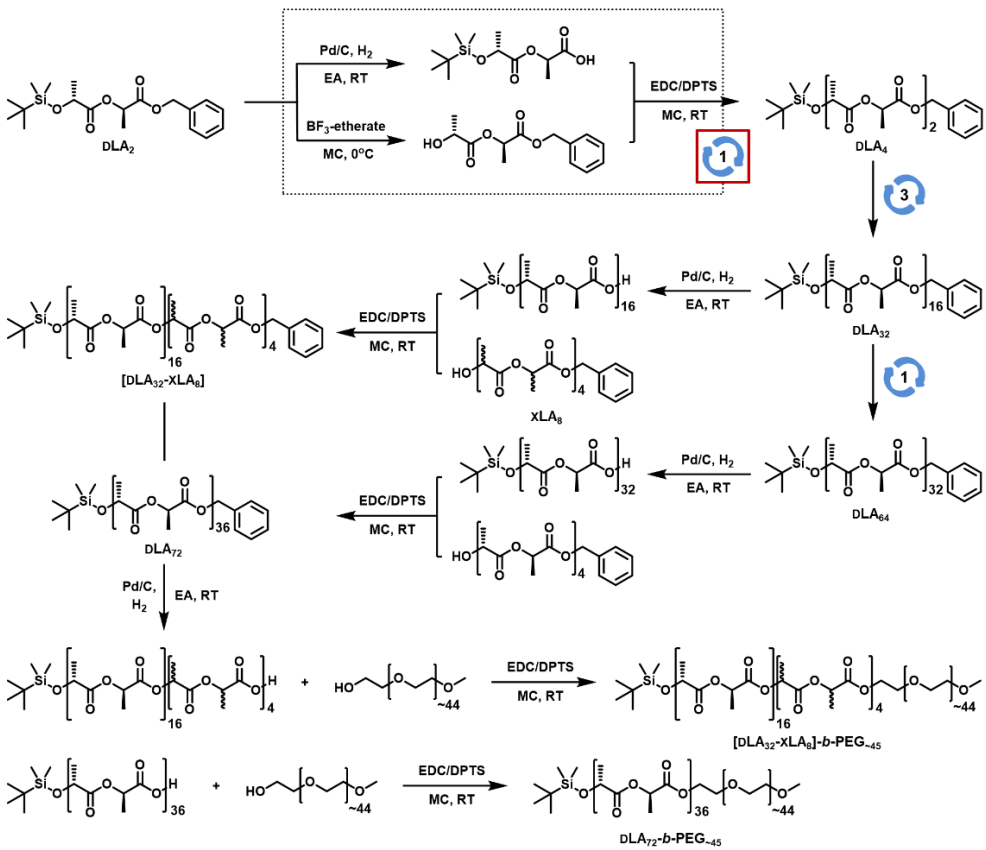

The enantiopure [LA_{40}] and [LA_{72}] were synthesized by the coupling of [LA_{32}] or [LA_{64}] with [LA_8] having the same stereochemical configuration in the final convergent step. Similarly, MPLAs with terminal

octameric residues and different stereochemical sequences such as [DLA_{32}-D/LLA_8] and [DLA_{32}-LLA_8] at the carboxy-terminus (*C*-terminus) were synthesized using an octameric building block having a desired stereochemical arrangement. All synthesized MPLAs were purified by preparative size-exclusion chromatography (prep-SEC) running on a commercially available recycling prep-SEC instrument equipped with large-capacity columns, which yielded pure MPLAs in a multi-gram quantity. The purities of MPLAs and BCPs were verified by ^{1}H and ^{13}C NMR, analytical SEC, differential scanning calorimetry (DSC) and matrix-assisted laser desorption ionization-time of flight (MALDI-TOF) mass spectrometry (Figure 2-2, S1–19). The *C*-terminus of the MPLA was subsequently exposed via Pd-catalyzed hydrogenation for esterification with mono-methoxy PEG (PEG, M_n = 2 kDa, $Đ$ = 1.04), resulting in a series of amphiphilic BCPs ([LA_n]-*b*-PEG), having stereospecific MPLAs as core-forming crystalline polymer blocks (Table 2-1). We assumed that the presence of PEG ($Đ$ = 1.04) as a solvent-soluble block would have a minimal influence on the CDSA of the resulting BCP because the driving force of CDSA should be the crystallization of the core-forming MPLA blocks. Therefore, a small change in the molecular weight ratios between PEG and MPLA blocks originating from the molecular weight distributions of PEG should have negligible influence on the morphology of nanostructures formed by CDSA.

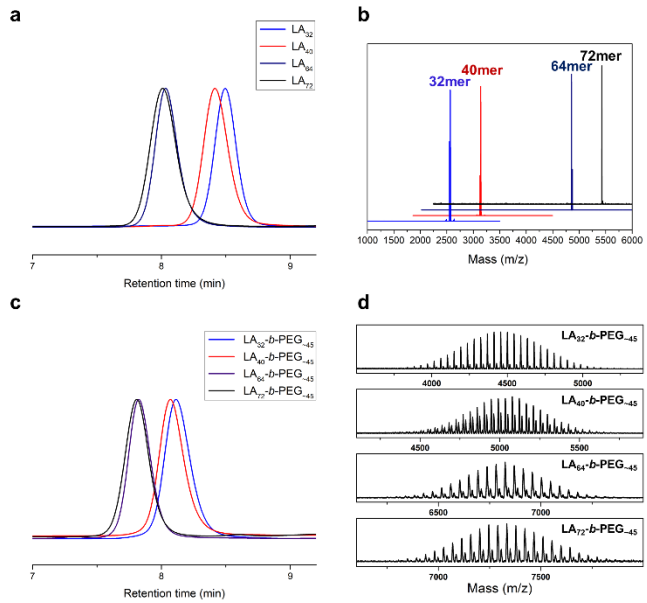

Figure 2-2. (a) Gel-permeation chromatography (GPC) analysis of [LA_n] (b) Combined MALDI-TOF mass spectra of MPLA. (c) GPC analysis of [LA_n]-*b*-PEG. (d) Combined MALDI-TOF mass spectra of [LA_n]-*b*-PEG.

CDSA of [LA_n]-*b*-PEG. A series of BCPs containing MPLA as a crystallizable core-forming block and PEG as a solvent-selective block ([LA_n]-*b*-PEG) was allowed to form nanostructures by CDSA in EtOH. In a typical procedure, [LA_n]-*b*-PEG was molecularly dissolved in EtOH (1 mg/mL) at 75 °C, followed by a slow cooling and equilibration at 25 °C without perturbation for 24 h. The resulting solution was diluted with water (0.1 mg/mL) and equilibrated at 25 °C for 4 h. This diluted solution was studied by transmission electron microscopy (TEM), AFM, and dynamic light scattering (DLS). Due to the low electron density of [LA_n]-*b*-PEG, TEM grids were stained with phosphortungstic acid (1% in water).[39]

We investigated the morphology of the [DLA_{32}]-*b*-PEG nanostructures formed by CDSA. The TEM images obtained from the diluted solution of [DLA_{32}]-*b*-PEG after CDSA exhibited the formation of 2D diamond-shaped

(lozenge) crystallites (Figure 2-3a, S20), which resulted from the crystallization of MPLA blocks forming the core of the 2D structure. While the previous study showed vesicular structures, cylindrical and spherical micelles were formed by the self-assembly of oligoLLA$_{16}$-*b*-oligoEG$_{11,17,48}$, the 2D structures formed possibly due to the longer chain length of PLA and different self-assembly conditions.[48] We estimated the thickness of BCP crystallites on a silicon substrate using height profiles from the AFM images of the nanostructures recorded in a contact mode. The height profiles obtained from the AFM images of diamond-shaped structures of [DLA$_{32}$]-*b*-PEG showed that the edges of 2D platelets were ~ 10 nm high and the central part was ~16 nm high from the silicon substrate (Figure 2-3c,e). The MPLA folded at ~ 32 repeating units (~ 9.5 nm) to form a crystalline domain in bulk,[13,49] which suggested that the edges of 2D diamond-shaped structures were composed of a crystalline core consisting of stretched [DLA$_{32}$] blocks without chain folding. The AFM images of the EtOH solution of [DLA$_{32}$]-*b*-PEG before the dilution with water showed 2D diamond crystallites composed of a single layer (Figure S21a,c), suggesting that the epitaxial growth of an additional layer on the 3D diamonds (Figure 2-3) could be promoted by the dilution of the EtOH solution of the BCP with water.

Table 2-1. Characteristics of [LA_n]-*b*-PEG block copolymers

Entry	BCP	M_{exp}^{LA} (Da)[a]	M_n^{BCP} (Da)[a]	M_n^{BCP} (Da)[b]	$Đ^b$
1	[DLA_{32}]-*b*-PEG	2550.8	4431.3	7810	1.03
2	[LLA_{32}]-*b*-PEG	2550.8	4432.1	7840	1.03
3	[DLA_{40}]-*b*-PEG	3126.0	5040.5	8420	1.03
4	[DLA_{32}-D/LLA_8]-*b*-PEG	3126.0	5038.7	8510	1.02
5	[DLA_{32}-LLA_8]-*b*-PEG	3126.0	5033.2	8280	1.03
6	[LLA_{40}]-*b*-PEG	3126.0	5048.2	8460	1.03
7	[DLA_{64}]-*b*-PEG	4855.2	6815.5	12940	1.02
8	[LLA_{64}]-*b*-PEG	4855.2	6810.9	12770	1.03
9	[DLA_{72}]-*b*-PEG	5434.6	7330.0	13330	1.02

[a]Isotopic mass $[M+Na]^+$ of MPLAs including protecting groups (TBDMS and Bn) and number average molecular weight (M_n^{BCP}) determined by MALDI-TOF. [b]Number average molecular weight (M_n^{BCP}) and dispersity ($Đ$) determined by GPC using polystyrene (PS) standards. Elution was performed with THF at a flow rate of 1 mL/min at 25 °C.

To confirm the folding of MPLA at ~ 32 repeating units in the crystalline domain, we fabricated self-assembled BCPs having higher molecular weight MPLA block i.e., [DLA_{64}]-*b*-PEG. Truncated diamond crystallites were observed on examining the CDSA results of [DLA_{64}]-*b*-PEG obtained using TEM under the same experimental conditions (Figure 2-3b, S22). Lozenge and truncated-shaped crystals were determined by comparing the growth rates along (110) planes and (200) planes.[50] When the

length of the [DLA_n] block increased, the growth rate along (110) decreased, which resulted in the truncated crystals. The AFM images of the self-assembled 2D structures of [DLA_{64}]-*b*-PEG conformed with the morphology of the nanostructures observed using TEM (Figure 2-3d). The height profiles of the edges of crystallites confirmed the thicknesses of the nanostructures to be 9–10 nm even when the number of repeating units in MPLA block were twice as compared with that of [DLA_{32}] (Figure 2-3f). This observation confirmed that the MPLA block folded at 32 repeating units to form the crystalline domain of the 2D nanostructure in the solution. The higher height of central part (~14 nm) was not observed when the AFM images were obtained from the EtOH solution of [DLA_{64}]-*b*-PEG without dilution (Figure S21b,d).

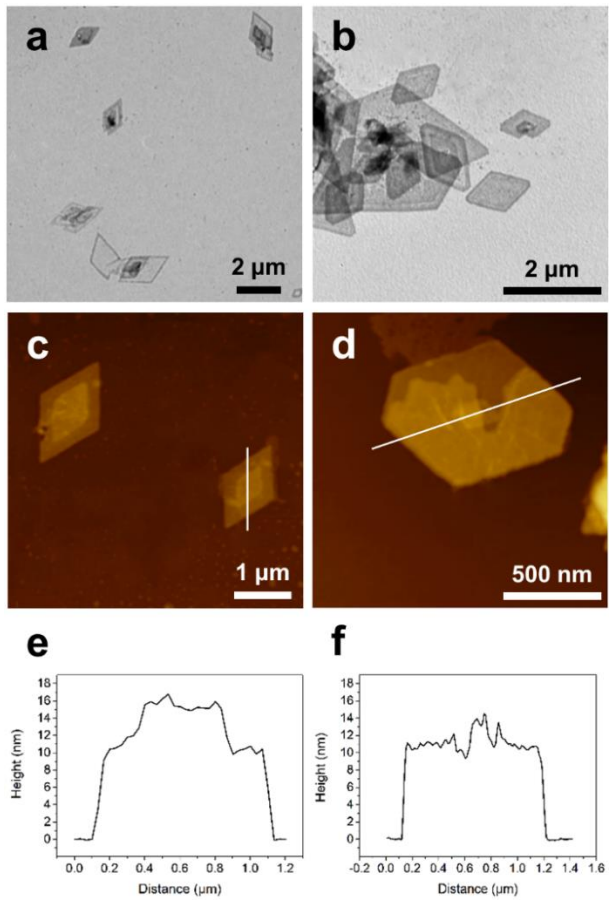

Figure 2-3. 2D nanostructures obtained from the CDSA of [DLA_{32n}]-*b*-PEG (n = 1, 2). (a,b) TEM images (c–f) AFM images, and height profiles of diamond- and truncated diamond crystallites. (a,c,e) [DLA_{32}]-*b*-PEG. (b,d,f) [DLA_{64}]-*b*-PEG. TEM samples were stained with a 1 wt% solution of phosphortungstic acid in water.

Effects of the stereochemical sequence of an MPLA block on CDSA. When the number of repeating units of the MPLA block increased from 32 to 40, the resulting BCP, [DLA_{40}]-*b*- PEG self-assembled to leaf-like crystallites deviating from the lozenge crystallite structure under the same CDSA condition (Figure 2-4a,e, S23). Similar leaf-shaped 2D nanostructures were also observed from the CDSA of [DLA_{72}]-*b*-PEG

(Figure 2-4b,f, S24). Measured by the height profiles of AFM images, these nanostructures possessed a thickness of ~ 10 nm for the edges of crystallites (Figure 2-4i,j). These results indicated that the further chain length attached to the [DLA_{32}] or [DLA_{64}] did not affect significantly the thicknesses of crystallites and the chain folded at ~ 32-repeating unit.[13,49] Based on these results, we assumed that the presence of additional D-lactic acid units participated in the crystallization of [DLA_{32}] blocks and resulted in the deviation of the shape of crystallites from lozenge to leaf-like structures. In case of [DLA_{72}]-*b*-PEG, the chain folding of [DLA_{72}] could produce the terminal segment composed of eight D-lactic acid units that might interfere with the crystallization of 32-repeating unit MPLA segments. This interference of the terminal residues could cause shape-irregularity of the [DLA_{72}]-*b*-PEG crystallites.

To investigate the effects of the additional repeating units on the crystallization of MPLA blocks, we inspected the CDSA results of the [DLA_{32}-D/LLA_8]-*b*-PEG having an octamer of rac-lactic acid at the C-terminus and the [DLA_{32}-LLA_8]-*b*-PEG having a repeating sequence comprising eight L-lactic acid units at the same position. The octamers of D/L-lactic acid or L-lactic acid were introduced because they did not exhibit any crystallization in bulk or solution,[49] and therefore, likely do not interfere in the crystallization of [DLA_{32}] domains. Under identical CDSA conditions, [DLA_{32}-D/LLA_8]-*b*-PEG and [DLA_{32}-LLA_8]-*b*-PEG only formed diamond-shaped 2D structures, which coincided with the lozenge platelets observed from the CDSA of [DLA_{32}]-*b*-PEG (Figure 2-4c,d,g,h, S25,26). The height profiles of the AFM images of these structures confirmed that the edges of lozenge structures were ~ 10 nm thick, indicating the formation of a crystalline domain by the packing of the unfolded [DLA_{32}] (Figure 2-4k,l).

This morphological resemblance among the nanostructures of [DLA_{32}]-*b*-PEG, [DLA_{32}-D/LLA_8]-*b*-PEG, and [DLA_{32}-LLA_8]-*b*-PEG led to the assumptions that the formation of the crystalline domain of the BCP was mainly affected by the long isotactic domain of the core-forming [DLA_{32}] block and that the terminal segment with opposite or randomized stereochemical sequence located at the C-terminus of MPLA block did not participate in the formation of the crystallites. The latter assumption was partly supported by the crystallization temperatures (T_c) of a series of BCPs having [LA_{40}] blocks of different stereochemical sequences measured using DSC. The crystallization temperature (T_c) of [DLA_{32}-*x*LA_8]-*b*-PEG (*x* = D, L, or D/L) increased proportionally with the number of D-lactic acids comprising the backbone (Figure 2-5). When the stereochemical structure of eight residues at the *C*-terminus was altered from the isotactic to the racemic arrangement, the T_c of the resulting BCP decreased from 106.5 °C for [DLA_{40}]-*b*-PEG to 96.4 °C for [DLA_{32}-D/LLA_8]-*b*-PEG. When the terminal segment was composed of eight L-lactic acid [LLA_8] units, the T_c of [DLA_{32}-LLA_8]-*b*-PEG was 93.6 °C which was close to the T_c of [DLA_{32}]-*b*-PEG (89.8 °C), indicating that the terminal segment with modulated stereoregularity did not contribute to the formation of MPLA crystals.

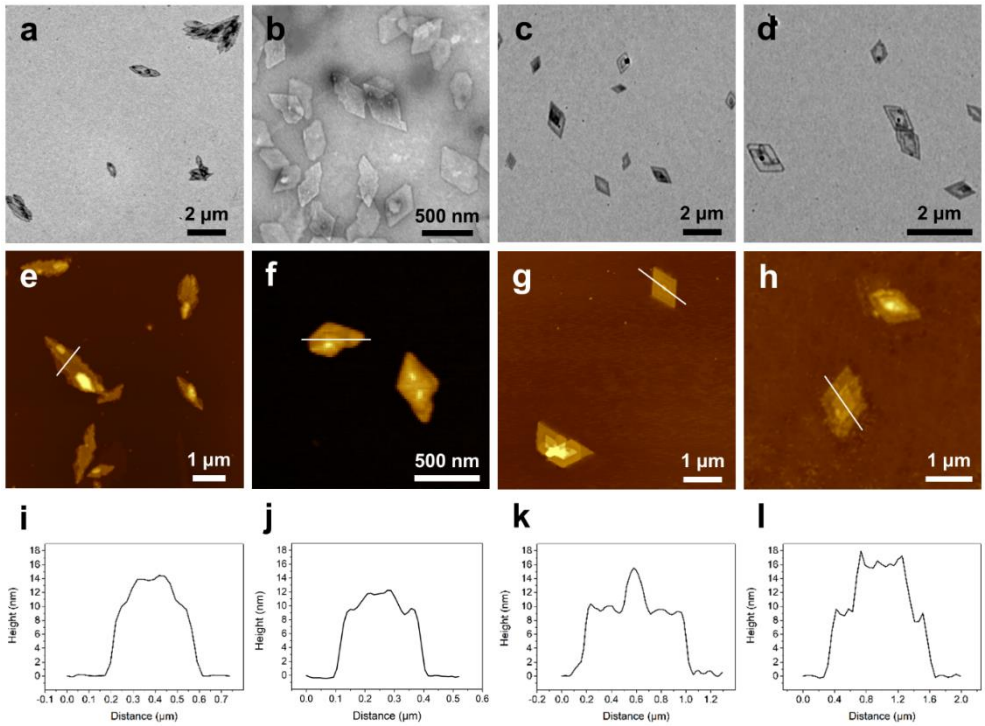

Figure 2-4. 2D crystallites with different shapes formed by the CDSA of diblock copolymers [DLA_{32}-*x*LA_8]-*b*-PEG (*x* = D, L, or D/L) or [DLA_{72}]-*b*-PEG. (a–d) TEM images, (e–h) AFM images, and (i–l) height profiles of leaf- and diamond-shaped crystallites. (a,e,i) [DLA_{40}]-*b*-PEG. (b,f,j) [DLA_{72}]-*b*-PEG. (c,g,k) [DLA_{32}-D/LLA_8]-*b*-PEG. (d,h,l) [DLA_{32}-LLA_8]-*b*-PEG. TEM samples were stained with a 1 wt% solution of phosphortungstic acid in water.

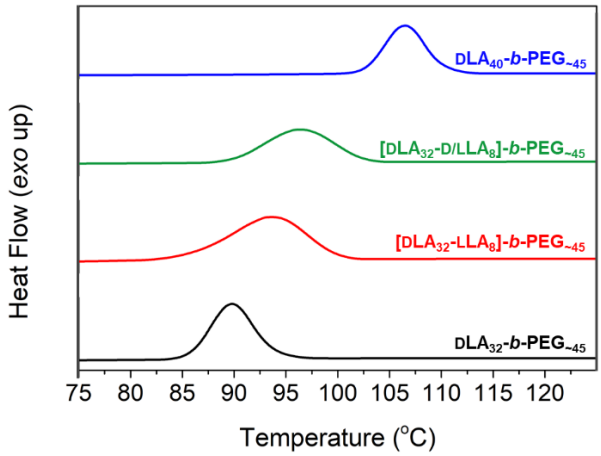

Figure 2-5. DSC results (second cooling scans, ramp rate = 10 °C min $^{-1}$, T_c) of MPLA-*b*-PEG prepared by the CDSA of [DLA_{32}-*x*LA_8]-*b*-PEG (*x* = D, L, or D/L) or [DLA_{32}]-*b*-PEG.

CDSA of the SCs of a pair of BCPs having complimentarily configured MPLA blocks. A pair of isotactic PLAs composed of enantiopure lactides forms a stereocomplex (SC) in condensed phase.[51–54] The molecular weight distributions and stereochemical irregularities of conventional PLAs could be detrimental to the formation of SCs, which requires the complementarity of the two PLA chains in both tacticity and molecular weight.[55,56] Therefore, an MPLA composed of a discrete number of enantiomerically pure repeating units arranged in a predetermined sequence could be used as a model system to explore the effects of the statistical uncertainty of molecular weight and stereochemical regularity of PLA on the formation of an SC.

The stereocomplexation of a pair of BCPs having complementarily configured MPLA blocks i.e., [DLA_n]-*b*-PEG/[LLA_n]-*b*-PEG (1:1 mol/mol), was induced during CDSA by allowing them to self-assemble in EtOH (1 mg/mL, 75°C). Slow cooling, equilibration and dilution conditions are

identical to the CDSA of [LA$_n$]-*b*-PEG. The TEM and AFM images obtained from the CDSA of the pair of [DLA$_{32}$]-*b*-PEG/[LLA$_{32}$]-*b*-PEG exhibited the formation of nanoparticulate crystallites (Figure S27a), which resembled the previously reported formation of the nanoparticles of a pair of BCPs having polydisperse PLAs as core-forming blocks.[35] The absence of diamond-shaped structures from the self-assembly of individual BCP indicated the preferential formation of the SC under the CDSA condition. On inspecting the CDSA of a BCP pair of [DLA$_{40}$]-*b*-PEG/[LLA$_{40}$]-*b*-PEG under the same condition, we observed that the pair of [DLA$_{40}$]-*b*-PEG/[LLA$_{40}$]-*b*-PEG self-assembled to elongated leaf-shaped structures that were different from the nanostructures observed from the CDSA of individual BCPs (Figure S27b). When the molecular weights of the MPLAs increased, the BCP pair, [DLA$_{64}$]-*b*-PEG/[LLA$_{64}$]-*b*-PEG, self-assembled to irregular shaped 2D platelets of thickness ~12 nm (Figure S27c). On the formation of an SC, MPLA adopted a denser conformation than that of the crystalline structure of a single enantiomer owing to the strong interactions between the chains with opposite configurations and improved packing.[57] This tight chain conformation increased the interaction between the oppositely configured MPLA chains forming the SC.

CDSA of the SCs of BCPs having a mismatch in the size. While assuming that the rapid crystallization of the SC of a BCP pair might be responsible for the formation of particulate or irregular nanostructures by CDSA, we speculated that the rate of crystallization of the BCP SC could be attenuated by introducing a mismatch in the number of repeating units or stereochemical sequences of the pair of MPLA blocks. To investigate the effects of the mismatch in the number of repeating units of MPLA blocks forming the SC during CDSA, we self-assembled a series of the BCP pairs experiencing incomplete stereocomplexation in CDSA by pairing [DLA$_n$]

with [LLA$_m$] ($n > m$). We defined the ratios between the number of D-lactic acids and L-lactic acids (D/L) as a degree of mismatch of the MPLA pair. The self-assembled structures resulting from the CDSA of these BCP pairs were studied by TEM and AFM.

The TEM images obtained from the SC of [DLA$_{40}$]-*b*-PEG/[LLA$_{32}$]-*b*-PEG (D/L = 1.25) exhibited the formation of nanoparticles (Figure 2-6a), which were analogous to the CDSA results of the SC of [DLA$_{32}$]-*b*-PEG/[LLA$_{32}$]-*b*-PEG without the size mismatch. When [DLA$_{64}$]-*b*-PEG/[LLA$_{32}$]-*b*-PEG (D/L = 2) were allowed to form the SC under the same CDSA condition, the BCP pair self-assembled into vesicle-like nanostructures having the average diameter of 760 nm ($Đ$ = 0.197) as determined by DLS (Figure 2-6b and S28). The height of collapsed structures of [DLA$_{64}$]-*b*-PEG/[LLA$_{32}$]-*b*-PEG was determined to be 46 nm by the AFM analysis (Figure 2-6d,e). The BCP pairs having MPLA blocks with a high D/L ratio (> 1.6) self-assembled to form vesicle-like nanostuctures via stereocomplexation of MPLA blocks during CDSA (Figure S29b,c). Interestingly, the pair of [DLA$_{72}$]-*b*-PEG/[LLA$_{64}$]-*b*-PEG (D/L = 1.12) self-assembled into triangular 2D crystallites with a thickness of 10 nm (Figure 2-6c,f,g). The crystallinity of these morphologies was confirmed by X-ray diffraction (XRD) results of the nanostructures (Figure S30).

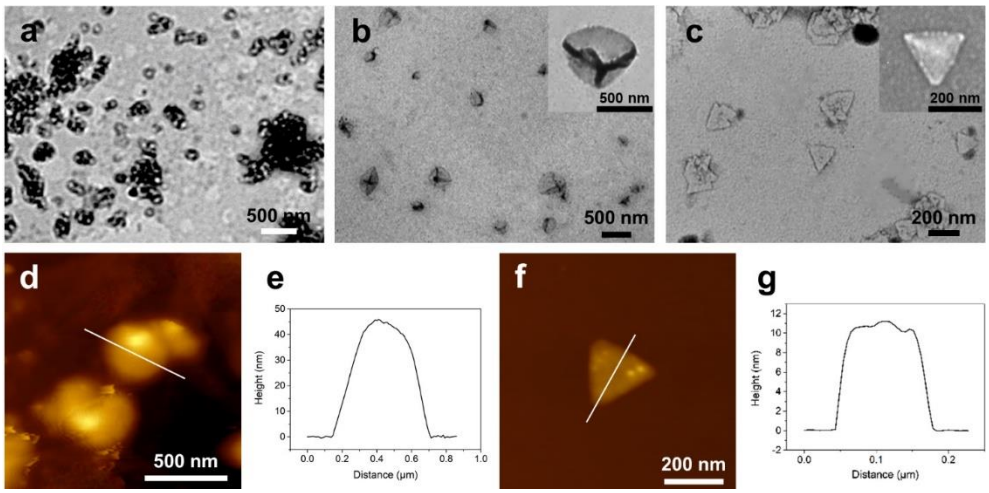

Figure 2-6. Assembled structures with different shapes from mismatched SCs. (a–c) TEM images of incomplete SC. (a) Nanoparticles prepared by co-self-assembly of [DLA_{40}]-*b*-PEG/[LLA_{32}]-*b*-PEG (1:1 mol/mol, D/L = 1.250). (b) Vesicles formed by co-self-assembly of [DLA_{64}]-*b*-PEG/[LLA_{32}]-*b*-PEG (1:1 mol/mol, D/L = 2.000). (c) Triangular 2D structures prepared by co-self-assembly of [DLA_{72}]-*b*-PEG/[LLA_{64}]-*b*-PEG (1:1 mol/mol, D/L = 1.125). (d,e) AFM image and height profile of vesicles formed by co-self-assembly of [DLA_{64}]-*b*-PEG/[LLA_{32}]-*b*-PEG (1:1 mol/mol, D/L = 2.000). (f,g) AFM image and height profile of triangular 2D structures by co-self-assembly of [DLA_{72}]-*b*-PEG/[LLA_{64}]-*b*-PEG (1:1 mol/mol, D/L = 1.125). TEM samples were stained with a 1 wt% solution of phosphortungstic acid in water.

The growth kinetics of CDSA of the complimentarily configured and size mismatched SCs. We surmised that the reason for the structural transformation from irregular structures to triangular plates and vesicle-like nanostructures was due to the crystallization kinetics of the SC of MPLAs. This assumption could be justified by the TEM images captured at different times during the stereocomplexation of a BCP pair of [DLA_n]-*b*-

PEG/[LLA_n]-*b*-PEG (n = 32, 40, 64) (Figure S31–33). After 2 hours, small aggregated particles were observed from the co-self-assembly of a pair of BCPs having complimentarily configured MPLA blocks (Figure S31–33a). Further 2 hours of aging (total 4 hours) was sufficient for the completion of crystallization and definitive morphologies were formed (Figure S31–33b). Additional aging time had no effect on the shape of complete SCs (Figure S31–33c,d). Whereas the TEM images obtained from different time points of the stereocomplexation of a BCP pair of [DLA_n]-*b*-PEG/[LLA_m]-*b*-PEG (n > m) showed the formation of premature structures until 6 hours of aging which is enough for the SCs of a pair of BCPs having complimentarily configured MPLA (Figure S34, 35). After 8 hours, the TEM images exhibited mixed structures which are composed of premature and regular nanostructures (Figure S34d, 35d). Additional 4 hours of aging (total 12 hours) finalized the crystallization of incomplete SCs and led to the transition from premature to regular structures (Figure S34e, 35e). These results suggested that the complimentarily configured SCs crystallized at a faster rate than that of the size mismatched SCs in solution, resulting in the formation of kinetically frozen structures during CDSA.

CDSA of the SCs of BCPs having a mismatch stereochemical sequence of the MPLA blocks. We assumed that the degree of the stereocomplexation of a pair of BCPs would decrease if the MPLA blocks possessed a mismatch in the stereochemical sequence. Therefore, we investigated the effects of the stereochemical mismatch of a pair of MPLA blocks on the self-assembly of [DLA_{32}-*x*LA_8]-*b*-PEG/[LLA_{40}]-*b*-PEG (*x* = D, L, and D/L). When there was no mismatch in the size and stereochemical sequence of the MPLA pairs, the BCP pairs, [DLA_{40}]-*b*-PEG/[LLA_{40}]-*b*-PEG formed 1D irregular structures under the CDSA condition (Figure S27a). By contrast, [DLA_{32}-D/LLA_8]-*b*-PEG/[LLA_{40}]-*b*-PEG self-

assembled into triangular 2D nanostructures that were analogous to the triangular 2D structures of [DLA_{72}]-*b*-PEG/[LLA_{64}]-*b*-PEG (Figure 2-7a,c, S36a). Under the identical CDSA condition, [DLA_{32}-LLA_{8}]-*b*-PEG/[LLA_{40}]-*b*-PEG self-assembled to form truncated triangular structures (Figure 2-7b,d, S36b). The XRD results obtained from these nanostructures indicated that the formation of these morphologies is derived from the crystallization (Figure S37). The thickness of the 2D triangle of the BCP pair was ~ 11 nm, which coincided with the thicknesses of the 2D triangles of [DLA_{72}]-*b*-PEG/[LLA_{64}]-*b*-PEG (10 nm) (Figure 2-7e–h and S29). This comparison strongly suggested that the MPLAs folded to form the SC in a similar manner to that of the MPLA in the crystalline core of the nanostructure of a single BCP. These results suggested that the stereochemical mismatch between MPLA blocks altered the crystallization of the SC of the BCP pair in a similar manner to the stereocomplexation of the BCP pairs with size mismatch in the MPLA blocks.

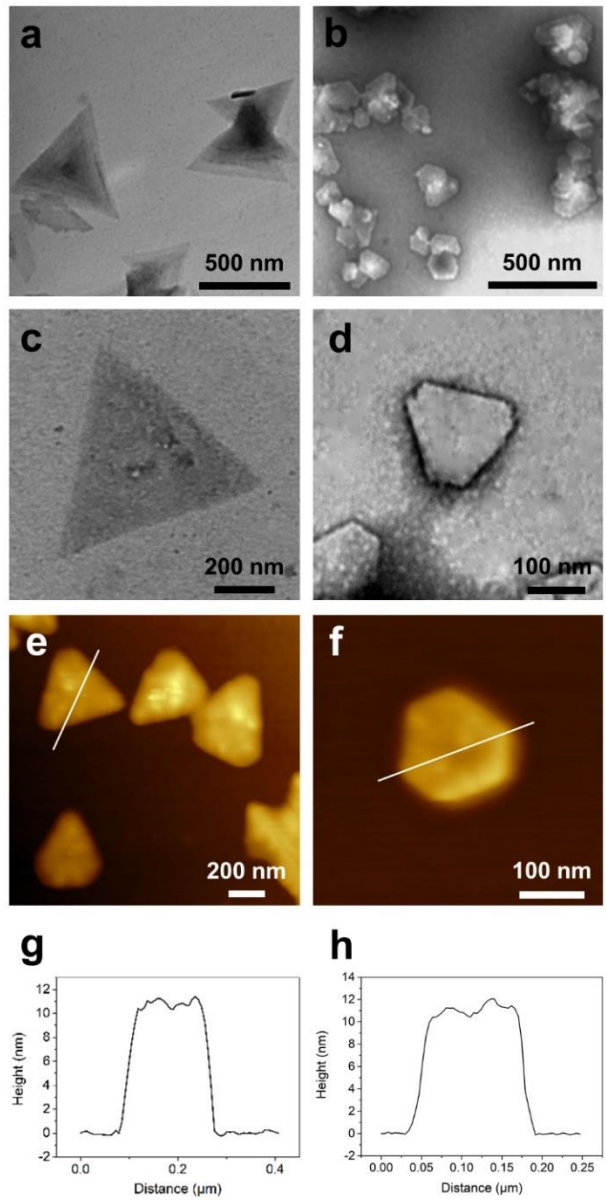

Figure 2-7. 2D crystallites formed from SCs having stereochemical sequence. (a–d) TEM images, (e–h) AFM images, and height profiles of SC crystallites. (a,c,e,g) Triangular 2D structures by co-self-assembly of [DLA_{32}-D/LLA_8]-*b*-PEG/[LLA_{40}]-*b*-PEG (1:1 mol/mol).

To assess the degree of the stereocomplexation, we measured the melting temperatures of the BCP pairs by DSC (Figure 2-8a). Comparing the T_m of the SCs of [DLA_{40}]-*b*-PEG/[LLA_{40}]-*b*-PEG (207.4 °C, ΔH_{fus} = 52.5 J/g), the T_m of the SCs of [DLA_{32}-D/LLA_8]-*b*-PEG/[LLA_{40}]-*b*-PEG was 190.4 °C (ΔH_{fus} = 46.1 J/g) and that of the SC of [DLA_{32}-LLA_8]-*b*-PEG/[LLA_{40}]-*b*-PEG was 182.0 °C (ΔH_{fus} = 32.6 J/g). Interestingly, the T_m of the SC of [DLA_{32}-D/LLA_8]-*b*-PEG/[LLA_{40}]-*b*-PEG was 8.4 °C higher than that of the SC formed with [DLA_{32}-LLA_8]-*b*-PEG, suggesting the contribution of four DLA units (in the terminal segment) to the formation of the SC. Assuming parallel stacking of MPLA blocks, the enthalpy of fusion (ΔH_{fus}) of the SCs increased proportionally with the increase in the number of pairs of repeating units with complementary stereochemical arrangements.

These results also coincided with the FT−IR results of the SC of BCPs (Figure 2-8b). The formation of the SC of PLA involved the formation of weak hydrogen bonds between the carbonyl group of one chain and the methyl hydrogen of the other chain.[54,58] The CO stretching band of the SCs of [DLA_{40}]-*b*-PEG/[LLA_{40}]-*b*-PEG shifted to a shorter wavenumber (1747 cm^{-1}) than that of the [LLA_{40}]-*b*-PEG, indicating the formation of SC crystallites by the mixture of BCPs.[58] Similar to the T_m of the SC of the BCP pair, with stereochemical mismatching, the degree of the shift in the CO stretching band of the SC was also proportional to the number of stereochemical pairs arranged in MPLA blocks forming the SC.

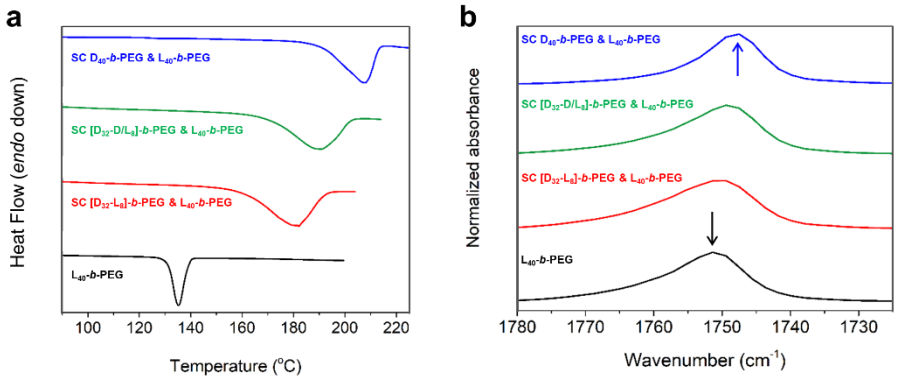

Figure 2-8. (a) DSC (second heating scans, ramp rate = 10 °C min^{-1}, T_m) and (b) FT-IR results of the SCs prepared by the CDSA of [DLA_{32}-*x*LA_8]-*b*-PEG/[LLA_{40}]-*b*-PEG.

2.4 Conclusion

In summary, we synthesized stereochemical sequence-defined MPLAs using iterative convergent methods. The PLAs with a discrete number of repeating units (up to 72) and stereochemical sequence such as [DLA_{32}-*x*LA_8] (x = D, L, or D/L) at the carboxy terminus were employed to explore the structural difference of their crystallites. MPLA-b-PEG BCPs prepared by ligating the MPLA with PEG allowed crystallization of MPLA blocks in EtOH. Structural differences derived from a discrete number of units, stereochemical sequences, and regulated SCs were monitored by TEM, AFM, DSC, DLS, and FT-IR analyses. Based on the AFM and DSC analyses of [DLA_n]-*b*-PEG and [DLA_{32}-*x*LA_8]-*b*-PEG, we suggest that PLAs folded at 32 repeating units to form the crystalline domain of the 2D nanostructure and the additional units having atactic or opposite stereochemistry do not participate in crystallization. Depending on the pair of BCPs (complementary, mismatch, and sequence), resulting SCs formed various nanostructures. A pair of BCPs having complementarily configured

MPLA blocks assembled to form irregular nanostructures. The fast crystallization kinetics of the SC of MPLAs was the reason for these irregular structures. These structures were transformed to triangular and vesicular nanostructures by attenuating crystallization with a mismatch in repeating units or stereochemical sequences. We believe that these results provide a deeper understanding of crystallization of PLAs and suggest that these properties of PLA crystallites provide a means to create advanced materials for future applications.

2.5 Reference

1. Lutz, J.-F.; Ouchi, M.; Liu, D. R.; Sawamoto, M. Sequence-Controlled Polymers. *Science* **2013,** *341,* 1238149.

2. van Genabeek, B.; de Waal, B. F. M.; Ligt, B.; Palmans, A. R. A.; Meijer, E. W. Dispersity under Scrutiny: Phase Behavior Differences between Disperse and Discrete Low Molecular Weight Block Co-Oligomers. *ACS Macro Lett.* **2017,** *6,* 674−678.

3. Gentekos, D. T.; Sifri, R. J.; Fors, B. P. Controlling polymer properties through the shape of the molecular-weight distribution. *Nat. Rev. Mater.* **2019,** *4,* 761−774.

4. Merrifield, R. B. Solid phase peptide synthesis. i. the synthesis of a tetrapeptide. *J. Am. Chem. Soc.* **1963,** *85,* 2149−2154.

5. Al Ouahabi, A.; Charles, L.; Lutz, J.-F. Synthesis of non-natural sequence-encoded polymers using phosphoramidite chemistry. *J. Am. Chem. Soc.* **2015,** *137,* 5629−5635.

6. Roy, R. K.; Meszynska, A.; Laure, C.; Charles, C.; Verchin, C.; Lutz, J.-F. Design and synthesis of digitally encoded polymers that can be decoded and erased. *Nat. Commun.* **2015,** *6,* No. 7237.

7. Porel, M.; Alabi, C. A. Sequence-defned polymers via orthogonal allyl acrylamide building blocks. *J. Am. Chem. Soc.* **2014,** *136,* 13162−13165.

8. Bootwicha, T.; Feilner, J. M.; Myers, E. L.; Aggarwal, V. K. Iterative assembly line synthesis of polypropionates with full stereocontrol. *Nat. Chem.* **2017,** *9,* 896−902.

9. Konrad, W.; Fengler, C.; Putwa, S.; Barner-Kowollik, C. Protection-group free synthesis of sequence-defined macromolecules via precision λ-orthogonal photochemistry. *Angew. Chem., Int. Ed.* **2019,** *58,* 7133−7137.

10. Solleder, S. C.; Schneider, R. V.; Wetzel, K. S.; Boukis, A. C.; Meier, M. A. R. Recent progress in the design of monodisperse, sequence-defned macromolecules. *Macromol. Rapid Commun.* **2017,** *38,* No. 1600711.

11. Barnes, J. C.; Ehrlich, D. J. C.; Gao, A. X.; Leibfarth, F. A.; Jiang, Y.; Zhou, E.; Jamison, T. F.; Johnson, J. A. Iterative Exponential Growth of Stereo- and Sequence-Controlled Polymers. *Nat. Chem.* **2015,** *7,* 810−815.

12. Jiang, Y.; Golder, M. R.; Nguyen, H. V.-T.; Wang, Y.; Zhong, M.; Barnes, J. C.; Ehrlich, D. J. C.; Johnson, J. A. Iterative Exponential Growth Synthesis and Assembly of Uniform Diblock Copolymers. *J. Am. Chem. Soc.* **2016,** *138,* 9369−9372.

13. Takizawa, K.; Nulwala, H.; Hu, J.; Yoshinaga, K.; Hawker, C. J. Molecularly Defined (L)-Lactic Acid Oligomers and Polymers: Synthesis and Characterization. *J. Polym. Sci., Part A: Polym. Chem.* **2008,** *46,* 5977−5990.

14. Takizawa, K.; Tang, C.; Hawker, C. J. Molecularly Defined oolactone Oligomers and Polymers: Synthesis and Characterization. *J. Am. Chem. Soc.* **2008,** *130,* 1718−1726.

15. Lee, J. M.; Koo, M. B.; Lee, S. W.; Lee, H.; Kwon, J.; Shim, Y. H.; Kim, S. Y.; Kim, K. T. High-Density Information Storage in an Absolutely

Defined Aperiodic Sequence of Monodisperse Copolyester. *Nat. Commun.* **2020,** *11,* No. 56.

16. Koo, M. B.; Lee, S. W.; Lee, J. M.; Kim, K. T. Iterative Convergent Synthesis of Large Cyclic Polymers and Block Copolymers with Discrete Molecular Weights. *J. Am. Chem. Soc.* **2020,** *142,* 14028−14032.

17. Sun, Y.; Tan, R.; Ma, Z.; Gan, Z.; Li, G.; Zhou, D.; Shao, Y.; Zhang, W.-B.; Zhang, R.; Dong, X.-H. Discrete Block Copolymers with Diverse Architectures: Resolving Complex Spherical Phases with One Monomer Resolution. *ACS Cent. Sci.* **2020,** *6,* 1386−1393.

18. van Genabeek, B.; de Waal, B. F. M.; Gosens, M. M. J.; Pitet, L. M.; Palmans, A. R. A.; Meijer, E. W. Synthesis and Self-Assembly of Discrete Dimethylsiloxane−Lactic Acid Diblock Co-oligomers: The Dononacontamer and Its Shorter Homologues. *J. Am. Chem. Soc.* **2016,** *138,* 4210−4218.

19. Perry, S. L.; Sing, C. E. 100th Anniversary of Macromolecular Science Viewpoint: Opportunities in the Physics of Sequence-Defined Polymers. *ACS Macro Lett.* **2020,** *9,* 216−225.

20. Nanjan, P.; Porel, M. Sequence-Defined Non-Natural Polymers: Synthesis and Applications. *Polym. Chem.* **2019,** *10,* 5406−5424.

21. Charles, L.; Lutz, J.-F. Design of Abiological Digital Poly(phosphodiester)s. *Acc. Chem. Res.* **2021,** *54,* 1791−1800.

22. Aksakal, R.; Mertens, C.; Soete, M.; Badi, N.; Du Prez, F. Applications of Discrete Synthetic Macromolecules in Life and Materials Science: Recent and Future Trends. *Adv. Sci.* **2021,** *8,* No. 2004038.

23. Terreau, O.; Luo, L.; Eisenberg, A. Effect of Poly(acrylic acid) Block Length Distribution on Polystyrene-b-Poly(acrylic acid) Aggregates in Solution. 1. Vesicles. *Langmuir* **2003,** *19,* 5601−5607.

24. Jiang, Y.; Chen, T.; Ye, F.; Liang, H.; Shi, A.-C. Effect of Polydispersity on the Formation of Vesicles from Amphiphilic Diblock Copolymers. *Macromolecules* **2005,** *38,* 6710−6717.

25. Doncom, K. E. B.; Blackman, L. D.; Wright, D. B.; Gibson, M. I.; O'Reilly, R. K. Dispersity effects in polymer self-assemblies: a matter of hierarchical control. *Chem. Soc. Rev.* **2017,** *46,* 4119−4134.

26. Ha, S.; La, Y.; Kim, K. T. Polymer Cubosomes: Infinite Cubic Mazes and Possibilities. *Acc. Chem. Res.* **2020,** *53,* 620−631.

27. Das, A.; Petkau-Milroy, K.; Klerks, G.; B van Genabeek, B.; Lafleur, R. P. M.; Palmans, A. R. A.; Meijer, E. W. Consequences of Dispersity on the Self-Assembly of ABA-Type Amphiphilic Block Co-Oligomers. *ACS Macro Lett.* **2018,** *7,* 546−550.

28. Ha, S.; Kim, K. T. Effect of the molecular weight distribution of the hydrophobic block on the formation of inverse cubic mesophases of block copolymers with a discrete branched hydrophilic block. *Polym. Chem.* **2019,** *10,* 5805−5813.

29. Hudson, Z. M.; Boott, C. E.; Robinson, M. E.; Rupar, P. A.; Winnik, M. A.; Manners, I. Tailored hierarchical micelle architectures using living crystallization-driven self-assembly in two dimensions. *Nat. Chem.* **2014,** *6,* 893−898.

30. Qiu, H.; Gao, Y.; Boott, C. E.; Gould, O. E. C.; Harniman, R. L.; Miles, M. J.; Webb, S. E. D.; Winnik, M. A.; Manners, I. Uniform patchy and hollow rectangular platelet micelles from crystallizable polymer blends. *Science* **2016,** *352,* 697−701.

31. Pearce, S.; He, X.; Hsiao, M.-S.; Harniman, R. L.; MacFarlane, L. R.; Manners, I. Uniform, High-Aspect-Ratio, and Patchy 2D Platelets by Living Crystallization-Driven Self-Assembly of Crystallizable

Poly(ferrocenyldimethylsilane)-Based Homopolymers with Hydrophilic Charged Termini. *Macromolecules* **2019,** *52,* 6068−6079.

32. He, X.; Hsiao, M.-S.; Boott, C. E.; Harniman, R. L.; Nazemi, A.; Li, X.; Winnik, M. A.; Manners, I. Two-dimensional assemblies from crystallizable homopolymers with charged termini. *Nat. Mater.* **2017,** *16,* 481−489.

33. Petzetakis, N.; Walker, D.; Dove, A. P.; O'Reilly, R. K. Crystallization-driven sphere-to-rod transition of poly(lactide)-b-poly(acrylic acid) diblock copolymers: mechanism and kinetics. *Soft matter* **2012,** *8,* 7408.

34. Sun, L.; Petzetakis, N.; Pitto-Barry, As.; Schiller, T. L.; Kirby, N.; Keddie, D. J.; Boyd, B. J.; O'Reilly, R. K.; Dove, A. P. Tuning the Size of Cylindrical Micelles from Poly(l-lactide)-b-poly(acrylic acid) Diblock Copolymers Based on Crystallization-Driven Self-Assembly. *Macromolecules* **2013,** *46,* 9074−9082.

35. Sun, L.; Pitto-Barry, A.; Kirby, N.; Schiller, T. L.; Sanchez, A. M.; Dyson, M. A.; Sloan, J.; Wilson, N. R.; O'Reilly, R. K.; Dove, A. P. Structural reorganization of cylindrical nanoparticles triggered by polylactide stereocomplexation. *Nat. Commun.* **2014,** *5,* No. 5746.

36. He, X.; He, Y.; Hsiao, M.-S.; Harniman, R. L.; Pearce, S.; Winnik, M. A.; Manners, I. Complex and Hierarchical 2D Assemblies via Crystallization-Driven Self-Assembly of Poly(L-lactide) Homopolymers with Charged Termini. *J. Am. Chem. Soc.* **2017,** *139,* 9221−9228.

37. Inam, M.; Cambridge, G.; Pitto-Barry, A.; Laker, Z. P. L.; Wilson, N. R.; Mathers, R. T.; Dove, A. P.; O'Reilly, R. K. 1D vs. 2D shape selectivity in the crystallization-driven self-assembly of polylactide block copolymers. *Chem. Sci.* **2017,** *8,* 4223−4230.

38. Hurst, P. J.; Rakowski, A. M.; Patterson, J. P. Ring-opening polymerization-induced crystallization-driven self-assembly of poly-L-

lactide-block-polyethylene glycol block copolymer (ROPI-CDSA). *Nat. Commun.* **2020,** *11,* No. 4690.

39. He, Y.; Eloi, J.-C.; Harniman, R. L.; Richardson, R. M.; Whittell, G. R.; Mathers, R. T.; Dove, A. P.; O'Reilly, R. K.; Manners, I. Uniform Biodegradable Fiber-Like Micelles and Block Comicelles via "Living" Crystallization-Driven Self-Assembly of Poly(l-lactide) Block Copolymers: The Importance of Reducing Unimer Self-Nucleation via Hydrogen Bond Disruption. *J. Am. Chem. Soc.* **2019,** *141,* 19088−19098.

40. Inam, M.; Jones, J. R.; Pérez-Madrigal, M. M.; Arno, M. C.; Dove, A. P.; O'Reilly, R. K. Controlling the Size of Two-Dimensional Polymer Platelets for Water-in-Water Emulsifiers. *ACS Cent. Sci.* **2018,** *4,* 63−70.

41. Yang, S.; Kang, S.-Y.; Choi, T. L. Semi-conducting 2D rectangles with tunable length via uniaxial living crystallization-driven self-assembly of homopolymer. *Nat Commun.* **2021,** *12,* No. 2602.

42. Yang, S.; Choi, T.-L. Rapid formation and real-time observation of micron-sized conjugated nanofibers with tunable lengths and widths in 20 minutes by living crystallization-driven self-assembly. *Chem. Sci.* **2020,** *11,* 8416−8424.

43. Yang, S.; Kang, S.-Y.; Choi, T.-L. Morphologically Tunable Square and Rectangular Nanosheets of a Simple Conjugated Homopolymer by Changing Solvents. *J. Am. Chem. Soc.* **2019,** *141,* 19138−19143.

44. Rizis, G.; van de Ven, T. G. M.; Eisenberg, A. "Raft" Formation by Two-Dimensional Self-Assembly of Block Copolymer Rod Micelles in Aqueous Solution. *Angew. Chem., Int. Ed.* **2014,** *53,* 9000−9003.

45. Han, L.; Wang, M.; Jia, X.; Chen, W.; Qian, H.; He, F. Uniform two-dimensional square assemblies from conjugated block copolymers driven by π−π interactions with controllable sizes. *Nat. Commun.* **2018,** *9,* No. 865.

46. Zhu, Y.; Han, L.; Fan, H.; Wang, M.; Qi, R.; Zhao, Y.; He, F. Three-Dimensional Spirals of Conjugated Block Copolymers Driven by Screw Dislocation. *Macromolecules* **2020,** *53,* 3217−3223.

47. Petkau-Milroy, K.; Ianiro, A.; Ahn, M. M. L.; Magana, J. R.; Vleugels, M. E. J.; Lamers, B. A. G.; Tuinier, R.; Voets, I. K.; Palmans, A. R. A.; Meijer, E. W. Architecture-Dependent Interplay between Self-Assembly and Crystallization in Discrete Block Co-Oligomers. *ACS Macro Lett.* **2020,** *9,* 38−42.

48. Vleugels, M. E. J.; de Zwart, M. E.; Magana, J. R.; Lamers, B. A. G.; Voets, I. K.; Meijer, E. W.; Petkau-Milroy, K.; Palmans, A. R. A. Effects of crystallinity and dispersity on the self-assembly behavior of block co-oligomers in water. *Polym. Chem.* **2020,** *11,* 7170−7177.

49. Lamers, B. A. G.; van Genabeek, B.; Hennissen, J.; de Waal, B. F. M.; Palmans, A. R. A.; Meijer, E. W. Stereocomplexes of Discrete, Isotactic Lactic Acid Oligomers Conjugated with Oligodimethylsiloxanes. *Macromolecules* **2019,** *52,* 1200−1209.

50. Yang, J.; Zhao, T.; Zhou, Y.; Liu, L.; Li, G.; Zhou, E.; Chen, X. Single Crystals of the Poly(L-lactide) Block and the Poly(ethylene glycol) Block in Poly(L-lactide)-poly(ethylene glycol) Diblock Copolymer. *Macromolecules* **2007,** *40,* 2791−2797.

51. Tsuji, H. Poly(lactic acid) stereocomplexes: A decade of progress. *Adv. Drug. Delivery Rev.* **2016,** *107,* 97−135.

52. Worch, J. C.; Prydderch, H.; Jimaja, S.; Bexis, P.; Becker, M. L.; Dove, A. P. Stereochemical enhancement of polymer properties. *Nat. Rev. Chem.* **2019,** *3,* 514−535.

53. Tsuji, H.; Ikada, Y. Stereocomplex formation between enantiomeric poly(lactic acid)s. XI. Mechanical properties and morphology of solution-cast films. *Polymer* **1999,** *40,* 6699−6708.

54. Tsuji, H. Poly(lactide) Stereocomplexes: Formation, Structure, Properties, Degradation, and Applications. *Macromol. Biosci.* **2005,** *5,* 569−597.

55. Tsuji, H.; Ikada, Y. Stereocomplex formation between enantiomeric poly(lactic acid)s. 6. Binary blends from copolymers. *Macromolecules* **1992,** *25,* 5719−5723.

56. Tsuji, H.; Hyon, S. H.; Ikada, Y. Stereocomplex formation between enantiomeric poly(lactic acid)s. 4. Differential scanning calorimetric studies on precipitates from mixed solutions of poly(D-lactic acid) and poly(L-lactic acid). *Macromolecules* **1991,** *24,* 5657−5662.

57. Okihara, T.; Tsuji, M.; Kawaguchi, A.; Katayama, K.-I.; Tsuji, H.; Hyon, S.-H.; Ikada, Y. Crystal structure of stereocomplex of poly(L-lactide) and poly(D-lactide). *J. Macromol. Sci., Part B: Phys.* **1991,** *30,* 119−140.

58. Zhang, J.; Sato, H.; Tsuji, H.; Noda, I.; Ozaki, Y. Infrared spectroscopic study of $CH_3\cdots O{=}C$ interaction during poly(L-lactide)/poly(D-lactide) stereocomplex formation. *Macromolecules* **2005,** *38,* 1822−1828.

Chapter 3. Self-Assembly of Stereoblock Copolymers Driven by the Chain-Folding of Discrete Poly(D-lactic acid-*b*-L-lactic acid) via Intramolecular Stereocomplexation

3.1 Abstract

The encoding of information by defining the sequence of monomers is a highly anticipated strategy for controlling the three-dimensional structures of polymers via information-driven chain-folding and self-assembly. In this paper, we report the controlled chain-folding of stereoblock poly(lactic acid)s (PLAs) composed of two oligo(lactic acid) domains, [DLA$_n$] and [LLA$_n$] constructed using precisely defined numbers of D- and L-lactic acids, respectively. Under the crystallization-driven self-assembly (CDSA) condition, block copolymers (BCPs) of stereoblock PLA and poly(ethylene glycol) formed planar nanostructures having unilamellar crystalline cores of stereoblock PLA. [DLA$_n$]-[LLA$_n$] stereoblocks were folded predominantly by intramolecular stereocomplexation (SCN) in dilute solutions in which the intermolecular interaction between BCPs was suppressed**.** The thickness of the planar nanostructures was precisely defined by the number of repeating units constituted of [DLA$_n$] and [LLA$_n$] domains. The convergent synthesis of PLA permitted the addition of a single monomer unit between the [DLA$_n$] and [LLA$_n$] domains, resulting in the introduction of a desired functional group at the apex of the folded chain. Our results demonstrate that information encoded in the form of a monomer sequence may shape the polymer chain and guide its self-assembly toward specific nanostructures having the desired dimensions and functions.

3.2 Introduction

A polypeptide chain encodes information as a sequence of amino acid residues.[1–3] This information directs the polypeptide chain to construct its three-dimensional (3D) structure by programmed chain-folding in solution, which is essential for its biological function.[4–7] In contrast, the majority of synthetic polymers lack sequence-specificity in their constituting monomers and, therefore, exhibit undefined 3D shapes. The folding of polymer chains is critical to their crystallization.[8,9] Stereoregular polymers such as poly(L-lactic acid) (PLLA) and poly(D-lactic acid) (PDLA) crystallize by the regular packing of folded segments of polymer chains. Therefore, the interval of intramolecular chain-folding, measured by the number of repeating units, determines the thickness of the crystalline lamella formed by the packing of folded polymer domains.[10,11] For example, PLLA folds after every 32 repeating units in solution to form lamellar structures having a periodicity of ~9 nm.[12–14] This lamellar thickness persists when the degree of polymerization of PLLA significantly exceeds the interval of chain-folding.[15]

When stereoregular poly(lactic acid) (PLA) is covalently connected to a solvent-soluble coil polymer such as poly(ethylene glycol) (PEG), the resulting block copolymers (BCPs) self-assemble in solution to form two-dimensional (2D) nanostructures having unilamellar PLA cores stabilized by coronal chains.[16–19] This crystallization-driven self-assembly (CDSA) of BCPs can achieve remarkable control over the shape, and surface chemistry of the resulting low-dimensional nanostructures by the controlled crystallization of various core-forming blocks.[20–28] Recently, a seeded growth method, termed living CDSA, has been utilized to obtain precisely controlled dimensions.[29–38] However, the thickness of the nanostructures, primarily decided by the number of repeating units required for the chain-

folding of the core-forming polymer blocks, remains uncontrollable because of the persistence of the chain-folding interval of the core-forming blocks in solution regardless of the number of repeating units of PLA blocks.

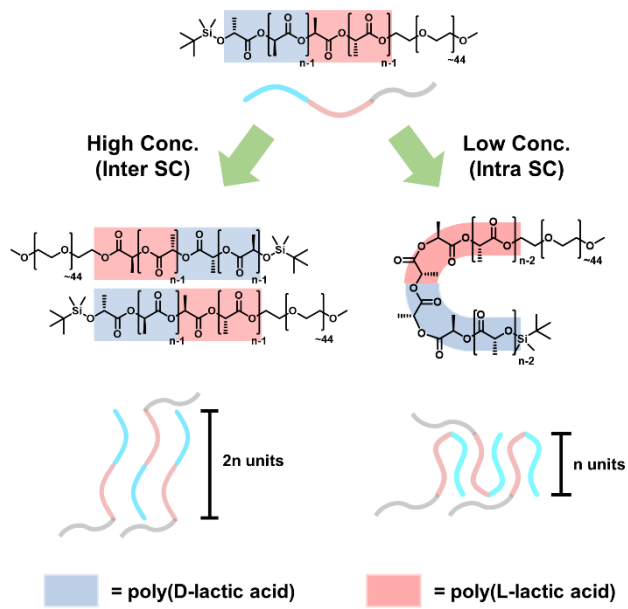

Figure 3-1. Schematic representation of the intermolecular and intramolecular stereocomplexation of [DLA$_n$]-[LLA$_n$]-*b*-PEG.

Exploiting the encoding of information in synthetic polymers to define its sequence has been highly anticipated as a bio-inspired strategy for defining the 3D shape of synthetic polymers by sequence-specific intramolecular/intermolecular interactions and chain-folding.[39–41] We envisaged that the enthalpically favored stereocomplexation (SCN) of PLLA and PLDA in solution[42–44] would induce chain-folding with a precisely chosen interval if a PLA chain was composed of two discrete PLA domains having stereochemical complementarity, which are termed stereoblocks in this work (Figure 3-1).[45–47] Achieving exact control over the number of D- or L-lactic acids and their sequence in stereoblock PLAs may provide an

opportunity to explore the information-directed formation of conformations and assemblies, which might realize synthetic superstructures having specific desired functions similar to those exhibited by their natural counterparts.

In this article, we report the controlled chain-folding of stereoblock PLAs composed of two oligo(lactic acid) (oLA) domains, [DLA$_n$] and [LLA$_n$], constructed using precisely defined numbers of D- and L-lactic acids, respectively. To identify the chain-folding, we analyzed the crystallites of BCPs composed of stereoblock PLAs and PEG created by CDSA. The CDSA of these BCPs, [DLA$_n$]-[LLA$_n$]-*b*-PEG, resulted in the formation of platelets having crystalline cores composed of the folded stereoblock PLAs via intramolecular SCN of [DLA$_n$] and [LLA$_n$] in solution. The intramolecular SCN predominantly occurred upon the suppression of intermolecular SCN of stereoblock PLAs by decreasing the concentration or increasing the solubility of BCPs in solution. The thickness of the folded crystalline core of 2D nanostructures was proportional to the number of repeating units of the domains forming stereocomplexes (SCs). The convergent synthesis of stereoblock PLAs permitted the addition of a single monomer unit between the [DLA$_n$] and [LLA$_n$] domains, which could be utilized to precisely introduce a desired functional group at the apex of the folded PLA block.[12]

3.3 Results and Discussion

CDSA of a BCP containing [DLA$_{16}$]-[LLA$_{16}$]. Stereopure oLAs, [DLA$_n$] and [LLA$_n$], were synthesized by convergent synthesis using the dimers of D-lactic acid or L-lactic acid having *t*-butyldimetylsilyl (TBDMS) and benzyl (Bn) protective groups as the building blocks. The as-synthesized [DLA$_{16}$] and [LLA$_{16}$] were orthogonally deprotected and

coupled by esterification with 1-(3-Dimethylaminopropyl)-3-ethylcarbodiimide hydrochloride (EDC·HCl) to form stereoblock PLAs, which were coupled with monomethoxy poly(ethylene glycol) (PEG, M_n = 2000 g/mol, $Đ$ = 1.03) by esterification (Supporting Information page 5). [DLA_{24}] and [LLA_{24}] formed stereocomplexes in common organic solvents, which resulted in precipitation. Therefore, [LLA_{24}] was initially coupled with PEG to enhance its solubility during esterification with [DLA_{24}] to afford the desired BCP. (Scheme 3-1). The as-synthesized BCPs, [DLA_n]-[LLA_n]-*b*-PEG (n = 16, 24), were characterized by proton nuclear magnetic resonance (^{1}H NMR), gel permeation chromatography (GPC), circular dichroism (CD), and matrix-assisted laser desorption/ionization-time of flight (MALDI-TOF) mass spectrometry (Figure 3-2, S1,2 and Table S1).

Scheme 3-1. Iterative convergent syntheses of stereopure discrete oligo(lactic acid)s and [DLA_{24}]-[LLA_{24}]-*b*-PEG.

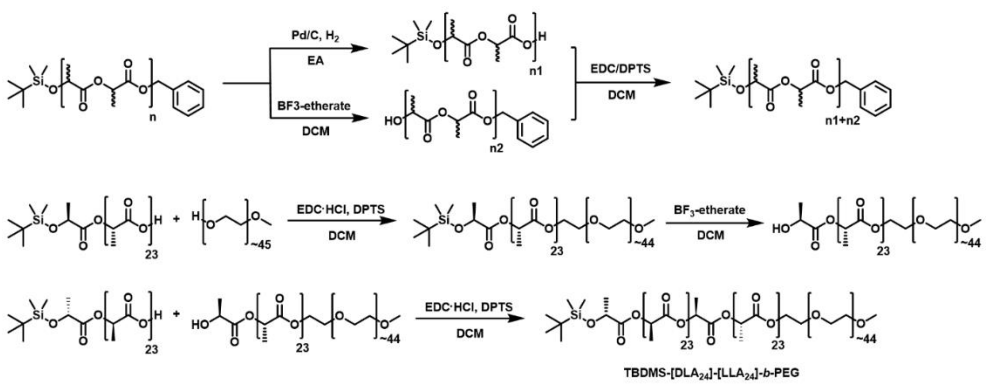

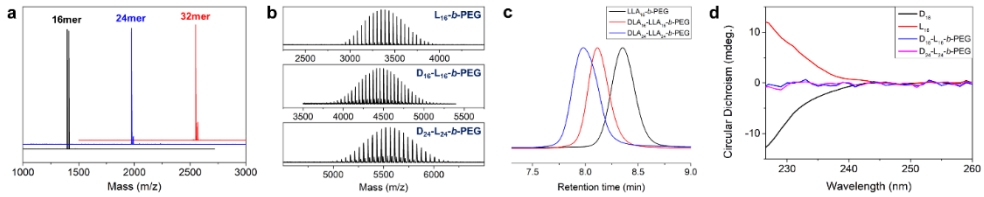

Figure 3-2. (a) Combined MALDI-TOF spectra of monodisperse PLA. (b) Combined MALDI-TOF spectra of [LLA$_{16}$]-*b*-PEG and [DLA$_n$]-[LLA$_n$]-*b*-PEG. (c) GPC analysis of [LLA$_{16}$]-*b*-PEG and [DLA$_n$]-[LLA$_n$]-*b*-PEG. (d) CD spectra of [DLA$_{16}$], [LLA$_{16}$], and [DLA$_n$]-[LLA$_n$]-*b*-PEG.

Initially, we investigated the CDSA of [DLA$_{16}$]-[LLA$_{16}$]-*b*-PEG in ethanol, conducted by dissolving the BCP in ethanol at 75 °C for 8 h, followed by cooling the reaction mixture to 25 °C at a rate of 0.2 °C/min.[14,17] The solution was equilibrated at 25 °C for 16 h and diluted with water, followed by 4 h of aging prior to analysis. Transmission electron microscopy (TEM) and atomic force microscopy (AFM) analyses of the CDSA result showed that at a concentration of 1 mg/mL in ethanol (0.226 μmol), [DLA$_{16}$]-[LLA$_{16}$]-*b*-PEG self-assembled into truncated triangular structures having protruding hairy peripheries (Figure 3-3a,c and S3). The truncated triangular morphology was clearly distinguishable from the commonly observed 2D diamond-shaped structures obtained under identical self-assembly conditions from the CDSA of [DLA$_{32}$]-*b*-PEG or [DLA$_{64}$]-*b*-PEG having stereopure PLA blocks.[14] The thickness of these structures, estimated from the atomic force microscopy (AFM) height profiles, was 9.0 ± 0.8 nm (Figure 3-3e), which was identical to the thickness of 2D structures of [DLA$_{32}$]-*b*-PEG or [DLA$_{64}$]-*b*-PEG having crystalline cores composed of stretched 32-repeating unit segments (0.29 nm height/repeating unit).[13,14,48] This result indicated that the cores of the truncated triangles of

[DLA_{16}]-[LLA_{16}]-*b*-PEG were composed of the crystallites of the intermolecular SCs of completely stretched [DLA_{16}]-[LLA_{16}].

Interestingly, the AFM height profiles of the hairy peripheries of the self-assembled structures of [DLA_{16}]-[LLA_{16}]-*b*-PEG indicated that the structures were ~ 4 nm thick (Figure 3-3e). This observation suggests that the hairy structures may have resulted from the crystallization of folded stereoblock PLAs via intramolecular SCN between [DLA_{16}] and [LLA_{16}] during the CDSA. We hypothesized that the intermolecular SCN of [DLA_{16}]-[LLA_{16}]-*b*-PEG could be suppressed by sufficiently reducing the concentration of the BCP in solution, which would promote the intramolecular SCN of [DLA_{16}] and [LLA_{16}] stereoblocks.

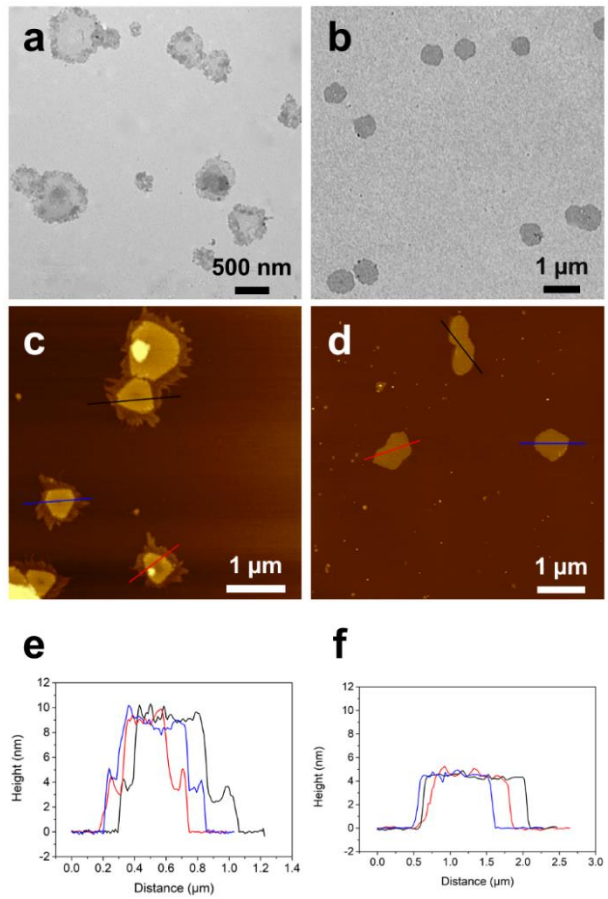

Figure 3-3. 2D nanostructures obtained from the CDSA of [DLA_{16}]-[LLA_{16}]-b-PEG (ethanol, 75°C, slow cooling, 16 h aging, dilution with water). (a, b) TEM images, (c–f) AFM images, and height profiles of ill-defined nanostructures. (a, c, e) 1 mg/mL, (b, d, f) 0.01 mg/mL. TEM samples were stained using a 1 wt% solution of phosphotungstic acid in water.

The rate of the crystallization of the core-forming blocks in solution may significantly influence the shape of the crystallite formed by the CDSA of BCPs having stereoregular PLA blocks.[14] We estimated the rate of crystallization of BCPs by measuring the change in the size of the

crystallites formed during the course of CDSA in a given solvent by dynamic light scattering (DLS) and TEM. We compared the rates of crystallization of [DLA_{16}]-[LLA_{16}]-*b*-PEG at the concentrations 1 mg/mL and 0.01 mg/mL in ethanol and 1 mg/mL in acetonitrile (Figure 3-4 and S4–6). The CDSA of [DLA_{16}]-[LLA_{16}]-*b*-PEG at the concentration of 1 mg/mL in ethanol exhibited a steady increase in the average diameter of crystallites for 6 h, whereafter the diameter remained constant. When the concentration of the BCP was reduced to 0.01 mg/mL, the average diameter increased continuously at a slower rate than that of the CDSA of [DLA_{16}]-[LLA_{16}]-*b*-PEG. Similarly, the diameters of the nanostructures formed by CDSA in acetonitrile attained their maximum values in 10 h and remained constant thereafter, which suggested that the crystallization of stereoblock PLAs was retarded by the change in solvent.

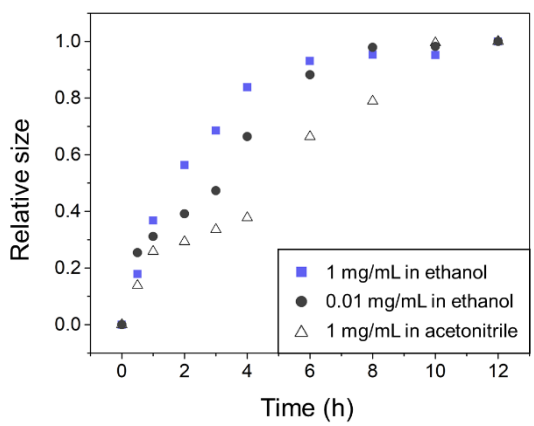

Figure 3-4. Plot of the relative size of the nanostructures of [DLA_{16}]-[LLA_{16}]-*b*-PEG in solution (filled square: concentration 1 mg/mL in ethanol, filled circle: 0.01 mg/mL in ethanol, and open triangle: 1 mg/mL acetonitrile) versus time. The relative size was determined by DLS. The sameple solution was slowly cooled from 75 °C to room temperature during the measurement.

The sizes after 12 h of aging: 390.5 nm (1 mg/mL in ethanol), 437.8 nm (0.01 mg/mL in ethanol), 183.7 nm (1 mg/mL in acetonitrile).

Therefore, we investigated the CDSA of [DLA_{16}]-[LLA_{16}]-*b*-PEG in acetonitrile to exploit the slower rate of crystallization of PLA blocks than that in ethanol. Upon examining the results of CDSA of [DLA_{16}]-[LLA_{16}]-*b*-PEG at the concentration of 1 mg/mL in acetonitrile, we discovered well-defined 2D triangular structures by AFM (Figure 3-5a). Analyzing the height profiles of the AFM images showed that the thickness of the triangles was 4.5 ± 0.4 nm (Figure 3-5c), indicating that chain-folding occurred at 16 repeating units via intramolecular SCN of [DLA_{16}]-[LLA_{16}] blocks. When the concentration of the BCP was increased to 2.5 mg/mL in acetonitrile, the CDSA resulted in the formation of platelets having an average thickness of 9 ± 0.6 nm (Figure 3-5b,d), which indicated the intermolecular SCN of completely stretched [DLA_{16}]-[LLA_{16}] blocks. These results strongly suggested that the attenuation of intermolecular interactions in the BCP is critical for ensuring that the chain-folding of [DLA_{16}]-[LLA_{16}] blocks occurs predominantly via intramolecular SC formation.

The presence of folded [DLA_{16}]-[LLA_{16}] in the triangular crystallites was supported by the results of CDSA performed using an equimolar mixture of stereopure [DLA_{16}] and [LLA_{16}]-*b*-PEG in acetonitrile (1 mg of the blend/mL). The CDSA of this blend resulted in the formation of irregularly shaped platelets having thicknesses of 4.5 ± 0.5 nm as measured by AFM (Figure S7). This result confirmed that the reduced thickness exhibited by the platelets of [DLA_{16}]-[LLA_{16}]-*b*-PEG self-assembled in a dilute solution was a result of the crystallization of folded stereoblock PLAs due to the intramolecular SCN of [DLA_{16}] and [LLA_{16}] domains.

The XRD patterns of the triangles of [DLA_{16}]-[LLA_{16}]-*b*-PEG formed in acetonitrile indicated the presence of SCs of [DLA_{16}]-[LLA_{16}] in the triangular crystallites (Figure 3-5e). The SCN of stereoblock PLAs during the CDSA of the BCP was also suggested by the value of the T_m of the self-assembled structures of [DLA_{16}]-[LLA_{16}]-*b*-PEG in acetonitrile, which was significantly higher in comparison to that of BCPs having a stereopure [LLA_{32}] block (Figure 3-5f).

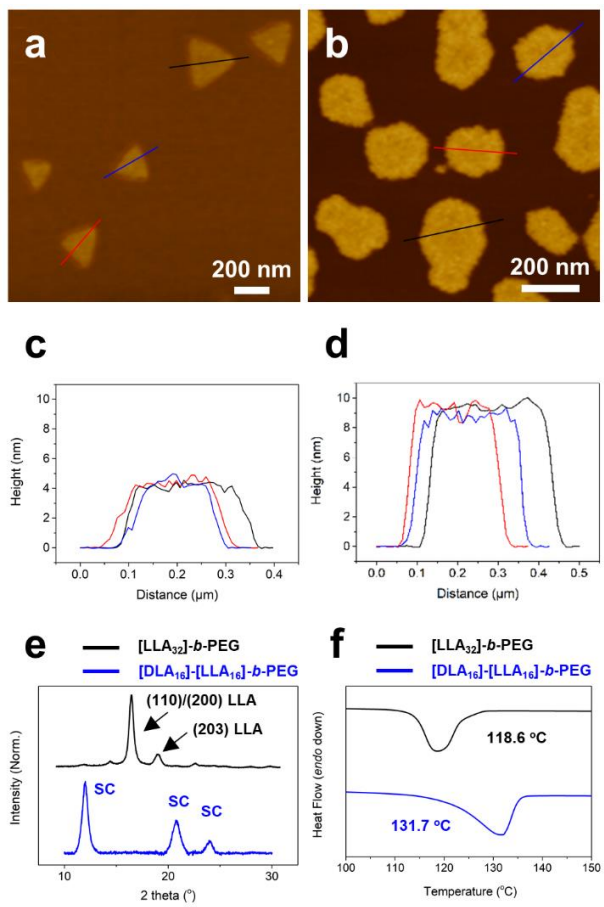

Figure 3-5. 2D nanostructures obtained from the CDSA of [DLA_{16}]-[LLA_{16}]-*b*-PEG (Acetonitrile, 75 °C, slow cooling, 16 h aging, dilution with water). (a–d) AFM images, and height profiles of defined nanostructures. (a,

c) 1 mg/mL, (b, d) 2.5 mg/mL. (e) XRD patterns of the crystallite obtained from [LLA_{32}]-*b*-PEG and [DLA_{16}]-[LLA_{16}]-*b*-PEG in acetonitrile solution. (f) Differential scanning calorimetry (DSC) thermograms (second heating scans, ramp rate = 10 ºC min^{-1}, T_m) of the nanostructures prepared by the CDSA of [LLA_{32}]-*b*-PEG and [DLA_{16}]-[LLA_{16}]-*b*-PEG.

The DSC thermograms recorded for the collected triangles of [DLA_{16}]-[LLA_{16}]-*b*-PEG exhibited a T_m of 129.7 ºC (**ΔH_{fus}** = 35.9 J/g) during the first heating scan, which shifted to 131.7 ºC (**ΔH_{fus}** = 23.3 J/g) during the second heating scan and remained unchanged during the third heating scan (Figure S8a). In contrast, the T_ms of the first and second heating scans of the SC of [DLA_{16}] and [LLA_{16}]-*b*-PEG were nearly identical at 137.5 ºC (**ΔH_{fus}** = 42.6 J/g) (Figure S8b).

CDSA of a BCP containing [DLA_{24}]-[LLA_{24}]. The formation of unilamellar structures of folded stereoblock PLA in CDSA may precisely control the thickness of the crystallites by changing the number of repeating units in the [DLA_n] and [LLA_n] domains. Therefore, the effect of the number of repeating units of the stereoblocks on their SCN was investigated by analyzing the CDSA results of [DLA_{24}]-[LLA_{24}]-*b*-PEG. Following CDSA in acetonitrile (1 mg/mL, 0.180 μmol), we only observed small nanoparticles of [DLA_{24}]-[LLA_{24}]-*b*-PEG in TEM and AFM analyses (Figure S9), which was reminiscent of the particulates formed by the CDSA of a blend of [DLA_{32}]-*b*-PEG and [LLA_{32}]-*b*-PEG driven by the intermolecular SCN between stereopure PLA blocks.[14] The change in the mean diameter during the CDSA of [DLA_{24}]-[LLA_{24}])-*b*-PEG in acetonitrile (1 mg/mL) demonstrated that the size of crystallites rapidly increased and plateaued in 4 h, indicating more rapid intermolecular crystallization than that of [DLA_{16}]-[LLA_{16}]-*b*-PEG under identical condition (Figure S10). To

retard the rapid crystallization of the BCP, we performed the CDSA of [DLA_{24}]-[LLA_{24}]-*b*-PEG in an acetonitrile/chloroform mixture (9:1 v/v), utilizing the high affinity of chloroform toward PLA blocks. In the presence of chloroform as a solubilizing agent for PLA blocks, the DLS analysis of the average diameter of self-assembled structures indicated the retarded crystallization of BCPs (Figure S10). The TEM and AFM analyses of the BCP solution after CDSA showed necklace-like structures composed of linearly aggregated particulate crystallites (Figure S9). Further increase of the chloroform content in the solvent mixture (20% v/v) did not result in the formation of aggregates of [DLA_{24}]-[LLA_{24}]-*b*-PEG following CDSA.

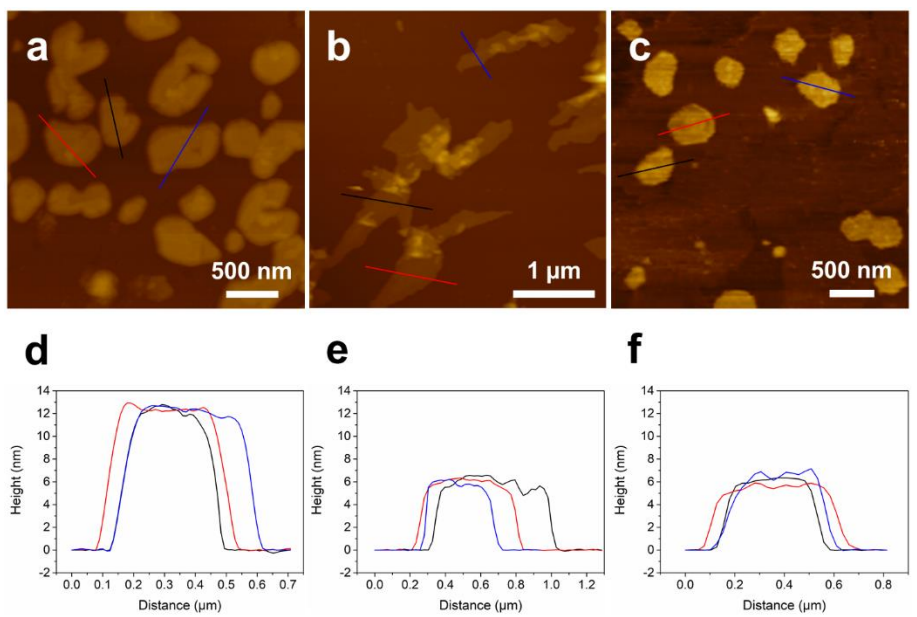

Figure 3-6. 2D nanostructures obtained from the CDSA of [DLA_{24}]-[LLA_{24}]-*b*-PEG (IPA/THF 9:1 or 3:1 vol %, 75°C, slow cooling, 24 h aging, dilution with water). (a–c) AFM images, (d–f) height profiles of nanostructures. (a, d) 1 mg/mL (IPA/THF 9:1 vol %), (b, e) 0.01 mg/mL (IPA/THF 9:1 vol %), (c, f) 1 mg/mL (IPA/THF 3:1 vol %).

We changed the solvent for the CDSA of [DLA_{24}]-[LLA_{24}]-*b*-PEG from acetonitrile to isopropyl alcohol (IPA) with tetrahydrofuran (THF) as a cosolvent, which further suppresses the intermolecular aggregation of the BCP during the CDSA (Figure S11). The CDSA of the BCP at 1 mg/mL in an IPA/THF mixture (9:1 vol%) resulted in the formation of ill-defined shaped crystallites (Figure S12). The average thickness of these crystallites was determined by AFM analysis to be 13 ± 0.5 nm (Figure 3-6a, d), which coincided with the length of stretched PLA having 48 repeating units. This result indicated that the formation of crystallites by CDSA in IPA and THF was driven by the regular packing of the stretched [DLA_{24}]-[LLA_{24}] blocks by their intermolecular SCN. Using an identical solvent mixture, reducing the concentration of BCP to 0.01 mg/mL resulted in the formation of needle-shaped crystallites of [DLA_{24}]-[LLA_{24}]-*b*-PEG by CDSA (Figure 3-6b). The AFM height profiles of these structures revealed their thickness to be 5.9 ± 0.4 nm, indicating the crystallization of folded [DLA_{24}]-[LLA_{24}] blocks (Figure 3-6e). An identical thickness was exhibited by the crystallites formed by the CDSA of the same BCP in a mixture of IPA and THF (3:1 v/v) (Figure 3-6c,f). These results proved that the thickness of the unilamellar crystallite of folded stereoblock PLAs is directly proportional to the number of repeating units of [DLA_n] and [LLA_n] domains, which could be unambiguously defined by the synthesis of stereoblock PLA. The DSC thermograms of the nanostructures prepared by the CDSA of [DLA_{24}]-[LLA_{24}]-*b*-PEG (1 mg/mL in IPA/THF 3:1 vol %) showed a T_m of 164.7 ºC (**(**ΔH_{fus} = 42.0 J/g) during the first heating scan, which shifted to 165.5 ºC (**(**ΔH_{fus} = 25.9 J/g) during the second heating scan (Figure S13). This tendency in which T_m obtained from first heating scan is lower than second heating scan is also observed from the triangular crystallites of [DLA_{16}]-[LLA_{16}]-*b*-PEG (Figure S8a). The XRD patterns of the crystallites demonstrated the SCN of [DLA_{24}]-[LLA_{24}] (Figure S14).

Apex-labeling of folded stereoblock PLAs. To confirm that the intramolecular SCN of [DLA_{16}]-[LLA_{16}] is a prerequisite for the formation of thin (4.5 ± 0.3 nm) crystallites in dilute solutions, we synthesized model stereoblock PLAs by incorporating a single *rac*-vinyllactic acid (*rac*VLA) unit between the [DLA_{16}] and [LLA_{16}] domains (Figure 3-7a).[49,50] The successful synthesis of [DLA_{16}]-*rac*VLA-[LLA_{16}]-*b*-PEG was confirmed by MALDI-TOF mass analysis and ^{1}H NMR (Figure 3-8 and S15–18).

For labelling using fluorescent dyes, we converted the vinyl group of [DLA_{16}]-*rac*VLA-[LLA_{16}]-*b*-PEG to an amino group by reacting the BCP with cysteamine by the thiol-ene click reaction in the presence of 2,2-dimethoxy-2-phenylacetophenone.[34] The complete conversion of the vinyl group of the BCP [DLA_{16}]-*rac*VLA^{NH2}-[LLA_{16}]-*b*-PEG was confirmed by the MALDI-TOF analysis showing the increase of the mass peaks of the parent BCPs by 77 Da, which corresponds to the mass of cysteamine (Figure 3-8b).

We expected that the presence of *rac*VLA^{NH2} unit in the middle (17th monomer) of the stereoblock PLA would prevent the intermolecular SCN of [DLA_{16}]-*rac*VLA^{NH2}-[LLA_{16}] during the CDSA of the BCP. We hypothesized that this forced intramolecular SCN of [DLA_{16}]-*rac*VLA^{NH2}-[LLA_{16}] would expose an amine by placing the *rac*VLA^{NH2} unit at the apex of the folded PLA (Figure 3-7b). The CDSA of [DLA_{16}]-*rac*VLA^{NH2}-[LLA_{16}]-*b*-PEG in ethanol (1 mg/mL, 0.217 μmol) resulted in the formation of 2D crystallites of folded [DLA_{16}]-*rac*VLA^{NH2}-[LLA_{16}] (4.1 ± 0.3) (Figure 3-9a–c). In comparison to the formation of the crystallites of completely stretched stereoblock PLAs from the CDSA of [DLA_{16}]-[LLA_{16}]-*b*-PEG in 1 mg/mL ethanol solution (Figure 3-3a,c,e), this result indicates that the additional *rac*VLA^{NH2} unit causes steric repulsion between stereoblock

PLAs, resulting in the exclusive intramolecular SCN between [DLA_{16}] and [LLA_{16}] domains.

The exclusive formation of the crystallites of folded [DLA_{16}]-*rac*VLA^{NH2}-[LLA_{16}] during CDSA suggested that the *rac*VLA^{NH2} unit placed between [DLA_{16}] and [LLA_{16}] domains may be located at the apex of the folded PLA block in order to maximize the interaction caused by the intramolecular SCN between stereoblocks having identical numbers of enantiomeric repeating units. Upon the crystallization of the aforementioned folded PLA block, *rac*VLA^{NH2} units should be placed on the surface of the crystallites formed by CDSA of the BCP.

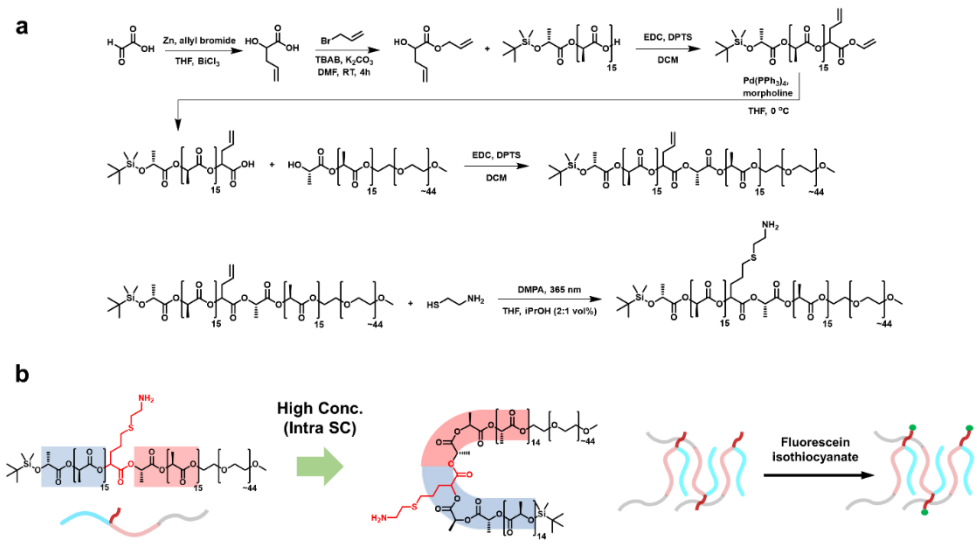

Figure 3-7. (a) Synthesis of [DLA_{16}]-*rac*VLA^{NH2}-[LLA_{16}]-*b*-PEG. (b) Schematic representation of the intramolecular stereocomplexation and apex-labeling of [DLA_{16}]-*rac*VLA^{NH2}-[LLA_{16}]-*b*-PEG.

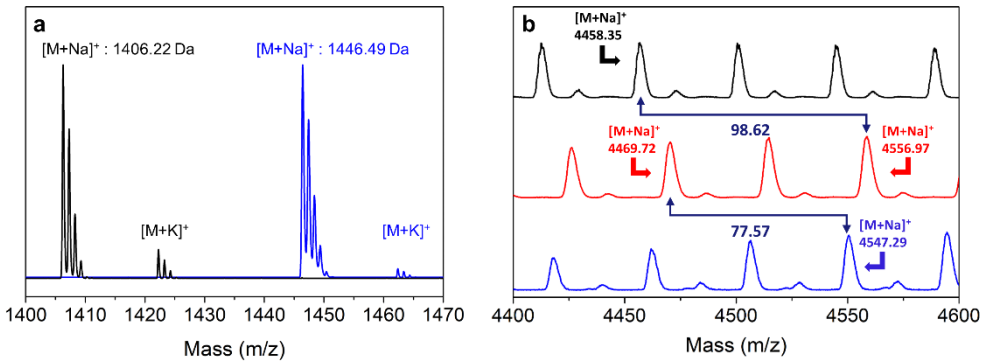

Figure 3-8. (a) MALDI-TOF spectra of [DLA_{16}]-*rac*VLA-allyl (blue) and [DLA_{16}]-*rac*VLA (black). (b) Combined MALDI-TOF spectra of [DLA_{16}]-[LLA_{16}]-*b*-PEG (black), [DLA_{16}]-*rac*VLA-[LLA_{16}]-*b*-PEG (red), and [DLA_{16}]-*rac*VLA^{NH2}-[LLA_{16}]-*b*-PEG (blue). Mass of VLA–H_2O: 98.10 Da, cysteamine: 77.15 Da.

The crystallites of [DLA_{16}]-*rac*VLA^{NH2}-[LLA_{16}]-*b*-PEG were labeled using fluorescent dyes by selectively reacting the amino groups of the crystallites of the BCP with fluorescein isothiocyanate (5 eq.).[34] Following the removal of unreacted labeling reagents by dialysis, the resulting solution was examined by confocal laser scanning microscopy (CLSM). We observed that the crystallites were fluorescently labeled, which indicated that the amino groups of the *rac*VLA^{NH2} units were located at the apexes of the folded stereoblock PLAs, and, consequently, were exposed to the surfaces of the crystallites (Figure 3-9d).

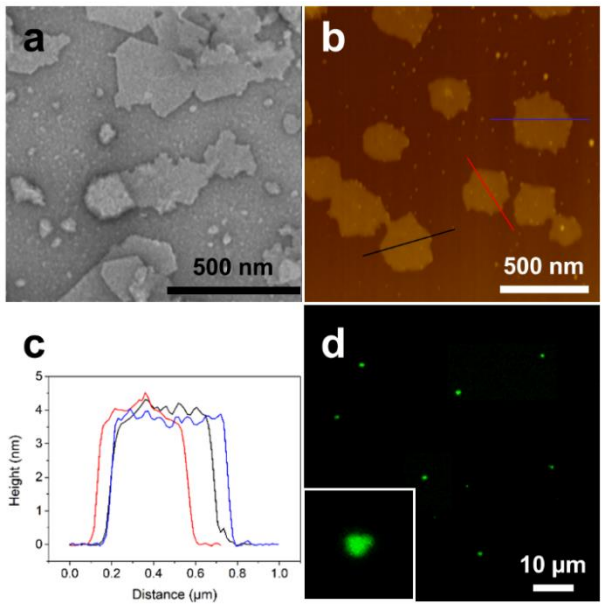

Figure 3-9. 2D nanostructures obtained from the CDSA of (a–c) [DLA$_{16}$]-*rac*VLA^{NH2}-[LLA$_{16}$]-*b*-PEG and (d) [DLA$_{16}$]-*rac*VLA^{F}-[LLA$_{16}$]-*b*-PEG (1 mg/mL in ethanol, 75 °C, slow cooling, 16 h aging, dilution with water). (a) TEM image, (b,c) AFM images and height profiles, (d) CLSM image of the nanostructures.

3.4 Conclusion

In this work, we demonstrated the controlled chain-folding of stereoblock PLAs composed of two oLA domains, [DLA$_n$] and [LLA$_n$], built using precisely defined numbers of D- and L-lactic acids. The discrete stereoblock PLAs were synthesized in a molecular weight- and sequence-defined manner by the convergent synthetic approach. The resulting stereoblock PLAs were conjugated with PEG to form BCPs that self-assembled into unilamellar crystallites in solution, driven by the crystallization of stereoblock PLAs. We discovered that the intramolecular stereocomplexation between [DLA$_n$] and [LLA$_n$] resulted in the controlled folding of the stereoblock PLAs. The intramolecular SCN predominantly

occurred upon the suppression of intermolecular SCN of stereoblock PLAs by decreasing the concentration of BCPs or increasing the solubility of BCPs in solution. The thickness of the folded crystalline core of 2D nanostructures was proportional to the number of repeating units of the domains forming the stereocomplexes (SCs). The convergent synthesis of stereoblock PLAs permitted the addition of a single monomer unit between the [DLA_n] and [LLA_n] domains, which could be utilized to precisely introduce a specific desired functional group at the apex of the folded PLA block. Our results demonstrate that the encoding of information in the form of a monomer sequence can shape the polymer chain and guide its self-assembly toward nanostructures having the desired dimensions and functions.

3.5 Reference

1. Fox, S. W. Terminal Amino Acids in Peptides and Proteins. *Advances in Protein Chem.* **1945,** *2,* 155–177.

2. Sanger, F. Some Peptides from Insulin. *Nature* **1948,** *162,* 491–492.

3. Edman, P. Method for Determination of the Amino Acid Sequence in Peptides. *Acta Chem. Scand.* **1950,** *4,* 283–293.

4. Anfinsen, C. B. Principles that Govern the Folding of Protein Chains. *Science* **1973,** *181,* 223–230.

5. Anfinsen, C. B.; Scheraga, H. A. Experimental and Theoretical Aspects of Protein Folding. *Adv. Protein Chem.* **1975,** *29,* 205–300.

6. Lewis, P. N.; Momany, F. A.; Scheraga, H. A. Folding of Polypeptide Chains in Proteins: A Proposed Mechanism for Folding. *Proc. Natl. Acad. Sci. U.S.A.* **1971,** *68,* 2293–2297.

7. Karplus, M.; Weaver, D. L. Protein-folding dynamics. *Nature* **1976,** *260,* 404–406.

8. Storks, K. H. An electron-diffraction examination of some linear high polymers. *J. Am. Chem. Soc.* **1938,** *60,* 1753−1761.

9. Keller, A. A note on single crystals in polymers: Evidence of a folded-chain configuration. *Philos. Mag.* **1957,** *2,* 1171−1175.

10. Lotz, B.; Miyoshi, T.; Cheng, S. Z. D. 50th Anniversary Perspective: Polymer Crystals and Crystallization: Personal Journeys in a Challenging Research Field. *Macromolecules* **2017,** *50,* 5995–6025.

11. Tang, X.; Chen, W.; Li, L. The Tough Journey of Polymer Crystallization: Battling with Chain Flexibility and Connectivity. *Macromolecules* **2019,** *52,* 3575–3591.

12. Takizawa, K.; Nulwala, H.; Hu, J.; Yoshinaga, K.; Hawker, C. J. Molecularly Defined (L)-Lactic Acid Oligomers and Polymers: Synthesis and Characterization. *J. Polym. Sci., Part A: Polym. Chem.* **2008,** *46,* 5977−5990.

13. Lamers, B. A. G.; van Genabeek, B.; Hennissen, J.; de Waal, B. F. M.; Palmans, A. R. A.; Meijer, E. W. Stereocomplexes of Discrete, Isotactic Lactic Acid Oligomers Conjugated with Oligodimethylsiloxanes. *Macromolecules* **2019,** *52,* 1200–1209.

14. Kwon, Y.; Kim, K. T. Crystallization-Driven Self-Assembly of Block Copolymers Having Monodisperse Poly(lactic acid)s with Defined Stereochemical Sequences. *Macromolecules* **2021,** *54,* 10487−10498.

15. Wang, Z.; Cao, Y.; Song, J.; Xie, Z.; Wang, Y. Cooperation of Amphiphilicity and Crystallization for Regulating the Self-Assembly of Poly(ethylene glycol)-block-poly(lactic acid). *Langmuir* **2016,** *32,* 9633–9639.

16. He, X.; He, Y.; Hsiao, M.-S.; Harniman, R. L.; Pearce, S.; Winnik, M. A.; Manners, I. Complex and Hierarchical 2D Assemblies via Crystallization-Driven Self-Assembly of Poly(L-lactide) Homopolymers with Charged Termini. *J. Am. Chem. Soc.* **2017,** *139,* 9221−9228.

17. Inam, M.; Cambridge, G.; Pitto-Barry, A.; Laker, Z. P. L.; Wilson, N. R.; Mathers, R. T.; Dove, A. P.; O'Reilly, R. K. 1D vs. 2D shape selectivity in the crystallization-driven self-assembly of polylactide block copolymers. *Chem. Sci.* **2017,** *8,* 4223−4230.

18. Hurst, P. J.; Rakowski, A. M.; Patterson, J. P. Ring-opening polymerization-induced crystallization-driven self-assembly of poly-L-lactide-block-polyethylene glycol block copolymer (ROPI-CDSA). *Nat. Commun.* **2020,** *11,* 4690.

19. Inam, M.; Jones, J. R.; Pérez-Madrigal, M. M.; Arno, M. C.; Dove, A. P.; O'Reilly, R. K. Controlling the Size of Two-Dimensional Polymer Platelets for Water-in-Water Emulsifiers. *ACS Cent. Sci.* **2018,** *4,* 63−70.

20. Rizis, G.; van de Ven, T. G. M.; Eisenberg, A. "Raft" Formation by Two-Dimensional Self-Assembly of Block Copolymer Rod Micelles in Aqueous Solution. *Angew. Chem., Int. Ed.* **2014,** *53,* 9000−9003.

21. Han, L.; Wang, M.; Jia, X.; Chen, W.; Qian, H.; He, F. Uniform two-dimensional square assemblies from conjugated block copolymers driven by π−π interactions with controllable sizes. *Nat. Commun.* **2018**, *9*, 865–877.

22. Yang, S.; Kang, S.-Y.; Choi, T.-L. Morphologically Tunable Square and Rectangular Nanosheets of a Simple Conjugated Homopolymer by Changing Solvents. *J. Am. Chem. Soc.* **2019,** *141,* 19138–19143.

23. Sun, L.; Pitto-Barry, A.; Kirby, N.; Schiller, T. L.; Sanchez, A. M.; Dyson, M. A.; Sloan, J.; Wilson, N. R.; O'Reilly, R. K.; Dove, A. P. Structural reorganization of cylindrical nanoparticles triggered by polylactide stereocomplexation. *Nat. Commun.* **2014,** *5,* 5746.

24. Schmelz, J.; Schedl, A. E.; Steinlein, C.; Manners, I.; Schmalz, H. Length Control and Block-Type Architectures in Worm-like Micelles with Polyethylene Cores. *J. Am. Chem. Soc.* **2012,** *134,* 14217−14225.

25. Yu, W.; Foster, J. C.; Dove, A. P.; O'Reilly, R. K. Length Control of Biodegradable Fiber-Like Micelles via Tuning Solubility: A Self-Seeding Crystallization-Driven Self-Assembly of Poly(ϵ-Caprolactone)-Containing Triblock Copolymers. *Macromolecules* **2020,** *53,* 1514−1521.

26. Petzetakis, N.; Walker, D.; Dove, A. P.; O'Reilly, R. K. Crystallization-driven sphere-to-rod transition of poly(lactide)-b-poly(acrylic acid) diblock copolymers: mechanism and kinetics. *Soft matter* **2012,** *8,* 7408.

27. Sun, L.; Petzetakis, N.; Pitto-Barry, A. s.; Schiller, T. L.; Kirby, N.; Keddie, D. J.; Boyd, B. J.; O'Reilly, R. K.; Dove, A. P. Tuning the Size of Cylindrical Micelles from Poly(l-lactide)-b-poly(acrylic acid) Diblock Copolymers Based on Crystallization-Driven Self-Assembly. *Macromolecules* **2013,** *46,* 9074–9082.

28. Xu, L.; Wang, C.; Li, Y. X.; Xu, X. H.; Zhou, L.; Liu, N.; Wu, Z. Q. Crystallization-Driven Asymmetric Helical Assembly of Conjugated Block Copolymers and the Aggregation Induced White-light Emission and Circularly Polarized Luminescence. *Angew. Chem., Int. Ed.* **2020,** *59,* 16675−16682.

29. Gilroy, J. B.; Gädt, T.; Whittell, G. R.; Chabanne, L.; Mitchels, J. M.; Richardson, R. M.; Winnik, M. A.; Manners, I. Monodisperse Cylindrical Micelles by Crystallization-Driven Living Self-Assembly. *Nat. Chem.* **2010,** *2,* 566−570.

30. Wang, X.; Guerin, G.; Wang, H.; Wang, Y.; Manners, I.; Winnik, M. A. Cylindrical Block Copolymer Micelles and Co-Micelles of Controlled Length and Architecture. *Science* **2007,** *317,* 644−647.

31. Qiu, H.; Gao, Y.; Boott, C. E.; Gould, O. E. C.; Harniman, R. L.; Miles, M. J.; Webb, S. E. D.; Winnik, M. A.; Manners, I. Uniform Patchy and Hollow Rectangular Platelet Micelles from Crystallizable Polymer Blends. *Science* **2016,** *352,* 697−701.

32. Yang, S.; Kang, S.-Y.; Choi, T.-L. Semi-conducting 2D rectangles with tunable length via uniaxial living crystallization-driven self-assembly of homopolymer. *Nat Commun.* **2021,** *12,* 2602.

33. Yang, S.; Choi, T.-L. Rapid formation and real-time observation of micron-sized conjugated nanofibers with tunable lengths and widths in 20 minutes by living crystallization-driven self-assembly. *Chem. Sci.* **2020,** *11,* 8416–8424.

34. He, X.; Hsiao, M.-S.; Boott, C. E.; Harniman, R. L.; Nazemi, A.; Li, X.; Winnik, M. A.; Manners, I. Two-dimensional assemblies from crystallizable homopolymers with charged termini. *Nat. Mater.* **2017,** *16,* 481−489.

35. Song, S.; Zhou, H.; Hicks, G.; Jiang, J.; Zhang, Y.; Manners, I.; Winnik, M. A. An Amphiphilic Corona-Forming Block Promotes Formation of a Variety of 2D Platelets via Crystallization-Driven Block Copolymer Self-Assembly. *Macromolecules.* **2021,** *54,* 9761−9772.

36. Song, S.; Liu, X.; Nikbin, E.; Howe, J. Y.; Yu, Q.; Manners, I.; Winnik, M. A. Uniform 1D Micelles and Patchy & Block Comicelles via Scalable, One-Step Crystallization-Driven Block Copolymer Self-Assembly. *J. Am. Chem. Soc.* **2021,** *143,* 6266−6280.

37. He, Y.; Eloi, J.-C.; Harniman, R. L.; Richardson, R. M.; Whittell, G. R.; Mathers, R. T.; Dove, A. P.; O'Reilly, R. K.; Manners, I. Uniform Biodegradable Fiber-Like Micelles and Block Comicelles via "Living" Crystallization-Driven Self-Assembly of Poly(l-lactide) Block Copolymers: The Importance of Reducing Unimer Self-Nucleation via Hydrogen Bond Disruption. *J. Am. Chem. Soc.* **2019,** *141,* 19088–19098.

38. Nie, J. C.; Wang, Z. Q.; Huang, X. Y.; Lu, G. L.; Feng, C. Uniform Continuous and Segmented Nanofibers Containing A πconjugated Oligo(p-phenylene ethynylene) Core via "Living" Crystallization-driven Self-assembly: Importance of Oligo(p-phenylene ethynylene) Chain Length. *Macromolecules* **2020,** *53,* 6299−6313.

39. Hill, D. J.; Mio, M. J.; Prince, R. B.; Hughes, T. S.; Moore, J. S. A Field Guide to Foldamers. *Chem. Rev.* **2001,** *101,* 3893–4012.

40. Ouchi, M.; Badi, N.; Lutz, J.-F.; Sawamoto, M. Single-chain technology using discrete synthetic macromolecules. *Nat. Chem.* **2011,** *3,* 917–924.

41. Fukushima, T.; Tamaki, K.; Isobe, A.; Hirose, T.; Shimizu, N.; Takagi, H.; Haruki, R.; Adachi, S.-I.; Hollamby, M. J.; Yagai, S. Diarylethene-Powered Light-Induced Folding of Supramolecular Polymers. *J. Am. Chem. Soc.* **2021,** *143,* 5845–5854.

42. Tsuji, H. Poly(lactic acid) stereocomplexes: A decade of progress. *Adv. Drug. Deliv. Rev.* **2016,** *107,* 97–135.

43. Sun, C.; Zheng, Y.; Xu, S.; Ni, L.; Li, X.; Shan, G.; Bao, Y.; Pan, P. Role of Chain Entanglements in the Stereocomplex Crystallization between Poly(lactic acid) Enantiomers. *ACS Macro Lett.* **2021,** *10,* 1023–1028.

44. Bandelli, D.; Alex, J.; Weber, C.; Schubert, U. S. Polyester Stereocomplexes Beyond PLA: Could Synthetic Opportunities Revolutionize Established Material Blending? *Macromol. Rapid Commun.* **2020,** *41,* 1900560.

45. Rosen, T.; Goldberg, I.; Venditto, V.; Kol, M. Tailor-Made Stereoblock Copolymers of Poly(lactic acid) by a Truly Living Polymerization Catalyst. *J. Am. Chem. Soc.* **2016,** *138,* 12041–12044.

46. Rosen, T.; Goldberg, I.; Navarra, W.; Venditto, V.; Kol, M. Block–Stereoblock Copolymers of Poly(-Caprolactone) and Poly(Lactic Acid). *Angew. Chem., Int. Ed.* **2018,** *57,* 7191−7195.

47. Isono, T.; Kondo, Y.; Otsuka, I.; Nishiyama, Y.; Borsali, R.; Kakuchi, T.; Satoh, T. Synthesis and Stereocomplex Formation of Star-Shaped Stereoblock Polylactides Consisting of Poly(L-lactide) and Poly(D-lactide) Arms. *Macromolecules* **2013,** *46,* 8509–8518.

48. Okihara, T.; Tsuji, M.; Kawaguchi, A.; Katayama, K.-I.; Tsuji, H.; Hyon, S.-H.; Ikada, Y. Crystal structure of stereocomplex of poly(L-lactide) and poly(D-lactide). *J. Macromol.Sci., Part B: Phys.* **1991,** *30,* 119−140.

49. Leemhuis, M.; Akeroyd, N.; Kruijtzer, J. A. W.; van Nostrum, C. F.; Hennink, W. E. Synthesis and characterization of allyl functionalized poly(α-hydroxy)acids and their further dihydroxylation and epoxidation. *Eur. Polym. J.* **2008,** *44,* 308–317.

50. Franz, N.; Menin, L.; Klok, H.-A. A Post-Modification Strategy for the Synthesis of Uniform, Hydrophilic/Hydrophobic Patternedα-Hydroxy Acid Oligomers. *Eur. J. Org. Chem.* **2009,** *31,* 5390–5405.

Chapter 4. Micro-Sized Triangular Structures by Stacking of Stereocomplex

4.1 Abstract

Discrete polymers Herein, we fabricate mismatched stereoblock copolymer composed of two oligo(lactic acid) domains, [DLA_n] and [LLA_m] (n > m), by using an exact numbers of D- and L-lactic acids, respectively. Interestingly, stereoblock copolymer having a mismatch in lactic acid units formed micro-sized triangular structures. This is probably due to the stacking of stereocomplex which is induced by extra D-lactic acids constituting mismatched streoblock copolymers. The effect of the extra D-lactic acid unis in mismatched stereoblock copolymers were investigated by decreasing the extra units. Depending on the degree of extra units, size and thickness of assembled structures were changed. We believe that these results will help prepare materials of various sizes.

4.2 Introduction

Complete control over the number of monomers to form a discrete macromolecule is an important challenge in polymer chemistry.[1–4] Such macromolecules have precisely defined structures and can perform the functions of proteins and nucleic acids. They can also overcome the intrinsic uncertainty arising from the statistical distribution of the chemical structures of synthetic polymers. In addition, the study of discrete polymers having an exact number of monomers could revolutionize our understanding of how macromolecules behave, function, and interact in the environments required for new applications.[5–9] Due to the statistical nature of polymerization, the synthesis of discrete polymers mainly involves repetitive addition of individual monomers.[10–14] Recently, exponential growth has been witnessed

in the synthesis of linear polymers by iterative convergence of orthogonally protected repeating units.[15–20] In addition, many studies have investigated the synthesis of discrete polymers by protection or chromatography-free convergence.[21–23]

Crystallization-driven self-assembly (CDSA) of crystalline block copolymers has aroused great interest as the method to precisely control shape and dimension of materials.[24–26] The impact of crystallinity in discrete block copolymers was investigated by the CDSA of block copolymers with monodisperse crystalline core-forming block.[27–29] Self-assembly of discrete block copolymers showed uniform nanostructures, however such uniformity of assembled structures decreased when disperse block was used for self-assembly.

Recently, we have demonstrated that the shape and thickness of 2D structures could be controlled by the stereocomplexation between enantiomeric discrete poly(lactic acid)s (PLA).[30,31] Interestingly, co-self-assembly of complementarily configured discrete PLAs having a mismatch in the size formed uniform nanostructures by attenuating the crystallization kinetics.[30] Herein, we report the CDSA of mismatched stereoblock copolymers composed of discrete oligo(lactic acid)s, [DLA_n] and [LLA_m] ($n > m$). To examine the effect of extra DLAs on the self-assembled structures, we synthesized a series of mismatched stereoblock copolymers by iterative convergent method and analyzed the crystallite resulted from the CDSA of [DLA_n]-[LLA_m]-*b*-PEG. The mismatching in stereoblock leads to the uniform and micro-sized triangular structures. Extra DLAs inducing stacking of stereocomplex resulted in the formation of micro-sized structures. We suggested two crystal models on the basis of observed structures and x-ray diffraction (XRD) patterns.

Scheme 4-1. Iterative Convergent Syntheses of Stereopure Discrete Oligo(lactic acid)s and mismatched stereoblock copolymers.

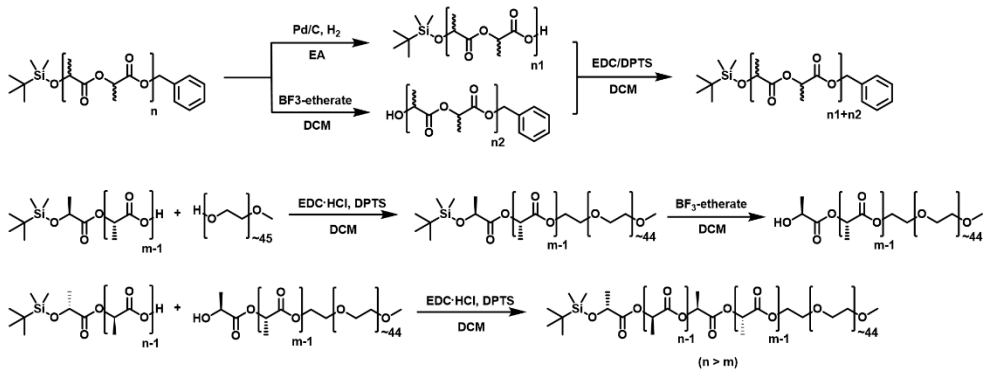

4.3 Results and Discussion

CDSA of Mismatched Stereoblock Copolymer Containing [DLA$_n$]-[LLA$_m$] (n>m). Discrete isotactic oligo(L-lactic acid) (oLLA) and oligo(D-lactic acid) (oDLA) comprising up to 32 repeating units were synthesized by the iterative convergent pathway.[15,16] [LLA$_{16}$] was initially conjugated with polyethylene glycol (PEG) (M_n = 2,000 g mol^{-1}, $Đ$ = 1.04) to improve the yield of stereoblock copolymers (Scheme 4-1). The as-synthesized [LLA$_{16}$]-*b*-PEG was deprotected and coupled with [DLA$_n$] to synthesize mismatched stereoblock copolymers. The mismatched stereoblock copolymers were characterized by circular dichroism (CD), and matrix-assisted laser desorption/ionization-time-of-flight (MALDI-TOF) mass spectrometry (Figure 4-1).

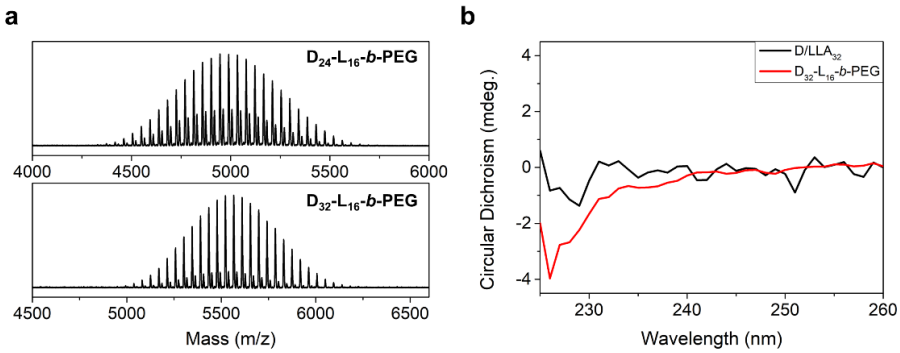

Figure 4-1. (a) Combined MALDI-TOF spectra of [DLA$_n$]-[LLA$_m$]-*b*-PEG. (b) CD spectra of [D/LLA$_{32}$], and [DLA$_{32}$]-[LLA$_{16}$]-*b*-PEG.

Firstly, the assembled structures obtained by the CDSA of [DLA$_{32}$]-[LLA$_{16}$]-*b*-PEG (ethanol, 75 °C for 8 h, cooling to 25 °C at a rate of 0.2 °C/min, aging for 12h) were investigated by transmission electron microscopy (TEM) and scanning electron microscopy (SEM). The TEM and SEM images obtained from the ethanol solution of [DLA$_{32}$]-[LLA$_{16}$]-*b*-PEG after CDSA showed the formation of micro-sized triangular structures (Figure 4-2a,b). While the previous study reported that triangular nanostructures were formed by the co-self-assembly of [DLA$_{72}$]-*b*-PEG/[LLA$_{64}$]-*b*-PEG (1:1 mol/mol) or intramolecular stereocomplexation of [DLA$_{16}$]-[LLA$_{16}$]-*b*-PEG, the formation of micro-sized structures is possibly due to the extra D-lactic acid units. The micro-sized structures of [DLA$_{32}$]-[LLA$_{16}$]-*b*-PEG were analyzed by atomic force microscopy (AFM) by placing the crystallites on silicon oxide wafer substrate. The AFM images of the self-assembled structures of [DLA$_{32}$]-[LLA$_{16}$]-*b*-PEG conform with the morphology observed by TEM and SEM (Figure 4-2c). We estimated the thickness of stereoblock copolymer crystallites on a silicon substrate using height profiles of the AFM images of the micro-sized structures recorded in a contact mode (Figure 4-2d). The thickness of the micro-sized structure was ~500 nm high from the silicon substrate.

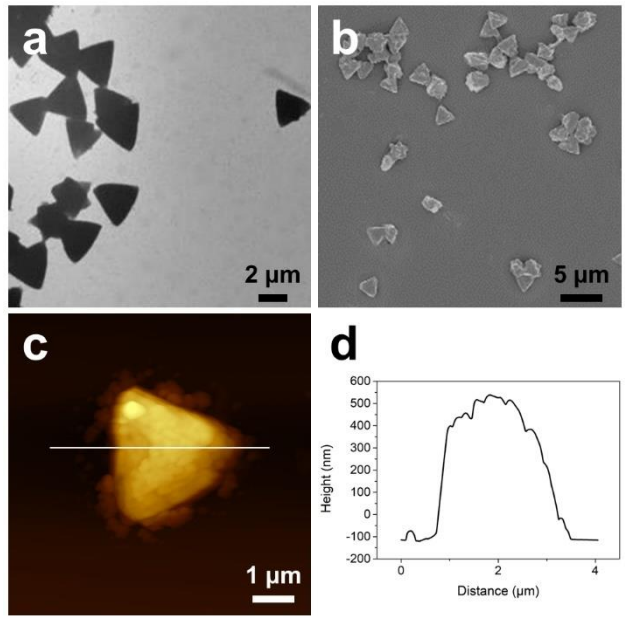

Figure 4-2. Micro-sized triangular structures obtained from the CDSA of [DLA_{32}]-[LLA_{16}]-*b*-PEG (ethanol, 75 ºC, slow cooling, 12 h aging). (a) TEM image, (b) SEM image, (c,d) AFM image and height profile of micro-sized structure.

The XRD pattern of the micro-sized triangular structures showed the stereocomplexation of [DLA_{32}]-[LLA_{16}]-*b*-PEG (Figure 4-3). Interestingly, not only stereocomplex peaks (12.0º, 20.8º, 24.1º), but a peak representing the diffraction of extra DLA (110)/(200) planes was observed at 16.8º.[32,33] This result means that the crystallization of extra DLAs contributed to the micro-sized triangular structures.

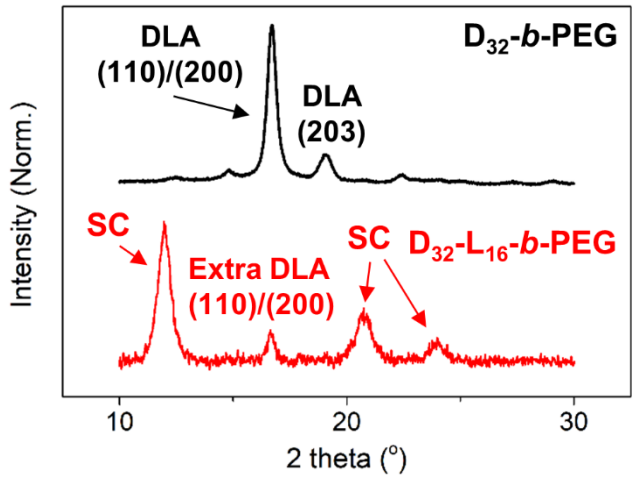

Figure 4-3. XRD patterns of the crystallite obtained from [DLA_{32}]-*b*-PEG and [DLA_{32}]-[LLA_{16}]-*b*-PEG in ethanol solution.

To investigate the effect of the degree of extra units on the CDSA, we decreased the number of D-lactic acids in mismatched stereoblock copolymers from 32 to 24 units and analyzed the CDSA results of [DLA_{24}]-[LLA_{16}]-*b*-PEG. The TEM images obtained from the CDSA of [DLA_{24}]-[LLA_{16}]-*b*-PEG also showed micro-sized triangular structures but decrease in size and thickness (Figure 4-4). This result suggested that the reduced number of D-lactic acids in mismatched stereoblock copolymers decrease stacking of stereocomplex.

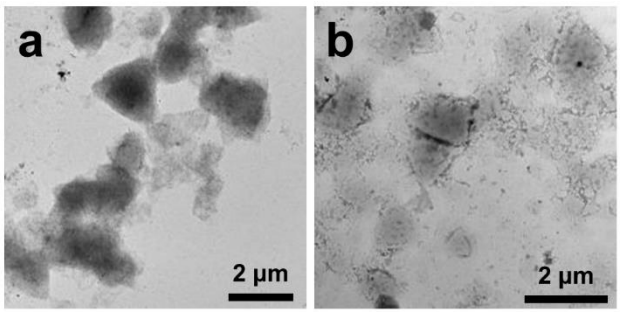

Figure 4-4. Micro-sized triangular structures obtained from the CDSA of [DLA_{24}]-[LLA_{16}]-*b*-PEG (ethanol, 75 ºC, slow cooling, 12 h aging). (a,b) TEM images of micro-sized structure.

The XRD pattern obtained from the CDSA of [DLA_{24}]-[LLA_{16}]-*b*-PEG indicated the formation of stereocomplex (Figure 4-5a). But the peak at 16.8 ºC representing the diffraction of extra DLA (110)/(200) planes almost disappeared. This difference in crystal structures might lead to the decrease of stacking of stereocomplex. Stereocomplexation was also confirmed by the differential scanning calorimetry (DSC) measurement of the melting temperature (T_m) of [DLA_{24}]-[LLA_{16}]-*b*-PEG. The ethanol solution of stereoblock copolymers after CDSA was dried and used for DSC analysis. The second heating scan of mismatched stereoblock copolymers by DSC showed a T_m of 140.2 °C, which was slightly higher than [DLA_{32}] homopolymer (T_m = 135.3 °C) (Figure 4-5b). Such an increase in the T_m of mismatched stereoblock copolymers indicates the formation of stereocomplex in solution. Comparing it with stereoblock copolymers having DLA_{16} and LLA_{16},[31] the increase of T_m of [DLA_{24}]-[LLA_{16}]-*b*-PEG (4.9 ºC) was much less than that of [DLA_{16}]-[LLA_{16}]-*b*-PEG (13.1 ºC). This result means that the degree of stereocomplexation was diminished by the mismatched lactic acid units.

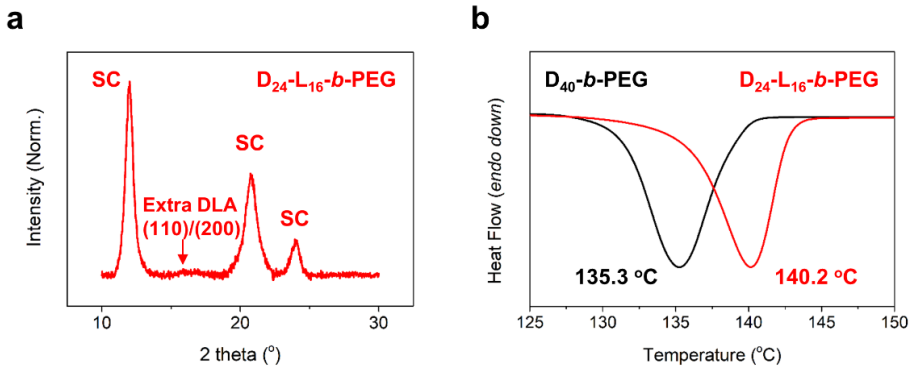

Figure 4-5. (a) XRD pattern of the crystallite obtained from [DLA_{24}]-[LLA_{16}]-*b*-PEG in ethanol solution. (b) DSC thermograms of the self-assembled structures prepared by the CDSA of [DLA_{40}]-*b*-PEG and [DLA_{24}]-[LLA_{16}]-*b*-PEG.

Crystal models of Mismatched Stereoblock Copolymers [DLA_{32}]-[LLA_{16}]-*b*-PEG. Based on these micro-sized structures and the XRD results, a schematic representation of crystal models is suggested (Figure 4-6). After the formation of intermolecular stereocomplex, homo-crystallization of extra DLAs in mismatched stereoblock copolymers could induce stacking of stereocomplex (Figure 4-6a). Considering the noticeable diffraction of extra DLAs obtained from XRD analysis, crystal layers of extra DLAs in the middle of stereocomplex are resonable. Micro-sized structures could also be triggered by stereocomplexation of extra DLAs (Figure 4-6b). Following the stereocomplexation between the mismatched stereoblocks, extra DLAs which did not participate in stereocomplexation formed additional stereocomplex with another mismatched stereoblock.

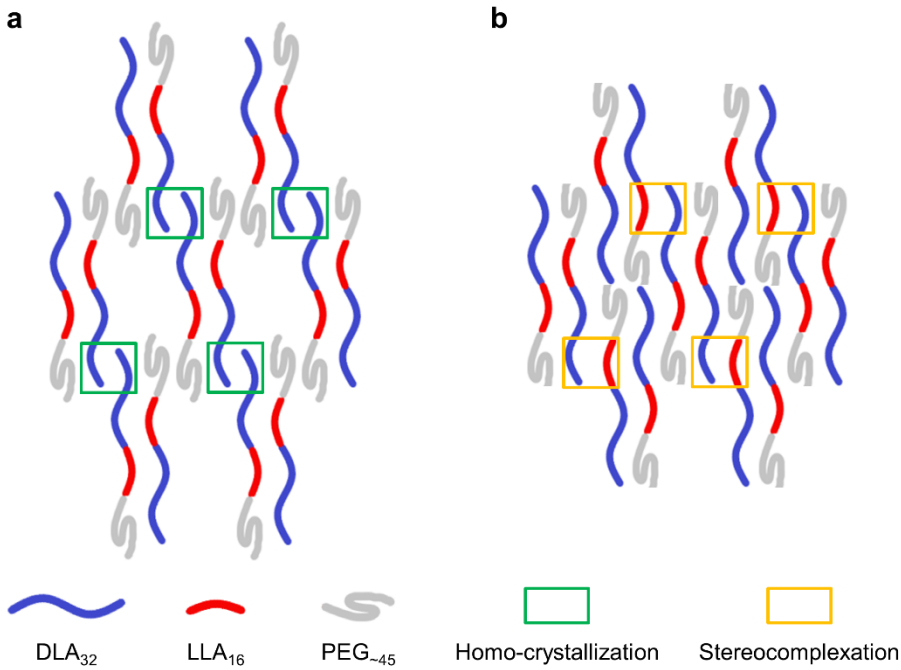

Figure 4-6. Schematic representation of the crystal models for [DLA_{32}]-[LLA_{16}]-*b*-PEG. Stacking of stereocomplex is induced by (a) homo crystallization or (b) stereocomplexation of extra DLA units.

4.4 Conclusion

In summary, we synthesized mismatched stereoblock copolymers with [DLA_n], [LLA_m] (n > m), and PEG. Self-assembly of [DLA_{32}]-[LLA_{16}]-*b*-PEG copolymers formed micro-sized triangular structures with a thickness of several hundred nanometers by stacking of stereocomplex. The contribution of extra DLAs in mismatched stereoblock copolymers to micro-sized structures was identified using XRD analysis. The diffraction of extra DLA (110)/(200) planes was observed along with the stereocomplex. CDSA of [DLA_{24}]-[LLA_{16}]-*b*-PEG showed that the size and thickness of microstructures were reduced. Decreasing the number of extra DLAs in mismatched stereoblock copolymers reduced the degree of stacking. We suggested two crystal models of mismatched stereoblock copolymers based

on the observed structures and the XRD results. We believe that our results provide a means to prepare materials of various sizes.

4.5 Reference

1. Ouchi, M.; Badi, N.; Lutz, J.-F.; Sawamoto, M. Single-chain technology using discrete synthetic macromolecules. *Nat. Chem.* **2011,** *3,* 917–924.

2. Lutz, J.-F.; Ouchi, M.; Liu, D. R.; Sawamoto, M. Sequence-Controlled Polymers. *Science* **2013,** *341,* 1238149–1238149.

3. Lodge, T. P. Celebrating 50 Years of Macromolecules. *Macromolecules* **2017,** *50,* 9525–9527.

4. Solleder, S. C.; Schneider, R. V.; Wetzel, K. S.; Boukis, A. C.; Meier, M. A. R. Recent Progress in the Design of Monodisperse, Sequence-Defined Macromolecules. *Macromol. Rapid Commun.* **2017,** *38,* 1600711.

5. Knight, A. S.; Zhou, E. Y.; Francis, M. B.; Zuckermann, R. N. Sequence Programmable Peptoid Polymers for Diverse Materials Applications. *Adv. Mater.* **2015,** *27,* 5665–5691.

6. Lutz, J.-F.; Lehn, J.-M.; Meijer, E. W.; Matyjaszewski, K. From precision polymers to complex materials and systems. *Nat. Rev. Mater.* **2016,** *1,* 16024.

7. Oschmann, B.; Lawrence, J.; Schulze, M. W.; Ren, J. M.; Anastasaki, A.; Luo, Y.; Nothling, M. D.; Pester, C. W.; Delaney, K. T.; Connal, L. A.; McGrath, A. J.; Clark, P. G.; Bates, C. M.; Hawker, C. J. Effects of Tailored Dispersity on the Self-Assembly of Dimethylsiloxane–Methyl Methacrylate Block Co-Oligomers. *ACS Macro Lett.* **2017,** *6,* 668–673.

8. van Genabeek, B.; de Waal, B. F. M.; Ligt, B.; Palmans, A. R. A.; Meijer, E. W. Dispersity under Scrutiny: Phase Behavior Differences between Disperse and Discrete Low Molecular Weight Block Co-Oligomers. *ACS Macro Lett.* **2017,** *6,* 674–678.

9. Golder, M. R.; Jiang, Y.; Teichen, P. E.; Nguyen, H. V. T.; Wang, W.; Milos, N.; Freedman, S. A.; Willard, A. P.; Johnson, J. A. Stereochemical Sequence Dictates Unimolecular Diblock Copolymer Assembly. *J. Am. Chem. Soc.* **2018,** *140,* 1596–1599.

10. Laurent, E.; Amalian, J.-A.; Parmentier, M.; Oswald, L.; Al Ouahabi, A.; Dufour, F.; Launay, K.; Clément, J.-L.; Gigmes, D.; Delsuc, M.-A.; Charles, L.; Lutz, J.-F. High-Capacity Digital Polymers: Storing Images in Single Molecules. *Macromolecules* **2020,** *53,* 4022–4029.

11. Porel, M.; Thornlow, D. N.; Phan, N. N.; Alabi, C. A. Sequence-defined bioactive macrocycles via an acid-catalysed cascade reaction. *Nat. Chem.* **2016,** *8,* 590–596.

12. Al Ouahabi, A.; Charles, L.; Lutz, J.-F. Synthesis of Non-Natural Sequence-Encoded Polymers Using Phosphoramidite Chemistry. *J. Am. Chem. Soc.* **2015,** *137,* 5629–5635.

13. Merrifield, R. B. Solid Phase Peptide Synthesis. I. The Synthesis of a Tetrapeptide. *J. Am. Chem. Soc.* **1963,** *85,* 2149–2154.

14. Roy, R. K.; Meszynska, A.; Laure, C.; Charles, L.; Verchin, C.; Lutz, J.-F. Design and synthesis of digitally encoded polymers that can be decoded and erased. *Nat. Commun.* **2015,** *6,* 7237.

15. Takizawa, K.; Tang, C.; Hawker, C. J. Molecularly Defined Caprolactone Oligomers and Polymers: Synthesis and Characterization. *J. Am. Chem. Soc.* **2008,** *130,* 1718–1726.

16. Takizawa, K.; Nulwala, H.; Hu, J.; Yoshinaga, K.; Hawker, C. J. Molecularly defined (L)-lactic acid oligomers and polymers: Synthesis and characterization. *J. Polym. Sci., Part A: Polym. Chem.* **2008,** *46,* 5977–5990.

17. Hawker, C. J.; Malmström, E. E.; Frank, C. W.; Kampf, J. P. Exact Linear Analogs of Dendritic Polyether Macromolecules: Design, Synthesis, and Unique Properties. *J. Am. Chem. Soc.* **1997,** *119,* 9903–9904.

18. Grayson, S. M.; Fréchet, J. M. J. Convergent Dendrons and Dendrimers: from Synthesis to Applications. *Chem. Rev.* **2001,** *101,* 3819–3868.

19. Binauld, S.; Damiron, D.; Connal, L. A.; Hawker, C. J.; Drockenmuller, E. Precise Synthesis of Molecularly Defined Oligomers and Polymers by Orthogonal Iterative Divergent/Convergent Approaches: Precise Synthesis of Molecularly Defined Oligomers and Polymers. *Macromole. Rapid Commun.* **2011,** *32,* 147–168.

20. Hawker, C. J.; Frechet, J. M. J. Preparation of polymers with controlled molecular architecture. A new convergent approach to dendritic macromolecules. *J. Am. Chem. Soc.* **1990,** *112,* 7638–7647.

21. Zhang, H.; Li, X.; Shi, Q.; Li, Y.; Xia, G.; Chen, L.; Yang, Z.; Jiang, Z.-X. Highly Efficient Synthesis of Monodisperse Poly(ethylene glycols) and Derivatives through Macrocyclization of Oligo(ethylene glycols). *Angew. Chem. Int. Ed.* **2015,** *54,* 3763–3767.

22. Loiseau, F. A.; Hii, K. K.; Hill, A. M. Multigram Synthesis of Well-Defined Extended Bifunctional Polyethylene Glycol (PEG) Chains. *J. Org. Chem.* **2004,** *69,* 639–647.

23. Wawro, A. M.; Muraoka, T.; Kinbara, K. Chromatography-free synthesis of monodisperse oligo(ethylene glycol) mono-p-toluenesulfonates and quantitative analysis of oligomer purity. *Polym. Chem.* **2016,** *7,* 2389–2394.

24. MacFarlane, L.; Zhao, C.; Cai, J.; Qiu, H.; Manners, I. Emerging applications for living crystallization-driven self-assembly. *Chem. Sci.* **2021,** *12,* 4661–4682.

25. Harniman, R. L.; Pearce, S.; Manners, I. Exploring the “Living” Growth of Block Copolymer Nanofibers from Surface-Confined Seeds by In Situ Solution-Phase Atomic Force Microscopy. *J. Am. Chem. Soc.* **2022,** *144,* 951–962.

26. Hwang, S.-H.; Kang, S.-Y.; Yang, S.; Lee, J.; Choi, T.-L. Synchronous Preparation of Length-Controllable 1D Nanoparticles via Crystallization-Driven *In Situ* Nanoparticlization of Conjugated Polymers. *J. Am. Chem. Soc.* **2022,** *144,* 5921–5929.

27. Petkau-Milroy, K.; Ianiro, A.; Ahn, M. M. L.; Magana, J. R.; Vleugels, M. E. J.; Lamers, B. A. G.; Tuinier, R.; Voets, I. K.; Palmans, A. R. A.; Meijer, E. W. Architecture-Dependent Interplay between Self-Assembly and Crystallization in Discrete Block Co-Oligomers. *ACS Macro Lett.* **2019,** *9,* 38–42.

28. van Genabeek, B.; Lamers, B. A. G.; de Waal, B. F. M.; van Son, M. H. C.; Palmans, A. R. A.; Meijer, E. W. Amplifying (Im)perfection: The Impact of Crystallinity in Discrete and Disperse Block Co-oligomers. *J. Am. Chem. Soc.* **2017,** *139,* 14869–14872.

29. Vleugels, M. E. J.; de Zwart, M. E.; Magana, J. R.; Lamers, B. A. G.; Voets, I. K.; Meijer, E. W.; Petkau-Milroy, K.; Palmans, A. R. A. Effects of crystallinity and dispersity on the self-assembly behavior of block co-oligomers in water. *Polym. Chem.* **2020,** *11,* 7170−7177.

30. Kwon, Y.; Kim, K. T. Crystallization-Driven Self-Assembly of Block Copolymers Having Monodisperse Poly(lactic acid)s with Defined Stereochemical Sequences. *Macromolecules* **2021,** *54,* 10487−10498.

31. Kwon, Y.; Ma, H.; Kim, K. T. Self-Assembly of Stereoblock Copolymers Driven by the Chain-Folding of Discrete Poly(D-lactic acid-*b*-L-lactic acid) via Intramolecular Stereocomplexation. *Macromolecules* **2022,** *55,* 2768−2776.

32. Yang, J.; Zhao, T.; Cui, J.; Liu, L.; Zhou, Y.; Li, G.; Zhou, E.; Chen, X. *J. Polym. Sci. Part B* **2006**, *44*, 3215–3226.

33. Lamers, B. A. G.; van Genabeek, B.; Hennissen, J.; de Waal, B. F. M.; Palmans, A. R. A.; Meijer, E. W. Stereocomplexes of Discrete, Isotactic

Lactic Acid Oligomers Conjugated with Oligodimethylsiloxanes. *Macromolecules* **2019,** *52,* 1200–1209.

Experimental Section

Chapter 2. Crystallization-Driven Self-Assembly of Block Copolymers having Monodisperse Poly(lactic acid)s with Defined Stereochemical Sequences

General Procedure of Deprotection of the benzyl group by hydrogenation

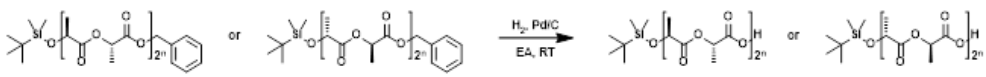

In an oven-dried Schlenk flask, discrete poly(D or L-lactic acid) protected with tert-butyldimethylsilyl (TBDMS) and benzyl groups (1 eq.) was dissolved in ethyl acetate under nitrogen. Palladium on activated charcoal (10% Pd/C, 10 wt%) was added to the solution, and the suspension was purged with nitrogen for 15 min. The nitrogen atmosphere was then changed with hydrogen, and the reaction mixture was stirred for 2h at room temperature. The suspension was filtered through a Celite cake to remove Pd/C. After removal of Pd/C, the product was obtained by evaporating the solvent under reduced pressure.

General Procedure of Deprotection of the TBDMS group with fluoride

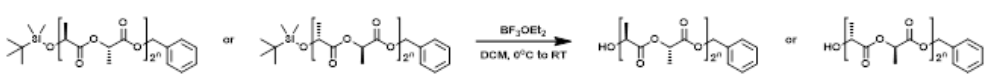

In an oven-dried Schlenk flask, discrete poly(D or L-lactic acid) protected with TBDMS and benzyl groups (1 eq.) was dissolved in dry dichloromethane. Boron trifluoride diethyl etherate (1.5 eq.) was added dropwise to a stirred solution at 0°C. The reaction mixture was stirred for 4h at room temperature. The reaction was quenched with saturated aqueous $NaHCO_3$. The organic layer was washed with $NaHCO_3$, water and brine. The combined organic layer was dried over $MgSO_4$, and the solvent was removed under reduced pressure. The crude product was purified via flash column chromatography using hexane & ethyl acetate as eluent.

General Procedure of Coupling Reaction: Esterification

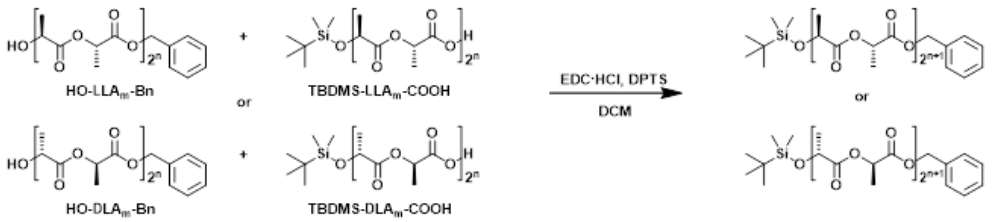

In an oven-dried Schlenk flask, TBDMS-D or LLA$_m$-COOH and HO-D or LLA$_m$-Bn were dissolved in dry dichloromethane. To the solution, *N*,*N*-dimethylaminopyridinium *p*-toluene sulfonate (DPTS, 0.2 eq.) and 1-(3-dimethylaminopropyl)-3-ethylcarbodiimide hydrochloride (EDC•HCl, 2 eq.) were added. The reaction mixture was stirred overnight at room temperature. The reaction mixture was washed with water and brine. The combined organic layer was dried over MgSO4, and the solvent was removed under reduced pressure. The crude product was purified via flash column chromatography using hexane & ethyl acetate as eluent. Products with 32 repeating units or more were purified by preparative-size exclusion chromatography (prep-SEC) with a series of columns using chloroform as an eluent.

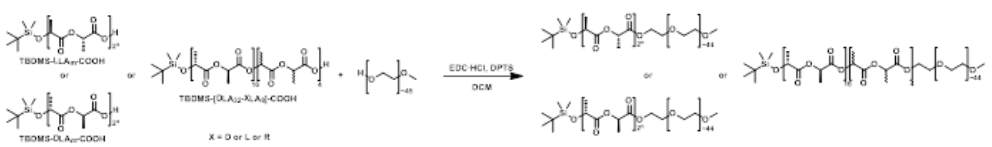

In an oven-dried Schlenk flask, TBDMS-D or LLA$_m$-COOH or TBDMS-[DLA$_{32}$-XLA$_8$]-COOH (X = D or L or D/L) and poly(ethylene glycol) methyl ether (PEG, 3 eq.) were dissolved in dry dichloromethane. To the solution, DPTS (0.2 eq.) and EDC•HCl, (2 eq.) were added. The reaction mixture was stirred overnight at room temperature. The reaction mixture was washed with water and brine. The combined organic layer was dried over MgSO4, and the solvent was removed under reduced pressure. Products were purified by preparative-size exclusion chromatography (prep-SEC) with a series of columns using chloroform as an eluent.

Synthesis of TBDMS-L or DLA$_2$-Bn

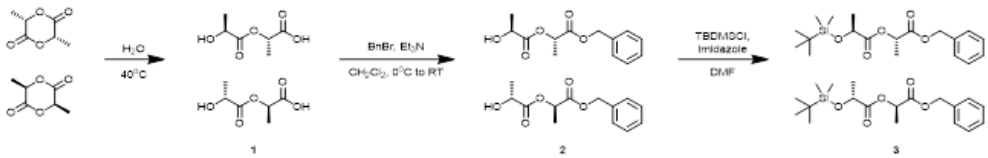

In an oven-dried round-bottom flask, a suspension of L-lactide or D-lactide (25 g) in water (100 mL) was stirred for 4h at 40ºC. The solvent was then evaporated under reduced pressure. The product **1** was obtained as colorless oil (28 g, 99% yield). ^{1}H NMR (400MHz, $CDCl_3$): 5.19 (q, J = 7.1 Hz, 1H, $CO_2C\mathbf{H}(CH_3)CO_2H$), 4.36 (q, J = 7.1 Hz, 1H, $HOC\mathbf{H}(CH_3)CO_2$), 1.56 (d, J = 7.1 Hz, 3H, $CO_2CH(C\mathbf{H_3})CO_2H$), 1.47 (d, J = 7.1 Hz, 3H, $HOCH(C\mathbf{H_3})CO_2$) ppm.

In an oven-dried Schlenk flask, **1** (28 g, 1 eq.) and triethylamine (34.9 g, 2 eq.) were dissolved in dry dichloromethane (200 mL). Benzyl bromide (26.5 g, 0.9 eq.) was added dropwise to a stirred solution at 0ºC. The reaction mixture was then stirred overnight at room temperature. The reaction mixture was washed with saturated aqueous NH_4Cl, water and brine. The combined organic layer was dried over MgSO4, and the solvent was removed under reduced pressure. The crude product was purified via flash column chromatography using 1:1 hexane: ethyl acetate as eluent. The product **2** was obtained as colorless oil (29.6 g, 68% yield). ^{1}H NMR (400MHz, $CDCl_3$): 7.36 (m, 5H, Ar), 5.20 (m, 3H, $CO_2C\mathbf{H}(CH_3)CO_2C\mathbf{H_2}Ph$), 4.34 (m, 1H, $HOC\mathbf{H}(CH_3)CO_2CH(CH_3)CO_2Ph$), 2.72 (b, 1H, O**H**), 1.54 (d, J = 7.1 Hz, 3H, $CO_2CH(C\mathbf{H_3})CO_2CH_2Ph$), 1.43 (d, J = 7.1 Hz, 3H, $HOCH(C\mathbf{H_3})CO_2$) ppm.

In an oven-dried round-bottom flask, **2** (29.6 g, 1 eq.) and *tert*-butyldimethylsilyl chloride (21.2 g, 1.2 eq.) and imidazole (15.9 g, 2 eq.) were dissolved in DMF (150 mL). The reaction mixture was then stirred overnight at room temperature. The reaction was quenched with saturated aqueous $NaHCO_3$ and extracted with hexane. The combined organic layer was dried over MgSO4, and the solvent was removed under reduced pressure. The crude product was purified via flash column chromatography using 5:1 hexane: ethyl acetate as eluent. The product **3** was obtained as colorless oil (36.5 g, 85% yield). ^{1}H NMR (400MHz, $CDCl_3$): 7.35 (m, 5H, Ar), 5.16 (m, 3H, $CO_2C\mathbf{H}(CH_3)CO_2C\mathbf{H_2}Ph$), 4.38 (q, J = 6.8 Hz, 1H, $SiOC\mathbf{H}(CH_3)CO_2CH(CH_3)CO_2Ph$), 1.52 (d, J = 7.1 Hz, 3H, $CO_2CH(C\mathbf{H_3})CO_2CH_2Ph$), 1.41 (d, J = 7.1 Hz, 3H, $SiOCH(C\mathbf{H_3})CO_2$), 0.90 (s, 9H, $(C\mathbf{H_3})_3CSi$), 0.10 (s, 3H, $(C\mathbf{H_3})_2Si$), 0.08 (s, 3H, $(C\mathbf{H_3})_2Si$) ppm.

Synthesis of TBDMS-[DLA$_{32}$-XLA$_8$]-Bn (X = D or L or D/L)

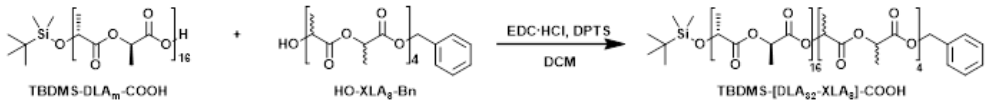

In an oven-dried Schlenk flask, TBDMS-DLA$_{32}$-COOH (0.1 g, 1eq.) and HO-XLA$_8$-Bn (0.042 g, 1.5 eq.) were dissolved in dry dichloromethane (10 mL). To the solution, DPTS (2 mg, 0.2 eq.) and EDC•HCl, (0.12 g, 1.5 eq.) were added. The reaction mixture was stirred overnight at room temperature. The reaction mixture was washed with water and brine. The combined organic layer was dried over MgSO4, and the solvent was removed under reduced pressure. The crude product was washed with 7:3 hexane:ethyl acetate to remove unreacted HO-XLA$_8$-Bn and purified via flash column chromatography using 2:8 hexane:ethyl acetate as eluent. The product was obtained as a white solid (0.091 g, yield 71%). ^{1}H NMR (400MHz, $CDCl_3$): 7.35 (m, 5H, Ar), 5.16 (m, 21H, CO_2[C**H**(CH_3)CO_2]C**H$_2$**Ph), 4.39 (q, J = 6.8 Hz, 1H, SiOC**H**(CH_3)CO_2), 1.54 (m, J = 7.1 Hz, 120H, CO_2CH(C**H$_3$**)CO_2), 0.90 (s, 9H, (C**H$_3$**)$_3$CSi), 0.10 (s, 3H, (C**H$_3$**)$_2$Si), 0.08 (s, 3H, (C**H$_3$**)$_2$Si) ppm.

Crystallization-Driven Self-Assembly

BCP was added to 1 mL of ethanol in a 4 mL vial. The samples were heated in oil bath at 75 ºC, followed by a slow cooling and equilibration at 25 °C without perturbation for 24 h. The resulting solution was diluted with water (0.1 mg/mL) and equilibrated at 25 °C for 4 h. The diluted solution was studied by TEM, AFM.

[DLA$_{32}$-XLA$_8$]-*b*-PEG$_{\sim 45}$ (0.5 mg) and LLA$_{40}$-*b*-PEG$_{\sim 45}$ (0.5 mg) were mixed and added to 1 mL of ethanol in a 4 mL vial. The samples were heated in oil bath at 75 ºC, followed by a slow cooling and equilibration at 25 °C without perturbation for 24 h. The resulting solution was diluted with water (0.1 mg/mL) and equilibrated at 25 °C for 4 h. The diluted solution was studied by TEM, AFM.

DLA$_n$-*b*-PEG$_{\sim 45}$ (0.5 mg) and LLA$_m$-*b*-PEG$_{\sim 45}$ (equivalent molar ratio) (n ≥ m) were mixed and added to 1 mL of ethanol in a 4 mL vial. The samples were heated in oil bath at 75 ºC, followed by a slow cooling and equilibration at 25 °C without perturbation for 24 h. The resulting solution was diluted with water (0.1 mg/mL) and equilibrated at 25 °C for 4 h. The diluted solution was studied by TEM, AFM.

Chapter 3. Self-Assembly of Stereoblock Copolymers Driven by the Chain-Folding of Discrete Poly(D-lactic acid-*b*-L-lactic acid) via Intramolecular Stereocomplexation

Synthesis of TBDMS-[DLA16]-[LLA16]-Bn stereoblock copolymers

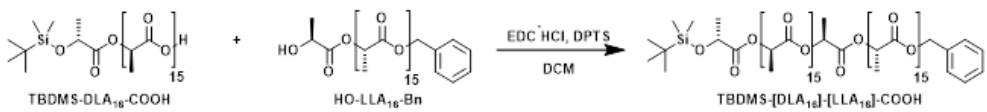

In an oven-dried Schlenk flask, TBDMS-DLA16-COOH (0.1 g, 1 eq.) and HO-LLA16-Bn (0.15 g, 1.5 eq.) were dissolved in dry dichloromethane (10 mL). To the solution, DPTS (2 mg, 0.2 eq.) and EDC•HCl, (22 mg, 1.5 eq.) were added. The reaction mixture was stirred for 3 h at room temperature. The reaction mixture was washed with water and brine. The combined organic layer was dried over MgSO4, and the solvent was removed under reduced pressure. The crude product was purified by preparative-size exclusion chromatography (prep-SEC) with a series of columns using chloroform as an eluent. The product was obtained as white powder (0.13 g, 68 % yield).

Synthesis of TBDMS-[DLA16]-[LLA16]-*b*-PEG

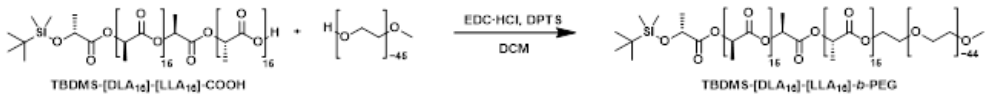

In an oven-dried Schlenk flask, TBDMS-[DLA16]-[LLA16]-COOH (0.13 g, 1 eq.) and poly(ethylene glycol) methyl ether (PEG, 0.26 g, 2.5 eq.) were dissolved in dry dichloromethane (10 mL). To the solution, DPTS (1.2 mg, 0.2 eq.) and EDC•HCl, (15 mg, 1.5 eq.) were added. The reaction mixture was stirred for 3 h at room temperature. The reaction mixture was washed with water and brine. The combined organic layer was dried over MgSO4, and the solvent was removed under reduced pressure. The crude product was purified by preparative-size exclusion chromatography (prep-SEC) with a series of columns using chloroform as an eluent. The product was obtained as white powder (0.15 g, 66 % yield).

Synthesis of TBDMS-[LLA$_{24}$]-*b*-PEG

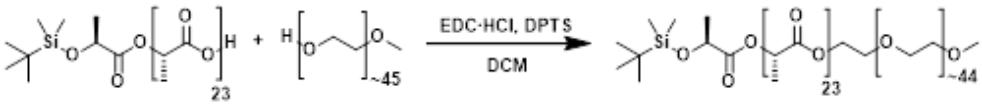

In an oven-dried Schlenk flask, TBDMS-[LLA$_{24}$]-COOH (90 mg, 1 eq.) and poly(ethylene glycol) methyl ether (PEG, 0.24 g, 2.5 eq.) were dissolved in dry dichloromethane (10 mL). To the solution, DPTS (1.1 mg, 0.2 eq.) and EDC•HCl, (13 mg, 1.5 eq.) were added. The reaction mixture was stirred for 3 h at room temperature. The reaction mixture was washed with water and brine. The combined organic layer was dried over MgSO4, and the solvent was removed under reduced pressure. The crude product was purified by preparative-size exclusion chromatography (prep-SEC) with a series of columns using chloroform as an eluent. The product was obtained as white powder (0.13 g, 72 % yield).

Deprotection of TBDMS-[LLA$_{24}$]-*b*-PEG

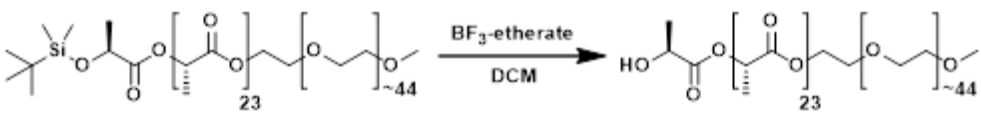

In an oven-dried Schlenk flask, TBDMS-[LLA$_{24}$]-*b*-PEG (0.13 g, 1 eq.) was dissolved in dry dichloromethane (5 mL). Boron trifluoride diethyl etherate (6 µL, 1.25 eq.) was added to a stirred solution at 0 ^{o}C. The reaction mixture was stirred for 4 h at room temperature. The reaction was quenched with saturated aqueous $NaHCO_3$. The organic layer was washed with $NaHCO_3$, water and brine. The combined organic layer was dried over $MgSO_4$, and the solvent was removed under reduced pressure. The product was obtained as white powder (0.12 g, 98 % yield).

Synthesis of TBDMS-[DLA$_{24}$]-[LLA$_{24}$]-*b*-PEG

In an oven-dried Schlenk flask, TBDMS-[DLA$_{24}$]-COOH (71 mg, 1.2 eq.) and HO-[LLA$_{24}$]-*b*-PEG (0.12 g, 1 eq.) were dissolved in dry dichloromethane (10 mL). To the solution, DPTS (0.7 mg, 0.2 eq.) and

EDC•HCl, (10 mg, 1.5 eq.) were added. The reaction mixture was stirred for 3 h at room temperature. The reaction mixture was washed with water and brine. The combined organic layer was dried over MgSO4, and the solvent was removed under reduced pressure. The crude product was purified by preparative-size exclusion chromatography (prep-SEC) with a series of columns using chloroform as an eluent. The product was obtained as white powder (85 mg, 48 % yield).

Crystallization-Driven Self-Assembly

[DLA_n]-[LLA_n]-*b*-PEG (n = 16, 24) (1 mg, 0.226 μmol-16, 0.180 μmol-24) was added to 1 mL of ethanol or acetonitrile in a 4 mL vial. The samples were heated in oil bath at 75 °C, followed by the cooling to 25 °C at a rate of 0.2 °C/min and equilibration at 25 °C without perturbation for 16 h. The resulting solution was diluted with water (0.1 mg/mL) and equilibrated at 25 °C for 4 h. The diluted solution was studied by TEM, AFM. TEM samples were stained with a 1 wt% solution of phosphortungstic acid in water.

[DLA_{16}] (0.30 mg, 0.218 μmol, TBDMS and benzyl protected) and LLA_{16}-*b*-PEG (0.72 mg, 0.218 μmol) were mixed and added to 1 mL of acetonitrile in a 4 mL vial. The samples were heated in oil bath at 75 °C, followed by the cooling to 25 °C at a rate of 0.2 °C/min and equilibration at 25 °C without perturbation for 16 h. The resulting solution was diluted with water (0.1 mg/mL) and equilibrated at 25 °C for 4 h. The diluted solution was studied by TEM, AFM. TEM samples were stained with a 1 wt% solution of phosphortungstic acid in water.

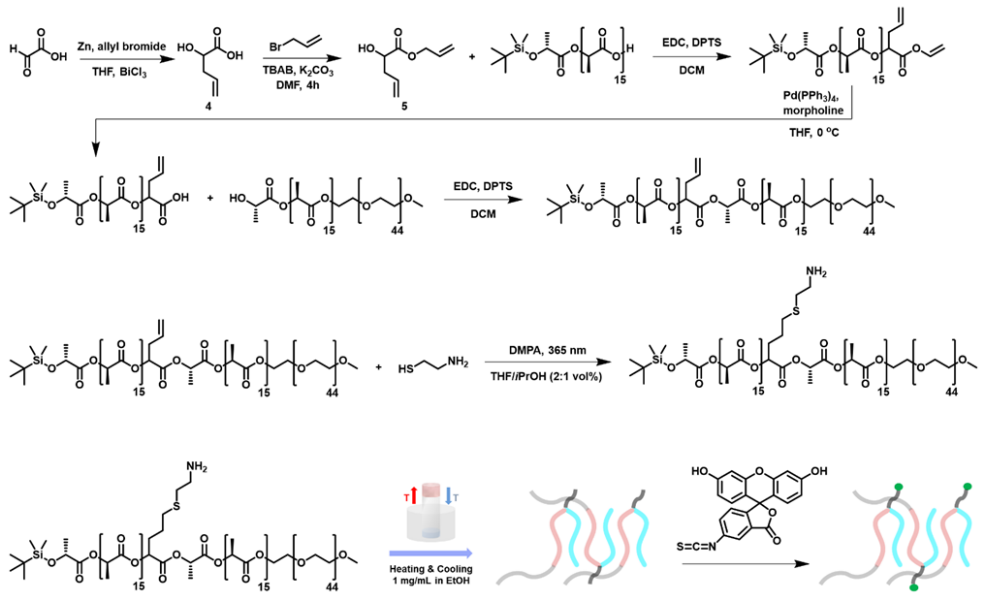

Scheme S3-1. Synthesis and CDSA of [DLA_{16}]-*rac*VLA^{NH2}-[LLA_{16}]-*b*-PEG and the resulting crystallites labeling with fluorescein isothiocyanate.

Synthesis of TBDMS-DLA_{16}-*rac*VLA-COOH

In an oven-dried round-bottom flask, glyoxylic acid monohydrate (2 g, 1 eq.) was dissolved in dry THF (50 mL) and the solution was cooled to 0 °C. Zn powder (3.1 g, 2 eq.) was added to this solution. $BiCl_3$ (10 g, 1.5 eq.) was dissolved in dry THF (20 mL) and added to the cooled mixture of Zn powder and glyoxylic acid monohydrate in THF. Allyl bromide (2.8 g, 2eq.) was added to a stirred solution at 0 °C. The reaction mixture was then stirred overnight at room temperature. The reaction was quenched by addition of 120 mL of 1 N HCl. After stirring for 2 h at room temperature, Zn salts was removed by filtration. Extraction of the water/THF phase was done with diethyl ether. The combined organic layer was dried over MgSO4, and the solvent was removed under reduced pressure. The product **4** was obtained as pale yellow oil (2.9 g, 93 % yield). ^{1}H NMR (400MHz, $CDCl_3$): 5.76 – 5.85 (m, 1H, C**H**=CH_2), 5.20 (t, 2H, C**H**$_2$=CH), 4.34 (q, 1H, HOC**H**CH_2), 2.46 – 2.64 (m, 2H, C**H**$_2$CH=CH_2) ppm.

In an oven-dried Schlenk flask, tetrabutyl ammonium bromide (0.7 g, 1 eq.) and K_2CO_3 (3.6 g, 1.2 eq.) were suspended in DMF (50 mL). Allyl bromide (2.2 mL, 1.2 eq.) and **4** (2.9 g, 1 eq.) were added. The reaction mixture was stirred for 4 h at room temperature. The reaction mixture was concentrated to a quarter of its initial volume and diethyl ether (60 mL), 5% aq. citric acid

solution (40 mL) and water (10 mL) were added. The aqueous phase was separated and extracted with diethyl ether. The combined organic phases were washed with 5 % $NaHCO_3$ and saturated NaCl solutions. The combined organic layer was dried over MgSO4, and the solvent was removed under reduced pressure. The crude product was purified via flash column chromatography using 1:4 diethyl ether : pentane as eluent. The product **5** was obtained as light yellow oil (3.3 g, 85% yield).

In an oven-dried Schlenk flask, **5** (45 mg, 2.5 eq.) and TBDMS-DLA_{16}-COOH (0.15 g, 1 eq.) were dissolved in dry DCM (10 mL). To the solution, DPTS (2.8 mg, 0.2 eq.) and EDC•HCl, (33 mg, 1.5 eq.) were added. The reaction mixture was stirred for 3 h at room temperature. The reaction mixture was washed with water and brine. The combined organic layer was dried over MgSO4, and the solvent was removed under reduced pressure. The crude product was purified via flash column chromatography using 7:3 hexane : ethyl acetate as eluent. The product TBDMS-DLA_{16}-*rac*VLA-allyl was obtained as white powder (0.14 g, 86% yield).

In an oven-dried Schlenk flask, TBDMS-DLA_{16}-*rac*VLA-allyl (0.14 g, 1 eq.) and $Pd(PPh_3)_4$ (11 mg, 0.1 eq.) were dissolved in dry THF (20 mL) and the solution was cooled to 0 ºC. Morpholine (0.01 mL, 1.2 eq.) was added to this solution. The reaction mixture was stirred for 2 h at 0 ºC. The solvent was removed under reduced pressure. The remaining residue dissolved in DCM, washed with 1 N HCl. The combined organic layer was dried over MgSO4, and the solvent was removed under reduced pressure. The product TBDMS-DLA_{16}-*rac*VLA-COOH was obtained as white powder (0.13 g, 97 % yield).

Synthesis of TBDMS-DLA_{16}-*rac*VLA^{NH2}-LLA_{16}-*b*-PEG

In an oven-dried Schlenk flask, TBDMS-DLA_{16}-*rac*VLA-COOH (0.43 mg, 1 eq.) and HO-LLA_{16}-*b*-PEG (0.1 g, 1 eq.) were dissolved in dry DCM (15 mL). To the solution, DPTS (1 mg, 0.2 eq.) and EDC•HCl, (10 mg, 1.5 eq.) were added. The reaction mixture was stirred for 3 h at room temperature. The reaction mixture was washed with water and brine. The combined organic layer was dried over MgSO4, and the solvent was removed under reduced pressure. The crude product was purified by preparative-size exclusion chromatography (prep-SEC) with a series of columns using chloroform as an eluent. The product was obtained as white powder (92 mg, 64 % yield).

In an oven-dried Schlenk tube, TBDMS-DLA_{16}-*rac*VLA-LLA_{16}-*b*-PEG (92

mg, 1 eq.), cysteamine (8 mg, 5 eq.) and DMPA (1 mg, 0.2 eq.) were dissolved in dry THF/*i*PrOH (2:1, v/v). The reaction mixture was irradiated UV lamp (365 nm) for 3 h. The solvent was removed under reduced pressure. The remaining residue was washed with methanol and dried under reduced pressure. The product TBDMS-DLA$_{16}$-*rac*VLA^{NH2}-LLA$_{16}$-*b*-PEG was obtained as white powder (83 mg, 89% yield).

Crystallization-Driven Self-Assembly of TBDMS-DLA$_{16}$-*rac*VLA^{NH2}-LLA$_{16}$-*b*-PEG

TBDMS-DLA$_{16}$-*rac*VLA^{NH2}-LLA$_{16}$-*b*-PEG (1 mg, 0.217 μmol) was added to 1 mL of ethanol in a 4 mL vial. The samples were heated in oil bath at 75 ºC, followed by the cooling to 25 °C at a rate of 0.2 °C/min and equilibration at 25 °C without perturbation for 16 h. The resulting solution was diluted with water (0.1 mg/mL) and equilibrated at 25 °C for 4 h. The diluted solution was studied by TEM, AFM. TEM samples were stained with a 1 wt% solution of phosphortungstic acid in water.

Synthesis of TBDMS-DLA$_{16}$-*rac*VLA^{F}-LLA$_{16}$-*b*-PEG

After CDSA, fluorescein isothiocyanate (0.42 mg, 5 eq.) was added to the resulting ethanol solution (1 mg/mL). The reaction mixture was stirred for 4 h at room temperature, followed by dialysis against water for 2 days. The resulting solution was diluted with water and studied by confocal laser scanning microscopy.

Table S3-1. Characteristics of [DLA_n]-[LLA_n]-*b*-PEG and [DLA_{16}]-*rac*VLA-[LLA_{16}]-*b*-PEG Block Copolymers.

Entry	BCP	M_n^{BCP} (Da)[a]	M_n^{BCP} (Da)[b]	$Đ^b$
1	[LLA_{16}]-*b*-PEG	3260.9	4400	1.04
2	[DLA_{16}]-[LLA_{16}]-*b*-PEG	4446.1	7600	1.03
3	[DLA_{24}]-[LLA_{24}]-*b*-PEG	5581.3	8500	1.04
4	[DLA_{16}]-*rac*VLA-[LLA_{16}]-*b*-PEG	4528.7	7900	1.03

[a]Number average molecular weight (M_n^{BCP}) determined by MALDI-TOF. [b]Number average molecular weight (M_n^{BCP}) and dispersity (Đ) determined by GPC using polystyrene (PS) standards. Elution was performed with THF at a flow rate of 1 mL/min at 25 °C.

국문초록

정확한 수의 반복 단위로 구성된 단일 분산 고분자는 통계적 분포없는 화학 구조를 갖는 고분자의 거동을 조사하는 모델 시스템으로 상당한 관심을 끌고 있다. 단일 분산 블록공중합체의 자기조립은 분산도가 자기조립 구조에 극적인 영향을 미치는 것을 보였다. 단일 분산 고분자의 자기 조립에의 활용은 형성되는 구조와 두께를 제어할 수 있는 수단이며, 이를 통해 보다 발전된 재료 생성을 이룰 수 있다. 이러한 맥락에서 단일 분산 폴리 락틱애씨드를 결정화 자기조립에 활용하여 형성되는 결정의 형태와 두께의 조절에 대해 논하고자 한다.

2장에서는 거울상 이성질체 반복단위로 이루어진 단일 분산 폴리 락틱애씨드로 구축된 블록 공중합체의 결정화 자기조립을 통해 결정의 형태를 조절하는 것을 성공하였다. 결정성을 갖는 단일 분산 폴리 락틱애씨드와 폴리 에틸렌 글리콜로 구성된 블록 공중합체의 결정화 자기 조립은 2차원의 나노 구조를 형성하였다. 단일 분산 폴리 락틱애씨드의 거울상 이성질체 반복 단위의 수와 배열을 조절함으로써 결정의 형태가 변화하는 것을 관찰하였으며, 이러한 결정 변화는 폴리 락틱애씨드 블록 공중합체의 입체 콤플렉스 형성 시 더 두드러진 것을 확인하였다.

3장에서는 고분자 사슬의 접힘을 조절하기 위해 단일 분산 폴리 락틱애씨드와 폴리 에틸렌 글리콜로 구성된 입체 블록 공중합체의 결정화 자기 조립을 진행하여 형성된 결정을 조사하였다. 결정화 자기 조립을 진행하는 고분자 용액의 농도에 따라 분자 간 또는 분자 내 입체 콤플렉스 형성이 이루어졌으며, 분자 내 입체 콤플렉스 형성 시 입체 블록이 접힌 구조를 갖는 것을 확인하였다. 폴리 락틱애씨드 입체 블록의 반복 단위를 정밀하게 제어하여 결정의 두께를 조절할 수 있었으며, 이는 락틱애씨드 단위 수에 비례하는 것을 확인하였다.

4장에서는 락틱애씨드 반복 단위가 일치하지 않는 입체 블록 공중합체를 합성하여 결정화 자기 조립을 진행하였다. 그 결과 선행연구들과는 달리 마이크로 크기의 결정이 형성된 것을 확인하였다. 입체 블록 공중합체에 존재하는 반복단위의 불균형이 입체 콤

플렉스의 적층에 기여했으며, 이로 인해 마이크로 크기의 결정 형성이 이루어졌다. 관찰된 결정 구조와 XRD 분석을 통해 가능한 결정 모델을 제안하였다.

주요어: 단일 분산 고분자, 반복 지수 합성법, 결정화 자기조립, 이차원 구조, 입체 블록 공중합체, 입체 콤플렉스

학번: 2016-20333